Study on Characteristic Evaluation and Control of an Upper Limb Rehabilitation System

by

Muye Pang

A thesis submitted for the degree of Doctor of Philosophy
Graduate School of Engineering, Kagawa University

Abstract

Stroke is the leading cause of disability, which severely affects the activity of daily living for patients. Benefitting from the found that neurons of humans are plastic, and the motor cortex functions can be altered by individual motor experiences, some strategies for rehabilitation training have been proposed, named neurorehabilitation training. Because the training process requires intensive, long duration and high-level exercise, it brings much burden to therapists. However, with the development of robotic technology, some robots have been designed for rehabilitation.

Considering the shortcoming of existing robots used in upper limb rehabilitation, in this thesis, a home-used upper limb rehabilitation training system was proposed.

In order to be able to be used at home, the device used for rehabilitation training should be more compact and portable. The developed Upper Limb Exoskeleton Rehabilitation Device (ULED) was thus applied in the system. To release the burden of therapists, a self-training concept, in which patients can finish the training exercises by themselves, was proposed. In self-training, the affected arm wore ULED and followed the motion of the intact arm. The control reference was based on surface electromyography (sEMG) signals recorded from the intact arm. A motion recognition method was applied to map raw sEMG signals into control reference firstly. An autoregression (AR) model was used to extract features and a back-propagation neural network (BPNN) classifier was trained to recognize motion patterns. For the purpose of improvement of recognition

rate, a wavelet packet transform method was applied to reduce noise and the features were extracted by a muscular model. The support vector machine was used to instead of BPNN to be the classifier. The recognition rate improved 10% average. Furthermore, to conquer the inherent drawback of the motion recognition based method that it can only provide a binary-like control reference, a muscular model based continuous angle prediction method was developed to predict elbow joint angle using only sEMG signals.

Another important issue for the home-used rehabilitation system is to evaluate training effect remotely. A remote force evaluation system was designed for this purpose. The evaluation system can predict human-environment contact force using only sEMG signals. The isometric downward touch and push motion were studied in this thesis. Seven muscles around upper limb were used for recording sEMG signals. Two musculoskeletal models were applied to derive dynamic equations for the two motions, respectively. The parameters involved were calibrated by a Bayesian Linear Regression (BLR) algorithm. The haptic device “Phantom Premium” was used in the remote side to represent the predicted force. The therapist can hold the handle of the Phantom to feel and evaluate the identical contact force exerted by the patient from a remote side.

The proposed system was evaluated by ten healthy subjects for the self-training function and force evaluation function. The RMS error for the elbow joint prediction method was below 10° while the ABS relevant error for force prediction method was below 20%

Acknowledgements

This dissertation is the result of 3 years study at Kagawa University. I would like to thank the people who have helped me.

First of foremost, I would like to express my sincere gratitude to my supervisor, Professor Shuxiang Guo for his invaluable guidance, support and encouragement throughout my Ph.D. For improving my thesis, he gave me so many useful advices. I appreciate him not only for his guidance on my research, but also the great encouragement and help on my life.

I wish to thank Dr Song who was the previous leader of the rehabilitation group in Guo Lab. He designed the device which was applied in my system. Most of all, he helped me a lot on my study when I got stuck on the study and showed me the way how to be an excellent researcher when I just started the doctoral program at KU.

I would like to express my thanks to my friends Songyuan Zhang, Mohan Qu, Qiang Fu, Chunhua Guo, Youichirou Sugi, Keiji Yamamoto, Chunfeng Yue, and Xuanchun Yin. Some of them are the members in rehabilitation group and some of them were room mates of mine. They gave me a happy living in Japan and helped me to grow up.

At last, I would like to thank my family because they provide strong spiritual and financial support to me. I will give my greatest apologizing to my grandma and grandpa, who have passed on during the period of my doctoral program, that I was not there at your last time of lives.

Declaration

I hereby declare that this submission is my own work and that, to the best of my knowledge and belief, it contains no material previously published or written by another person nor material which to a substantial extent has been accepted for the award of any other degree or diploma of the university or other institute of higher learning, except where due acknowledgment has been made in the text.

Table of Contents

Chapter 3 Motion Evaluation and Recognition using sEMG

Chapter 4 Continuous Motion Prediction using sEMG

List of Figures

List of Tables

Chapter 1 Introduction

1.1 Neurorehabilitation

It is reported by World Heart Federation that 15 million people worldwide suffer a stroke every year and nearly six million die and another five million are left permanently disabled [1]. Stroke is the second leading cause of disability, which wildly affects peoples' Activities of Daily Living (ADL) and the life style of their families. As it has been stated that 'Rehabilitation, for patients, is fundamentally a process of relearning how to move to carry out their needs successfully.' [2], rehabilitation is such kind of training process therapists help patients to recover their function of movement as they used to be before stroke. Fortunately, some researchers [3] found that the neurons of some animals and humans are plastic, and the motor cortex functions can be altered by individual motor experiences. Some training strategies are developed based on this found, such as intensive intervention [4], task orientation training [5-7], bilateral training [8], electromyographical biofeedback [9], and functional electrical stimulation training [10], towards the function of neurorehabilitation. Although the neurorehabilitation itself is at the infancy stage and remains lots of challenges to researchers and doctors, the basic concept of neurorehabilitation that practice will improve the performance of motor learning is advanced in the rehabilitation topic [11]. Normally, these strategies require intensive, long duration and high-level training periods

[12] which will bring much burden to therapists.

1.2 Robots for rehabilitation

Robots have been implemented on rehabilitation since 1980s [13]-[15]. MIT-Manus [16],[17], ARMin [18]-[19],[84]-[85] and MIME [20]-[21] have been thought to be the pioneers for developing therapeutic robot systems for rehabilitation and reporting treatment results on patients. Rather than other fields' requirements, more elaborate demands are needed to design robot systems for rehabilitation. Some literatures [22] divided these requirements into three aspects: psychological, medical and ergonomic. For psychological aspect, it is required that therapist and patient are both motivated. During the training process, the robot remains assistance or 'invisible' to the therapist and the therapist plays the main role for the patient. A 'human-friendly' design is also welcome for the psychological purpose [23]. For medical aspects, the robot should be adapted or adaptable to the human limb in terms of segment lengths, range of motion (ROM) and the number of degrees-of-freedom (DOFs). Although large DOFs may fit the patient well, it could make the device complex, inconvenient and expensive as well. No mention that it is still under discussion that whether large DOFs is good for rehabilitation or not. For ergonomic aspects, the rehabilitation robot set-up must be rather flexible to cope with a large variety of different applications and situations. The device should be suitable for different body heights and weights or gender.

Robots can provide more intensive, longer duration and higher-level training than therapists. A well programmed, backdrivable robot can

achieve active interactive training effort for patients. The impedance controller, which is introduced by Hogan [24], is widely used for the purpose of robotics and human-system interaction. Lum et al [20] developed the mirror image enhancer (MIME) arm therapy robot. The affected arm performs a mirror movement of the movement defined by the intact arm. The MIME can provide four different control models for patients. The virtual reality (VR) concept is also applied on rehabilitation [25]-[27]. This kind of system can mimic the real ADLs environment to enhance the activation for central nervous system.

1.3 Electromyography signals

As mentioned in section 1.1 that the electromyography (EMG) biofeedback technology is also applied on rehabilitation. EMG signals are detected when skeletal muscles are activated by the center nervous system. When activation comes from the nervous systems, action potential is achieved on membranes of muscle fiber cells in one motor unit. This excitation, which spreads along muscle fiber in both directions and inside muscle fiber through a tubular system, releases calcium ions in the intra cellular space [28]. Linked chemical processes finally shorten contractile elements of the muscle cell. Raw sEMG signals, which are detected through electrodes placed on the skin of the upper limb, are superposition of different Motor Unit Action Potentials [29] (MUAP). The two most important mechanisms influencing the magnitude and density of the observed signal are the recruitment of MUAPs and their firing frequency.

The mechanism of the generation of EMG signals indicates that this

kind of biological signals can be used for interpretation of muscle activation levels. Methods used for nowadays are very simple and direct to obtain muscle activation level from EMG signals. One of the simplest ways is to normalize the EMG signal by dividing it by the peak rectified EMG value obtained during a maximum voluntary contraction (MVC). This method may be the most conventional one for the researchers around the world to process EMG signals. Still it is open for discussion that whether it is appropriate to just use this simple way to obtain muscle activation level. Some researchers suggested that a more detailed model of muscle activation dynamics is warranted in order to characterize the time varying features of the EMG signal. One of such kind of model or method is called Discretized Recursive Filter (DRF) [30]. This method is based on the phenomenon that when a muscle fiber is activated by a single action potential, the muscle generates a twitch response. A damped linear second-order differential system can well represent this response and the DRF is just the discrete equation which describes this differential system. Although a linear approximation of muscle activation from EMG signals seems reasonable and suitable, the activation is nonlinearly related to EMG in many cases. Some equations [31]-[33] have been established based on the nonlinear concept.

1.4 Implementation of EMG signals

According to the different measurement method, EMG signals can be divided into surface ones, which are recorded by electrodes attached on the skin above the target muscle belly, and intrinsic ones, which are recorded

by needles inserted into the muscle fibers. Fig 1.1 shows the two kinds of recorded EMG signals. As using the needle requires professional anatomical and medical knowledge and it may bring pain to the subject, the surface EMG or sEMG is widely used for engineering purposes.

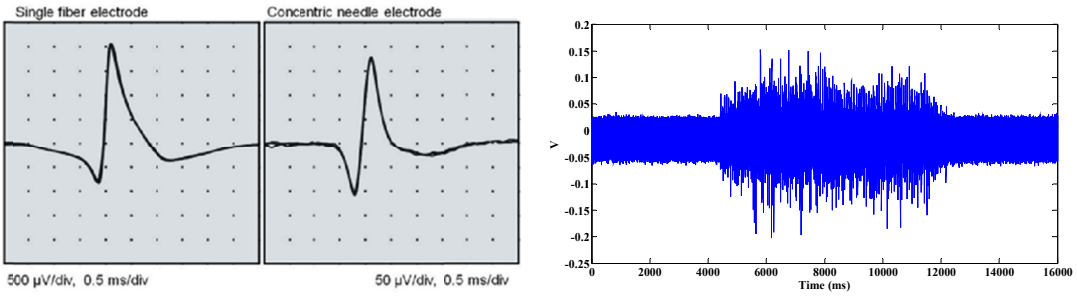

(a) (b)

Figure. 1.1: Two type of recording method for EMG signals. (a) shows the one recorded by needle [81]; (b) shows the ones recorded by surface electrode.

1.4.1 Utilization of EMG

Prediction of motions may be the most popular apply with sEMG signals. Fukuda et al. [34] used EMG signals to control a manipulator. They adopted a statistical neural network, named the log-linearized Gaussian mixture network, to achieve robust discrimination against differences among individuals, electrodes locations, and time variations caused by fatigue or sweat. They reported that the method can provide smooth control for the manipulator and it might allow a physically handicapped person to sense a feeling of prosthetic control similar to that of the original limb. Liarokapis et al. [35] used EMG signals from sixteen muscles of the upper

limb to study the muscular co-activation patterns during a variety of reach-to-grasp motions. Artemiadis et al. [36] developed a switching regime model to decode the EMG activity from 11 muscles into a continuous representation of arm motion in three-dimensional space. Ju et al. [37] designed a fuzzy Gaussian mixture model with non-linear feature extraction method to classify different hand grasps and in-hand manipulations. They reported that using their proposed non-linear method the highest recognition rate of 96.7% could be achieved. This kind of implementation is very meaningful for control of prostheses or robot arms intuitively. The operator doesn't need the control panel anymore but just performs his/her accustomed motions to control the device. Besides pattern recognition based methods, some researchers also proposed continuous prediction method. Earp, et al. [98], proposed a polynomial relation between EMG signals and knee angles. Vogel, et al. [99], recorded the EMG of atrophic muscles to control a robot arm continuously. Alternatively, An, et al. [100], offered a muscle synergy based method to mimic the human standing-up motion by recording EMG signals from lower limbs.

Another implementation is to use sEMG signals to calculate musculotendon forces [87-91]. Actually, besides the muscle activation level, the musculotendon force is the most direct one that EMG signals reflect. As the activation signals to muscle contraction, the EMG signal certainly has a strong relationship with musculotendon forces. Two physiological models are widely used for musculotendon forces prediction: Huxley- [38,39] and Hill-type models [40]. Compared with the complexity of Huxley-type

models, Hill-type models are more computationally viable. Cavallaro et al. [41] developed a Hill-type-model-based myoprocessor to predict joint torque. Seven muscles around the upper limb were recorded and a genetic algorithm was implemented to tune the parameters of the model. Manal et al. [42] used a Hill-typed model to calculate muscle force and implemented a forward dynamics approach to estimate joint angle. They used an optimal controller to map the relationship between measured and predicted joint moments. Fleischer and Hommel [43] used the sEMG signals and Hill-type based biomechanical model to control a lower-limb exoskeleton device. It should be noticed that the EMG signal is not the only one involved in the muscular model. For example in Hill-type model, the EMG signal is used to reflect the muscle activation level which is just one of the variables in the function, together with other hard to be measured ones, such as muscle changed length, changing velocity and the status of the tendon. Hogan also discussed the function of coactivation of antagonist muscles to maintain the posture of the forearm and hand [86].

Besides motion recognition and musculotendon force prediction, EMG signals are also applied on controlling of force enhance or power assistance system [95-97]. Lenzi et al. [44] proposed a simple sEMG signals based powered exoskeleton control method that can support the subject depending on the amplitude of detected sEMG signals. They reported that such kind of simple proportional control method can provide suitable results for their particular purpose. Kwon et al. [45] gave an analysis on the stability of sEMG-based elbow power assistance. They

wanted to set up a foundation for determining the appropriate amount of such kind of device. Moreover, some researchers used sEMG signals to perform impedance control. Ajoudani et al. [46] proposed a tele-impedance body-machine interface to perform a peg-in-the-hole and a ball-catching task. The sEMG signal was used to predict the stiffness of the operator's arm and a stiffness variable robot arm was applied to reflect the predicted stiffness.

1.4.2 Issues of EMG

Despite the attractive application of EMG signals on various fields, the EMG signal is still hard to be used outside the laboratory environment. Time-variable, non-stationarity, low signal-to-noise ratio, individual differences, and easily affected by external factors [92-94] become the primary factors that give rise to the 'hard-to-use' property of EMG signals.

As the complexity of mechanism of muscle activation procedure and the human musculoskeletal system, EMG signals seems non-linear and time-variable to every interesting targets, such as musculotendon force, to-be-predicted motions or stiffness of limbs. Compared with non-linear, the time-variable makes the problem even worse. For the same desired target or behavior, EMG signals change wildly and frequently. It is hard or impossible to find the exact mapping between EMG signals and the target. It seems like that a random noise is always added on the original EMG signals, which may be the reason that why researchers tend to apply machine learning algorithm to solve the problem concerned with EMG signals. Chen et al. [47] developed a multi-kernel learning support vector

machine method to classify multiple finger movements. In order to recognize hand motions, Tang et al. [48] applied a multi-channel energy ratio feature extraction method to overcome the influence of various forces for a given gesture. They used the proposed feature extraction method and a cascaded-structured classifier to recognize eleven hand gestures. Phinyomark et al. [49] implemented twelve anthropometric variables to design an automatic/semi-automatic calibration system for EMG recognition. Although many elegant algorithms have been developed [50-52], you still cannot treat this biological signal as the one obtained from conventional sensors, such as a force sensor or a position sensor.

For the low signal-to-noise ratio (SNR) aspect, Clancy [53],[54] proposed a time-varying selection of the smoothing window length method and white noise preprocessing method to improve SNR of EMG signals. The use of different cut-off frequency filters are also suggested by researchers [55]. Although this issue seems less important with the growing of signal processing technology, the researchers are still disturbed by the SNR problem, caused by inevitable factors, such as crosstalk.

1.5 Thesis contributions

In this thesis, a home-used upper-limb rehabilitation system was proposed, focusing on characteristic evaluation and the control method development.

Contributions of this thesis are:

(1). Development of bilateral self-training function using ULERD and sEMG signals.

The bilateral self-training function aimed to release the burden from therapists. Although the supervising from therapists is necessary for patients, for hemiparesis patients, they need training practice frequently at home in most of the time. In the proposed system, the patient is asked to wear the ULERD on his/her impaired upper-limb and electrodes are attached on the intact upper-limb. Then the patient is asked to perform training exercise bilaterally. The control reference is obtained from sEMG signals obtained from the intact upper-limb. One of the advantages of this system is that patient can guide by himself using the intact limb. Although it is still being studied, the research results indicate that positive exercise which is activated by Centeral Nervous System (CNS) or the willing of patient is more effective than passive exercise which is carried out by therapists or devices. Another advantage is that the control reference is obtained from the EMG signal. Rather than the conventional motion signals, such as angle value or trajectory obtained from motion capture system, the EMG signal reflect the intention of the motion and it is the original signal reflect the activation from CNS.

(2). Evaluation of motion to sEMG signals. A motion recognition method and a continuous elbow joint angle prediction method were proposed.

In order to map the sEMG to motions, a motion recognition based method was proposed firstly. The wavelet packet transform was applied to remove the influence from noise and a muscular model was used to extract features. Compared with conventional signal processing method, the muscular model based model reflects more natural property of the sEMG

signals. For classifier, the support vector machine (SVM) was chosen to recognize motions. In our particular cases, the SVM is more robust than the neural network classifier. Nevertheless, the motion recognition method has its own limit. It can only provide binary-like control reference, but in many cases, continuous prediction results are needed. For the purpose of providing continuous prediction results, a musculoskeletal model based elbow joint angle prediction method was proposed. A quadratic relationship was derived from the musculoskeletal model and Hill-type based muscular model. A state switching function was developed to conquer the problem of time-variable characteristic of sEMG signals. The proposed method can predict elbow joint angle continuously using only EMG signals.

(3). Development of human-environment contact force prediction method.

Another function of the home-used upper-limb rehabilitation system is that it can provide remote force evaluation. The force prediction is achieved by using only sEMG signals. To use sEMG signals can avoid the inconvenience of attaching force sensor and constrain of the motion of patients. Two isometric motions are focused on in this thesis, namely downward touch motion and push motion. Two dynamic equations were derived from the two motions, respectively. The parameters involved in the two equations were calibrated by Bayesian Linear Regression (BLR). The application of BLR can avoid the problem of over-fitting and the natural property of BLR treats the issue on the probability point of view which solves the problem of time-variable for sEMG signals. A haptic device ‘Phantom Premium’ was used to represent the predicted force on the

remote side.

Chapter 2 Motivation and Research Purpose

2.1 Motivation

Although many robotic rehabilitation systems have been developed since 1980s, home-used robotic rehabilitation systems are seldom seen. Large robotic systems are just suitable to be used in rehabilitation center for special purpose and under the supervision of therapists. Consider the amount of patients needed to be treated and the number of robotic systems being used, there is still a long way to go for the popularization of robotic system in rehabilitation training. On the other hand that the mild stroke patients don't quite need the medical treatment using such kind of large robotic system. Usually these patients are asked to perform rehabilitation training by themselves, with some simple assistance devices, and under the supervision of their families. In most of the cases, these patients are lack of supervision from the therapist and are not well motivated, as the families members are not well trained on concept of rehabilitation. With time going on, they may lose interest and feel bored for rehabilitation training. As a consequence, the training intension and duration is not enough to achieve a good result. And lacking of supervision from the therapist may lose some good opportunities for a better training timing.

It can be indicated that there are huge demand of relative small home-used robotic rehabilitation system. This kind of rehabilitation system should be small enough to be portable, to be able to provide active or

passive training assistance as needed and to be able to provide evaluation method to observe the status of patients. A remote function may be more attractive because it will save the time wasted on the road to rehabilitation center and waiting for the therapist. Furthermore, on the neurorehabilitation training point of view, just simple movement of the impaired limb is not good enough for rehabilitation. The patient should be inspired to perform the movement under his/her own will, i.e. under the command from CNS. The experimental results from Lum et al. [8] indicated that a 'bimanual mode' or bilateral training strategy will inspire the patient well. The bilateral type of rehabilitation may be helpful for patients to complete the training exercise at home. On the other hand, it will be also a useful function that the rehabilitation system can provide remote evaluation for the therapist to supervise the patients.

2.2 Upper-limb exoskeleton rehabilitation device

In our previous study, an Upper-Limb Exoskeleton Rehabilitation Device (ULERD) (as shown in Fig. 2.1) has been designed [56-59]. The total weight of ULERD is 1.3 kg which is light enough for portable purpose. It has seven DoFs, including three active DoFs (one for the elbow joint and tow for the wrist joint) and four passive DoFs (two for the elbow joint and two for the wrist joint). The passive DoFs aimed to achieve the requirement from ergonomic aspect as mentioned in section 1.2. This device can provide active training, in which a resistant force will be exerted on when patient performs rehabilitation exercise. The function is achieved by impedance control algorithm. Besides, a passive training model can also be

selected, in which the device will carry the impaired arm following the order from a supervisor.

The ULERD provide a hardware foundation for the home-used rehabilitation system. The weight is light enough to allow the patient to wear the device to perform the ADLs and the possible driven models (active and passive) are suitable to fit the various needs from patients.

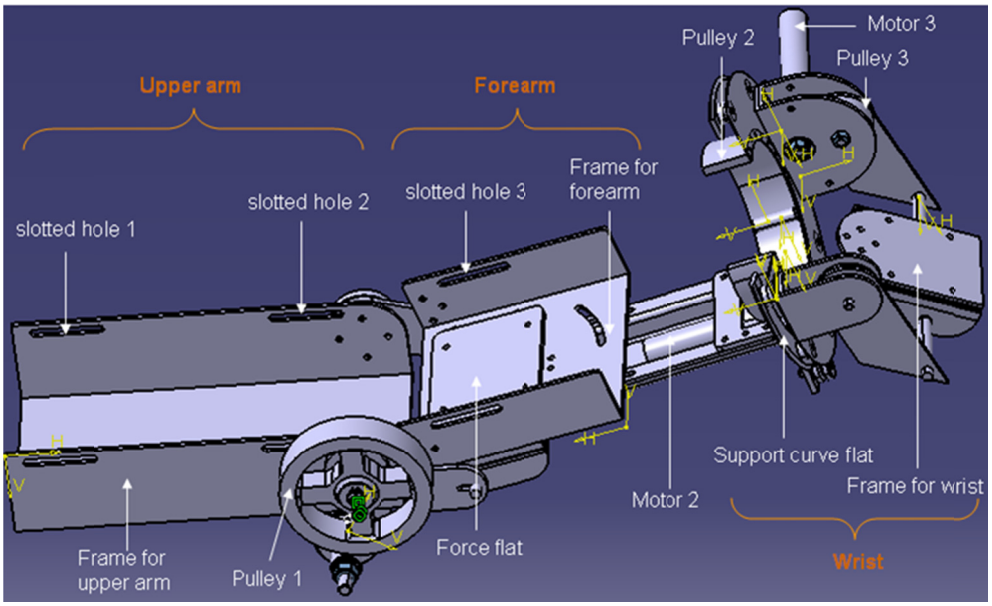

Figure 2.1: The Upper-Limb Exoskeleton Rehabilitation Device

2.3 Developed Tele-operation system for rehabilitation

We also developed a simple tele-operation interaction system (as shown in Fig. 2.1) to inspire patient. In the tele-operation system, patient wears the ULERD on the impaired arm and holds a haptic device. The task in the proposed training exercise is to control a beam to track a random appeared block displayed on the screen. The operation of the beam is executed by patient and therapist together. A spring-damping model was

designed for the operation. The system will provide assistance or resistance force to the patient via the haptic device and our ULERD. The exercise can be controlled by therapist on the remote side. The idea for this tele-operation system is that the training exercise can be performed by tele-operation, not required the therapist to be at present to supervise the training. The detailed information for this system can be found in [82, 83].

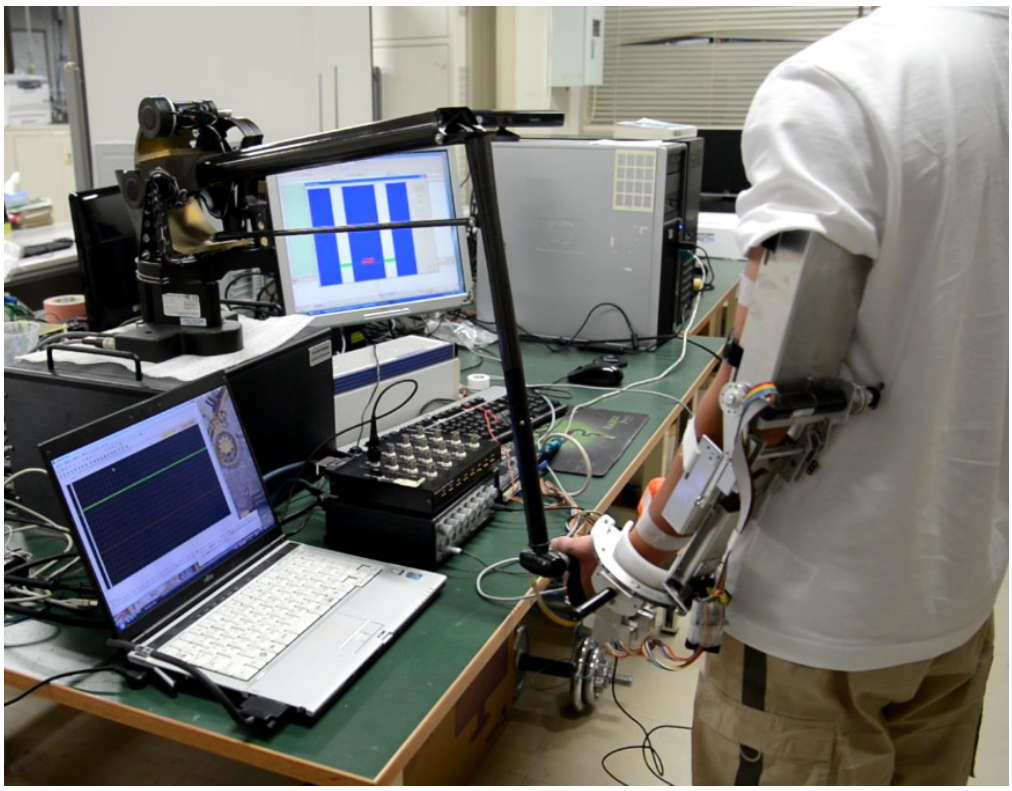

Figure. 2.2: Tele-operation system for rehabilitation training

2.3 Research purpose

The purpose of this thesis is to propose a home-used upper-limb rehabilitation system including the following properties:

(1) In order to release the burden from therapists, the system should be able

to provide self-training to the patient. The self-training should follow the concept of bilateral exercise from the neurorehabilitation point of view.

(2) To realize remote evaluation, a force prediction method should be developed. The method should reflect the status of the patient as entirely as possible. For such purpose, the force sensor may not be enough, because it can only reflect the end-effect performance of the patient.

(3) As one of the state-of-the-art technologies to control prostheses or robot arms, it is necessary to evaluate the relationship between sEMG signals and kinetics variable of human. A dynamic equation, if possible, is desired to interpret the relation between sEMG signals and motions.

Additionally, a deeper understanding of the relationship between human and exoskeleton device, e.g., how to improve the control interaction, how to improve the control algorithm to fit device better for subject, will be desired to release via the research.

Chapter 3 Motion Evaluation and Recognition using sEMG

3.1 Introduction

Using sEMG to recognize motion of human is one of the most prominent applications of this biological signal for engineering purpose. It is extremely useful toward intuitive control of prostheses or robot arms. The patient who loses his/her arm in an accident can mount the prostheses on the remaining part of the wounded arm and control signals will be extracted from sEMG signals recorded from the remaining muscles. In this way, the patient will feel like that controlling the prostheses is just like the original arm [34]. Some commercial products [60-62] have been developed towards this kind of application. These products are capable of performing complex motions by integrating more electrodes or sensory feedbacks. Furthermore, it has to be said that the remaining muscles may have no relationship with the target motions, depending on the wound situation. Under such circumstance, the patient, actually, uses an alternative way to perform the motion, i.e. using another group of muscles, because of lack of the original ones. However, it is still advanced than pushing bottoms on a control panel to control the prostheses.

From the neuromechanics point of view, human motion is just the output of CNS and musculoskeletal system. The EMG signal is a little previous than the measured movement (about 30 to 100 ms, namely

electromechanical delay (EMD) [63]). The existence of EMD indicates that it is theoretically possible to predict motion using EMG signals, which will bring much advance to control method.

In this chapter, the evaluation between human motion and sEMG signals will be discussed, and a motion recognition method will be introduced. Upper-limb motions, which include elbow flexion and extension, forearm pronation and supination, wrist flexion and extension, and adduction and abduction, are mainly focused on. These motions are involved in ADLs commonly. An autoregressive (AR) model based feature extraction and neural network based classification method will be introduced firstly, followed by an improved Hill-type muscular model based feature extraction and support vector machine (SVM) classifier recognition method.

3.2 Design of motion recognition method with neural network

3.2.1 Autoregressive based feature extraction

To extract features of sEMG signals, an autoregressive (AR) time series model is applied in this thesis [65]. The AR model was introduced in the study of EMG signals in 1975, when Graupe and Cline first used this model to represent electrical muscle activation behavior [64]. In statistics and signal processing, the AR model is a type of random process that is often used to model and predict various types of natural phenomena. Because EMG is a random natural signal, it is very suitable to use the AR model to extract features. The AR model is defined as follows

$$X_t = c + \sum_{i=1}^{p} \varphi_i X_{t-i} + \varepsilon_t \quad (3\text{-}1)$$

where p is the order of the AR model, X_t is the value of data, φ_i is coefficient, c is a constant and ε_t denotes the white noise.

For original purpose of the applying AR model, which is to predict output of a system based on previous outputs, it is reasonable to consider that coefficients (φ_i) of the model are representative of the sequence of input data or the model itself is capable of catching feature from the raw data. Fig. 3.1 provides some calculation results using the Burg method [78] to fit raw sEMG signals detected from biceps brachii with a 4th order AR model, where the above red line denotes the second coefficient of the AR model, and the below blue line represents for the raw sEMG signals. The upper line in Fig. 3.1 was calculated with a time interval of 50 ms (sampling frequency of 1000 Hz). The results show that changes of the coefficient follow the trend in sEMG signals. Additionally, it should be noticed here that this kind of phenomenon gave us the idea that whether we could find some way to extract the trend from the EMG signals to map the motion. The different sequences of coefficients represent different sequences of raw signals. For example, coefficients in Fig. 3.1 from time intervals 1 to 10 stand for raw signals from 1 to 500, coefficients from 11 to 25 stand for signals from 550 to 1250, coefficients from 26 to 40 stand for signals from 1300 to 2000, and so on. As the sEMG signals were recorded from the motions continuously, different sequences of the coefficients of the AR model are consequently representative of the different motions of the upper limb. So in this thesis, coefficients of the AR model are divided following different motions of the upper limb and then grouped coefficients

are used as input to the neural networks for pattern recognition.

Time consumed by AR model is low, and it is suitable in real-time calculation. sEMG signals were calculated using the AR model in real time with a certain time window (with 50 ms in this thesis), and then coefficients of the AR model are used as input to a well-trained neural network. The time consumption for the entire procedure was about 50 ms, as the time interval used for AR model computing was 50 ms and time consumption for motion recognition was only around 0.03 ms.

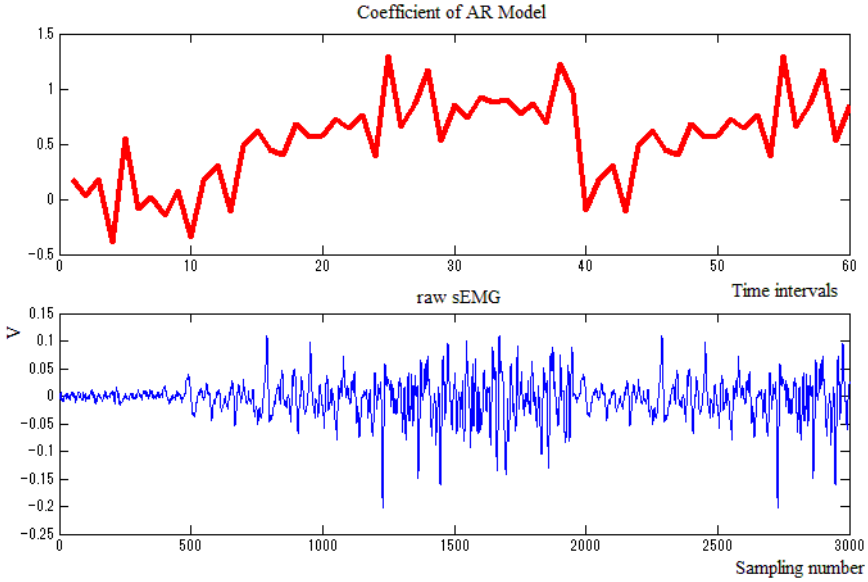

Figure. 3.1: Change in AR model coefficients compared to amplitude trend in sEMG signals [77]

There are two primary parameters in the AR model. One is the interval of the time window (t) used for data calculation and the other is the order (p) of the AR model.

There is the constraint that the AR model requires that predicted data be wide-sense stationary. It has been indicated that raw sEMG signals are

nonstationary [64], but with sufficient short time intervals, this nature of electrical behavior could be considered stationary. It is thus important to select a suitable processing time window when using the AR model in extracting the features of the sEMG signal. In order to judge the appropriateness of time intervals, all of the roots of polynomials, as described in equation (3-2), must lie within the unit circle in complex plane.

$$x^p + \sum_{i=1}^{p} \varphi_i \, x^{p-i} = 0 \qquad (3\text{-}2)$$

For this study, raw sEMG sequences were divided into 50 ms (each 50 samples at a 1000Hz sampling rate) intervals and the following figure shows calculation results using equation (3-2), where the circle represents the unit circle:

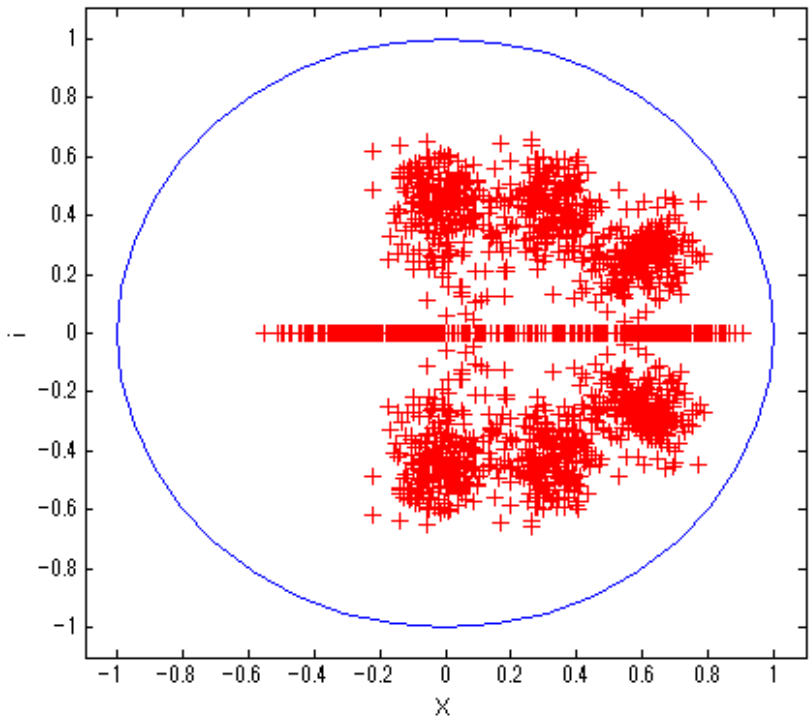

Figure. 3.2: Plot of all-roots with equation (3-2) [77]

Fig. 3.2 shows that all of the roots are in the unit circle, which means that all of the AR models remain wide-sense stationary.

It is also necessary to determine the optimal order before using the AR model fitting the sEMG signal. If the order is too small, the fitting effect will be so weak that the recognition accuracy rate will be adversely affected. Because in such condition, the feature losses the representation property for the sEMG signals and tends to be the signals themselves. As the consequence of the low signal-to-noise ratio characteristic of sEMG signals, the classifier can hardly convergence with such kind of training data. If the order is too big, however much computation time will be required, which will influence the real-time control effect as well.

To guarantee a suitable order, the Akaike Information Criterion (AIC) [79], which is a well-known criteria, was used as the judgment criterion. The following equation describes the AIC algorithm:

$$\mathrm{AIC(p)} = \ln(\mathrm{E_p}) + 2(\mathrm{p}+1)/\mathrm{N} \tag{3-3}$$

where E_p is the estimated linear prediction error variance for the model with order p and N is the number of input sEMG signals. The order that minimizes the AIC function results is selected as the optimal one.

The result of the AIC method is represented in Table 3.1 with AR model order P from 1 to 40, and Fig. 3.3 describes the general trend of change.

Table 3.1 Order P to AIC

P	AIC(10^{-4})	P	AIC(10^{-4})	P	AIC(10^{-4})	P	AIC(10^{-4})	P	AIC(10^{-4})
1	2.539	9	2.873	17	1.306	25	8.590	33	0.936
2	2.294	10	2.899	18	1.367	26	7.498	34	0.776
3	2.308	11	2.476	19	1.434	27	7.736	35	0.795
4	2.391	12	2.434	20	1.477	28	0.820	36	0.516
5	2.487	13	1.942	21	1.082	29	0.809	37	0.556
6	2.589	14	1.421	22	1.121	30	0.863	38	0.610
7	2.677	15	1.237	23	1.056	31	0.882	39	0.571
8	2.728	16	1.248	24	0.827	32	0.882	40	0.625

Fig. 3.3 shows that the trend of the AIC value decreases gradually although there is a small increasing trend during orders 2 to 10. From orders 10 to 15, there is a distinct decrease from 2.899x10^{-4} to 1.237x10^{-4}, and from 16 to 40, the decrease is not very overt. Considering calculation time cost, 15 was selected as the optimal order for the AR model at this time.

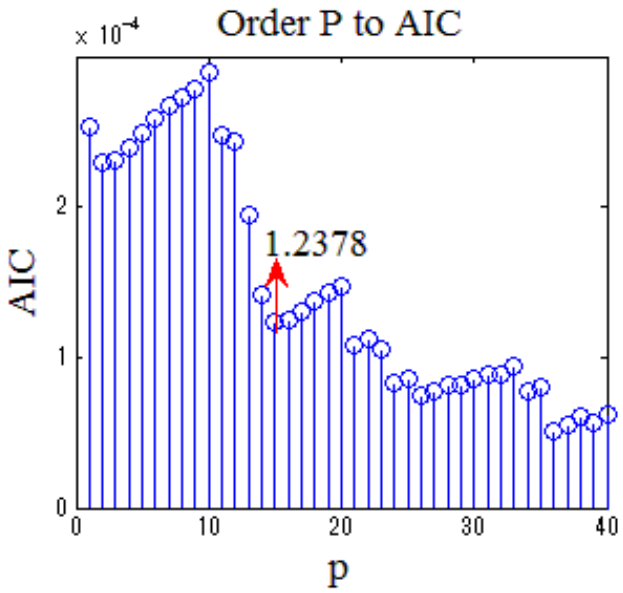

Figure. 3.3: Value of the AIC algorithm to increasing of order *p* [77]

3.2.2 Neural network as classifier

Before starting this section, I have to state that this section is just going to introduce the neural network classifier which I used and the consideration of using thus kind of classifier. There is no new point on the algorithm or network structure, as it is not my research focus to find a more effective and optimal neural network but looking for the relationship between sEMG signals and pattern recognition methods.

The term of 'neural network' is derived from the study of attempting to find mathematical representations of information processing in biological systems, for instance the human brain [66]-[68]. A mathematical function description for the neural network is:

$$y = \sigma(\sum_{j=1}^{M} \omega^{n}{}_{kj} h^{n-1}(\sum_{i_{n-1}=1}^{D_{n-1}} \omega_{ki_{n-1}}{}^{n-1}{}_{ji_{n-1}} h^{n-2}(...h^{1}(\sum_{i_1=1}^{D_1} \omega^{1}{}_{i_2 i_1} x_{i_1})))) \qquad (3\text{-}4)$$

where σ is the output layer activation function and h^{n-i} is the activation function of the hidden layer. The superscript *n-i* denotes the corresponding layer. ω represents the parameters which needs to be adjusted. x_i is the input for the neural network and y is the output. The diagram of such a neural network is plotted in Fig. 3.4.

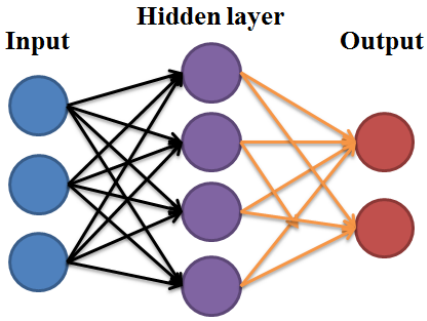

Figure. 3.4: The classic structure of Neural Network

The information flow in such a network structure is forward, from one layer to the next layer, and a network with such kind of structure is called feed-forward networks. The selection of the activation function for each layer is various, such as linear, logistic sigmoid and 'tanh' function. One property of feed-forward networks is that multiple distinct choices for the parameters of ω can lead to the same mapping function from inputs to outputs [69], which is called weight-space symmetries.

In most of cases, the training process is divided into two stages: the first one is to derivate the error function with respect to the parameters or weights; and the second one is to use the derivatives calculated in the first stage to compute the adjustments to be made to the weights. In the first stage, the error backpropagation algorithm is used to obtain a computationally efficient method for evaluating derivatives. And this is the very reason that such kind of network is called backpropagation neural network. And for the second stage, the conjugate gradients are widely adopted.

The steps for error backpropagation are:

(1) Apply an input vector $\boldsymbol{x}$ to the neural network and forward propagate to find the activations of all the hidden and output units of layers.

(2) Evaluate the δ_k for all the output units using equation 3-5:

$$\delta_k = y_k - t_k \tag{3-5}$$

(3) Backpropagate the δ using equation 3-6 to obtain δ_j for each hidden unit.

$$\delta_j = h'(a_j) \sum \omega_{kj} \delta_k \tag{3-6}$$

(4) Use equation 3-7 to evaluate the required derivatives:

$$\frac{\partial E_n}{\partial \omega_{ji}} = \delta_j \frac{\partial a_j}{\partial \omega_{ji}} \tag{3-7}$$

The steps for the scaled conjugate gradient algorithm are [72]:

(1) Choose arbitrary parameters of scalars $\sigma>0$, $\lambda_1>0$ and $\lambda'_1=0$. Set $p_1 = r_1 = -E(\omega 1)$ and a variable flag success = true.

(2) If success = true then used the derivatives calculated in the error backpropagation process:

$$\sigma_k = \frac{\sigma}{|p_k|} \tag{3-8}$$

$$s_k = \frac{E'(\omega_k+\sigma_k p_k)-E'(\omega_k)}{\sigma_k} \tag{3-9}$$

$$\delta_k = p_k^T s_k \tag{3-10}$$

(3) Scale s_k:

$$s_k = s_k + (\lambda_k - \lambda'_k)p_k \tag{3-11}$$

$$\delta_k = \delta_k + (\lambda_k - \lambda'_k)|p_k|^2 \tag{3-12}$$

(4) If $\delta_k \leq 0$ then make the Hessian matrix positive definite:

$$s_k = s_k + (\lambda_k - 2\frac{\delta_k}{|p_k|^2})p_k \tag{3-13}$$

$$\lambda'_k = 2(\lambda_k - \frac{\delta_k}{|p_k|^2}) \tag{3-14}$$

$$\delta_k = -\delta_k + \lambda_k|p_k|^2, \lambda_k = \lambda'_k \tag{3-15}$$

(5) Calculate step size:

$$s_k = s_k + (\lambda_k - \lambda'_k)p_k \tag{3-16}$$

(6) Calculate the comparison parameter:

$$\Delta_k = \frac{2\delta_k(E(\omega_k)-E(\omega_k+\sigma_k p_k))}{\mu_k^2} \tag{3-17}$$

(7) if $\Delta_k \geq 0$ then a successful reduction in error can be made:

$$\omega_{k+1} = \omega_k + \alpha_k p_k \tag{3-18}$$

$$r_{k+1} = -E'(\omega_{k+1}) \tag{3-19}$$

$$\lambda'_k = 0, \text{ success } = \text{ true.} \tag{3-20}$$

(7a) If k mod N = 0 then restart algorithm: $p_{k+1} = r_{k+1}$

else create new conjugate direction:

$$\beta_k = \frac{|r_{k+1}|^2 - r_{k+1} r_k}{\mu_k} \tag{3-21}$$

$$p_{k+1} = r_{k+1} + \beta_k p_k \tag{3-22}$$

(7b) If $\Delta_k \geq 0.75$ then reduce the scale parameter:

$$\lambda_k = 0.5\lambda_k \tag{3-23}$$

Else a reduction in error is not possible:

$$\lambda'_k = \lambda_k, \text{ success } = \text{ false} \tag{3-24}$$

(8) If $\Delta_k < 0.25$ then increase the scale parameter:

$$\lambda_k = 4\lambda_k \tag{3-25}$$

(9) If the steepest descent direction $r_k \neq 0$ then set k = k+1 and go to step 2 else terminate and return ω_{k+1} as the desired minimum.

It should be noticed that the error function used for parameters calibration is not convex over weight space. This property leads to one of the disadvantage that a local minimum may be found by the backpropagate process rather than a global minimum one. And there may be many local minimum points. Finding a proper one strongly depends on the starting point or the initial status of the parameters which in many cases are selected randomly.

In this thesis, a two-layer neural network with one hidden layer and one output layer was adopted to be the classifier. The activation function

for hidden layer and output layer is hyperbolic tangent sigmoid transfer function. The number of neurons in the hidden layer is n+2 where n is the dimension of input vector and in this particular circumstance it equals the number of muscles used for sEMG signals recording. The output are vectors structured by one-of-k coding scheme where k is the number of patterns.

3.3 Experimental results with neural network

3.3.1 Experimental setup

Three healthy volunteers aged from 22–26 years, all male, one left-handed and two right-handed, participated in the experiment. Before placing the electrode, which was aligned parallel to the muscle fibers, over the belly of the muscle, the skin was shaved and cleaned with alcohol in order to reduce skin impedance. The sampling rate was 1000 Hz with differential amplification (gain: 1000) and common mode rejection (104dB). A fourth-order high-pass Butterworth filter with a 10-Hz cut-off frequency was implemented in software to remove the DC offsets in EMG signals before they were rectified. The user interface was programmed using Visual C++ 2010 (Microsoft Co., USA). The analog/digital (A/D) data from the A/D board was collected through the application programming interface and processed with MATLAB (The MathWorks Co., USA). The software was run on a personal computer with a 2.8-GHz quad-core processor (Intel Core i7 860) and 4 GB of RAM. Two MTx sensors (Xsens Technologies B.V., USA) were attached on the subject's forearm and hand to record the elbow joint angle and wrist joint angle,

respectively, for calibration and comparison. Dry rectangle electrodes (Ag/AgCl, size: 26x14 mm), with a skin contact surface of 20 mm^2, and inter-electrode distance of 18 mm, were placed parallel to the muscle fibers, according to SENIAM references [70]. Electrode placements were confirmed by voluntary muscle contraction and followed the recommendation of [71]. The apparatus used in the experimental are shown in Fig. 3.5.

(a)

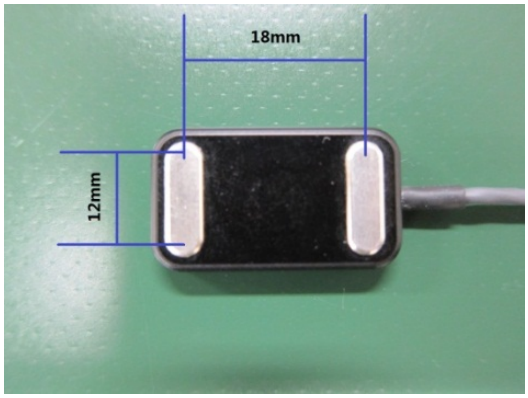

(b)

(c)

(d)

Figure. 3.5: sEMG signal recording system. (a): personal EMG filter box; (b): surface electrodes; (c): Profile of the MTx inertial sensor; (d): AD acquisition USB 4716.

The motions to be recognized are elbow flexion and extension, forearm pronation and supination, wrist flexion and extension, and wrist adduction and abduction. In order to generalization the upper-limb movement of the volunteers, their motions were restricted as requirement directing by a video. In the experiment of upper arm flexion and extension, the volunteer were asked to sit on a chair started with upper limbs relaxed vertically fitting to the vertical pillar of the benchmark apparatus (as shown in Fig. 3.6 a) and then contracted their experimental upper forearm to the horizontal beam (as shown in Fig. 3.6 b). After a short stop keeping the forearm to the horizontal position, the volunteer was asked to extend the forearm to the initial vertical position. In the experiment of forearm pronation and supination, the upper arm kept vertical and volunteer only pronated with his forearm, keeping the upper arm still. There is a cross mark on the ground to be the benchmark for pronation and supination (as shown in Fig. 3.7). In the experiment of palmar flexion and dorsiflexion, volunteer kept his forearm horizontal and flexed or dorsiflexed to the contracted bounds (as shown in Fig. 3.8). The movements are divided into two groups. In the first group, only elbow flexion and extension is focused. Motion patterns are elbow flexion, elbow holding, elbow extension and relaxing, i.e. there are four motions in the first group. In the second group, motion patterns are corresponded to the five main motions: elbow flexion and extension, forearm pronation and supination, wrist flexion and extension, and wrist adduction and abduction.

Each volunteer repeated these three experiments fifteen times with a

relaxation of one minute in every five tests. The raw sEMG signals were recorded separately from the three experiments and a special BP neural network coordinate to one experimenter would be trained using the collected data from the ten times repeated tests. After all the three volunteers finished their experiments, there were three independent neural networks belong to the different experimenters. The movement of each volunteer had been recognized with their own neural networks and the results were applied to the multi-motion recognition.

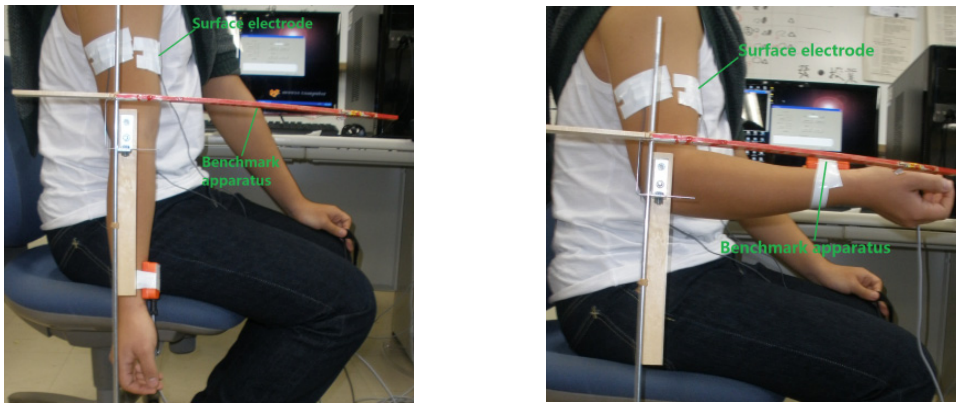

(a) (b)

Figure. 3.6: Experimental procedure A. (a): The start position of the experiment; (b): the vertical position when subject tries to hold his forearm

(a) (b)

Figure. 3.7: Experimental procedure B. (a): The forearm pronation; (b) the forearm supination.

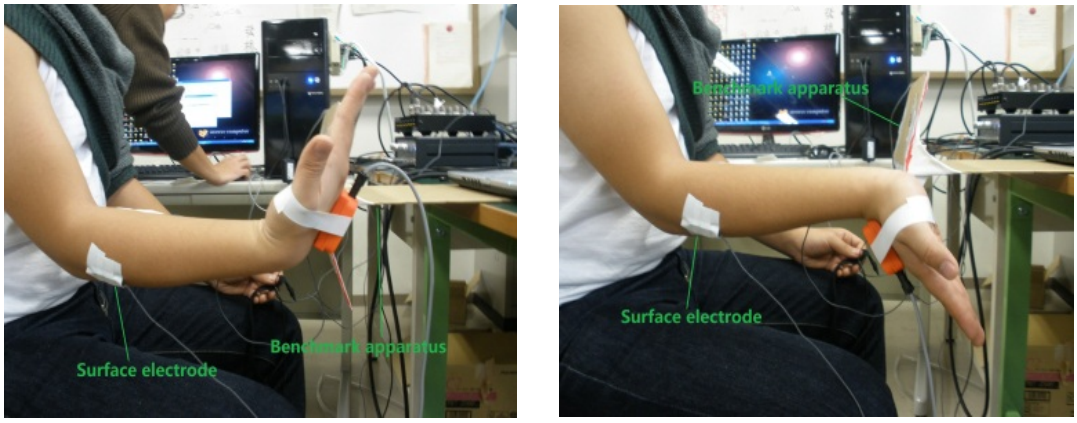

(a) (b)

Figure. 3.8: Experimental procedure C. (a) The palmar flexion; (b) the palmar dorsiflexion or extension

3.3.1 Experimental results

The experimental results for the first group are listed in Table 3.2. The confusion plots for the three subjects are shown in Fig. 3.9, respectively.

Table 3.2 Accuracy of artifical neural network

Subject	A	B	C
Recognition rate	81.5	82.1	94.6

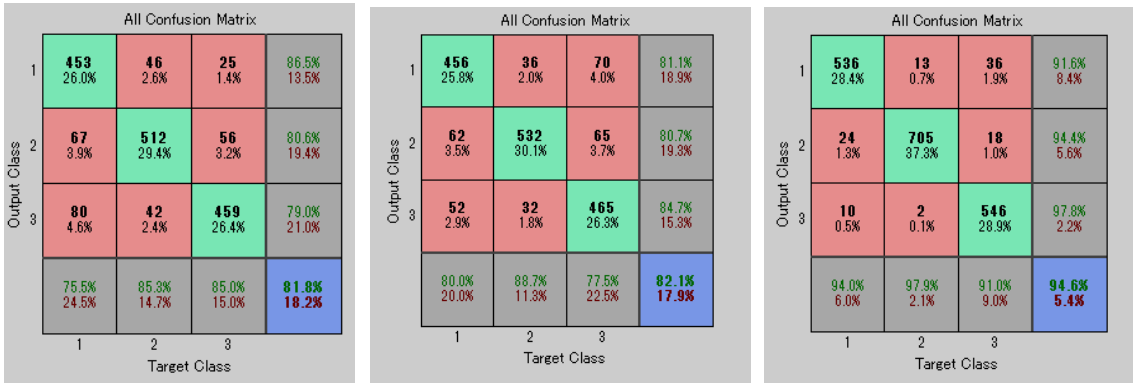

(a) Volunteer A (b) Volunteer B (c) Volunteer C

Figure. 3.9: The confusion matrix of the performance

Recognition results for each volunteer with his own neural network and with the others are presented in from Fig. 3.10 a to c, where three different colors of dots stand for the three parameters in the result vector and the horizontal lines of dashes are critical dividing lines by which all of the data is separated into ones and zeros. The result vector is described as follows, where the standard result for up, holding, down and relaxing movement is (1, 0, 0, 0), (0, 1, 0, 0), (0, 0, 1, 0), and (0, 0, 1, 1) respectively.

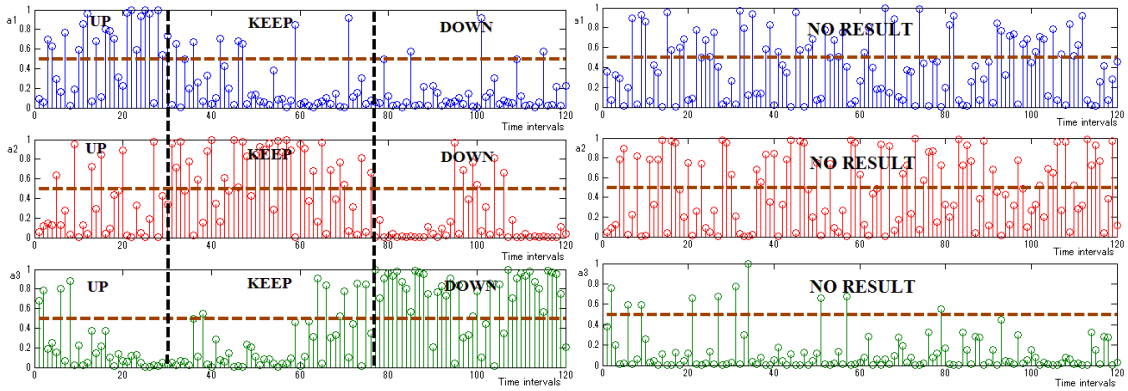

(a). Recognition rate of volunteer A with his own ANN (the left) and with volunteer B's ANN (the right)

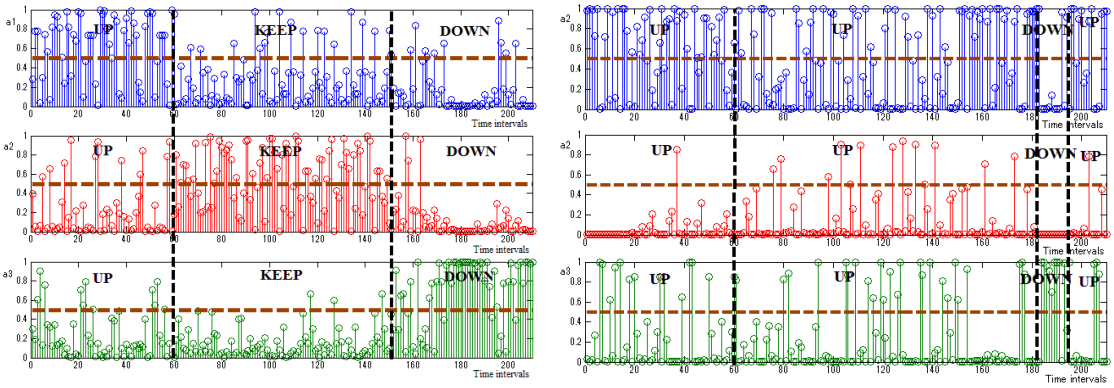

(b). Recognition rate of volunteer B with his own ANN (the left) and with volunteer C's ANN (the right)

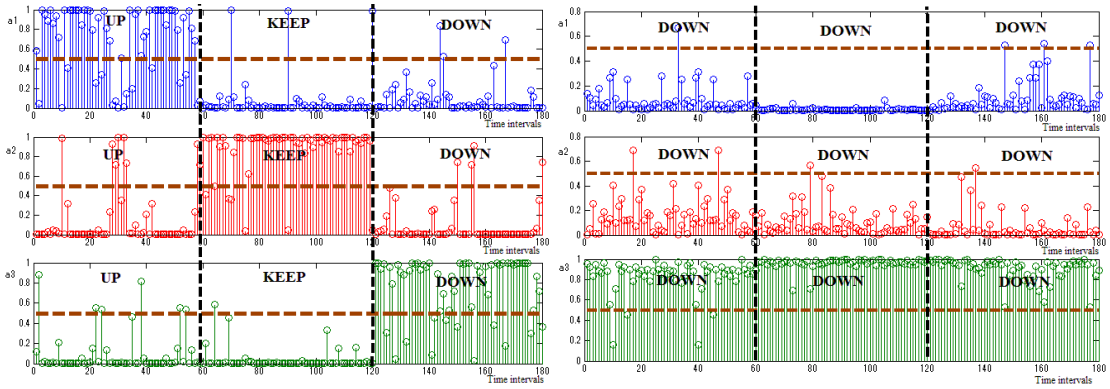

(c). Recognition rate of volunteer C with his own ANN (the left) and with volunteer A's ANN (the right)

Figure. 3.10: BP ANN recognition results for volunteers with their own ANN and the other's ANN [65]

As shown at left in Fig. 3.10, results were calculated on line, and were used as reference input for motor control of the ULERD. As shown in Fig. 3.10 (c), from time intervals 1 to 60, almost all of the dots in group a_1, which represents a_1 in equation (10), are positioned above the horizontal line. After normalization using a piecewise function defined in (11), these parts of data equaled 1. In contrast, dots in group a_2 and the dots in group a_1, are positioned below the horizontal line, equaled 0., These parts of recognition results consequently represented the vector of (1, 0, 0), which means the motion of the upper limb up.

The experimental results for the second group are listed in Table 3.3. The confusion plots for the three subjects are shown in Fig. 3.11, respectively.

Table 3.3 Accuracy of artifical neural network

Subject	A	B	C
Recognition rate	86.7	85.9	85.4

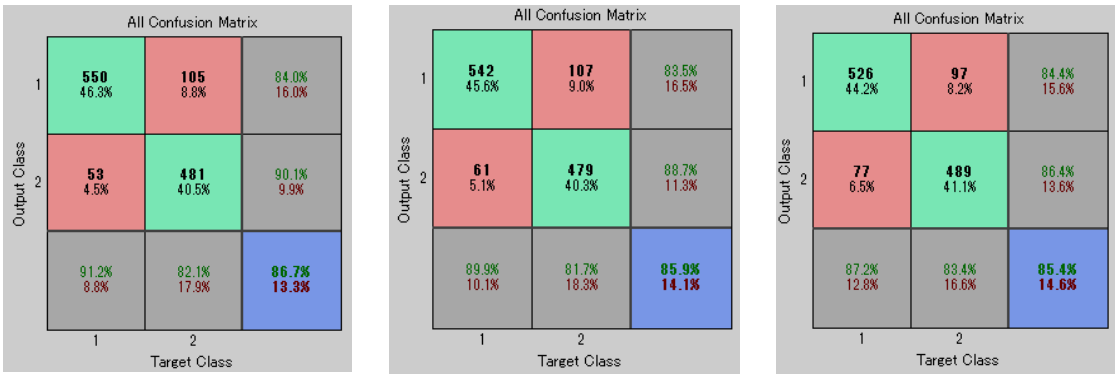

(a) Volunteer A (b) Volunteer B (c) Volunteer C

Figure. 3.11: The confusion matrix of the performance.

For the first group experiment, Biceps Brachii (BB) and Triceps Brachii (TB) muscles were chosen to record sEMG signals. As this pair of agonist and antagonist muscles take the main charge with the function of elbow flexion and extension, it is reasonable to choose this pair of muscles to study the movement of the elbow joint. Because the motion was performed in sagittal plane, TB was seldom activated. Furthermore, the involved movement includes concentric contraction motion (elbow flexion), isometric contraction motion (elbow holding) and active shortening motion (elbow extension). The muscle status is different among these motions. The behavior of EMG signals is different according to the different status of muscle. From this aspect point of view, the AR model used here is to extract features which represent the status of muscles as well. One set of the experimental results for AR model feature extraction is depicted in Fig. 3.12. The coefficients were calculated by Burg algorithm.

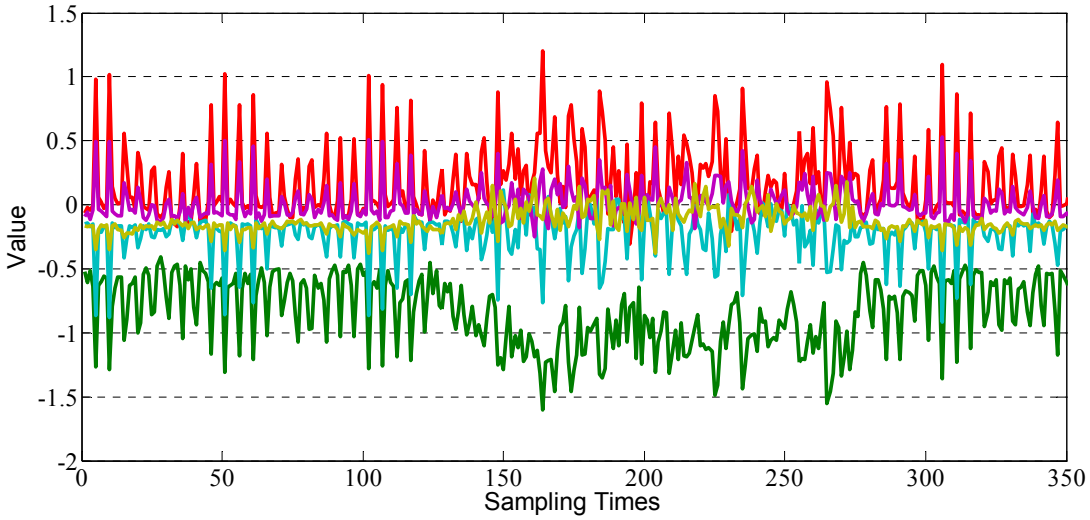

Figure. 3.12: Experimental results of features extracted by AR model

As there are 15 features in AR model, only five of these parameters are plotted in the above figure. It can be indicated, although not very distinctly, that the changes of features are correspond with the changes of elbow motion. However, this kind of change decreases with the increasing of order.

3.4 Improved recognition method

The Neural Network is not an ultra remedy for all the issue of classification, much less that the Neural Network itself has many trouble issues. On the other hand, any of the existing classifiers will lose their function if the features themselves are not separable. It can be indicated from the experimental results in 3.3.1 that the feathers extracted by AR model are not stable or distinct. Another problem is with the Neural Network that it needs many times to train in order to get a proper classification performance. As it is also mentioned that to improve the feature extraction method and classifier algorithm is the key factor for

motion recognition.

3.4.1 Support vector machine

SVM is proposed as a classification technique based on maximizing the margin between a data set and use optimal hyper plane to separate different data sets [72]. Compared with Neural Network, the advantage of SVM is that the target parameters depend on finding the optimal solution for a convex optimization problem, which is described as:

$$\varphi(\omega,\xi) = 0.5\left\|\omega^2\right\| + c\sum_{i=1}^{l}\xi_i \tag{3-26}$$

subject to

$$y_i[(x_i \cdot \omega) + b] \geq 1 - \xi_i, i = 1, 2, ..., l \tag{3-27}$$

where x is an n-dimensional vector and b is a scalar. c is the independent variable. l is the number of data points. y is the model to be learned. (3-26) and (3-27) can be rewritten in the dual Lagrangian form:

$$\tilde{L}(\boldsymbol{a}) = \sum_{n=1}^{l} a_n - 0.5\sum_{n=1}^{l}\sum_{m=1}^{l} a_n a_m t_n t_m k(x_n, x_m) \tag{3-28}$$

where $k(x_n,x_m)$ denotes the kernel function which plays the soul role in SVM. To classify new data using the trained model, (3-29) is used based on the conception of kernel function:

$$\mathrm{y}(\boldsymbol{x}) = \sum_{n=1}^{N} a_n t_n k(x, x_n) + b \tag{3-29}$$

where N denotes the number of support vectors.

One of the challenging issues in SVM is that the solution to a

quadratic programming problem in M variables in general has computational complexity that is $O(M^3)$. Considering that if there are 10,000 samples, which are just the number of variables in a quadratic programming problem, and each sample takes a 4-byte float type memory, a total 3725 GB memories are needed for computation. Fortunately, there is a popular approach to training SVM, which is called sequential minimal optimization (SMO) [73]. It is not until the discovery of the effective training algorithm that SVM has acquired a wide attention.

3.4.2 Improved feature extraction methods

It is intuitive to extract the trend of the EMG signal or finding some corresponded curve with low changing frequency to represent the changing for feature extraction.

A Weight Peaks algorithm was designed based on the above concept. The purpose of WP method is to try to catch the trend of original sEMG signals [74]. The reconstructed sEMG signals processed by WPT have the different frequency in different nodes. Therefore, the amount of peaks obtained in different nodes is different. Zero crossing which is defined as following is used to find where the peak exists.

$$ZC = \sum_{n=1}^{N-1} (\text{sgn}(s_n \times s_{n+1}) \cap |s_n - s_{n+1}| \geq threshold) \tag{3-30}$$

All the reconstructed sEMG signals of zero crossing are saved to obtain peaks and valleys among them.

The procedure of the WP method is described as following:

If max(sZC(i): sZC(i+1)) + min(sZC(i): sZC(i+1)) ≥ 0

$$P(i) = \max(sZC(i): sZC(i+1))$$

Else if $\max(sZC(i): sZC(i+1)) + \min(sZC(i): sZC(i+1)) < 0$

$$P(i) = (-1) \times \min(sZC(i): sZC(i+1))$$

where sZC(i) is the reconstructed sEMG signal of zero crossing. P(i) is the peak or valley between the data of zero crossing and valley is transformed into positive number.

During experiments, we found that the higher peaks reflect the trend of motion more than the lower peaks. Therefore the next step of weighted peaks is to increase the component of higher peak and decrease the component of lower peak to obtain the feature near to the trend of subject's motion. The algorithm is defined in (3-31), where parameter n is defined experientially.

$$P(i+1) = \frac{1-n}{n} P(i) + \frac{1}{n} P(i+1) \tag{3-31}$$

Actually, it is reasonable to extract the trend from the EMG signal to represent the feature. The actuator for human motion is the muscle-skeleton structure and the power is supplied by musculotendon force. Although EMG signals represents the activation propagation along muscle belly, the changing frequency of musculotendon force is much lower than that of EMG signals because of the low-pass-like filter property of the muscle [30].

Given this consideration, the Hill-type based muscular model was also applied to extract the feature from the EMG signal. For simplicity, the Hill-type model can be represented as a linear function of muscle activation

level, as to be discussed in the next chapter. Before processing raw EMG signals to muscle activation levels, they usually should be filtered by a high-pass filter to remove any DC offsets or low-frequency noise and then rectified. Sometimes, these rectified signals are directly transformed into muscle activation levels by dividing them by the peak rectified EMG value obtained during the MVC test. Some researchers [30] suggest that a more detailed model of muscle activation dynamics is warranted in order to characterize the time-varying features of the EMG signal. In this paper, a discretized recursive filter is used.

A discretized recursive filter with a continuous form of a second-order differential equation was implemented:

$$u(t) = Md^2e(t)/d^2t + Bde(t)/dt + Ke(t) \tag{3-32}$$

where M, B, and K are the constants that define the dynamics of muscle activation level and $e(t)$ is the processed EMG signal. This equation can be expressed in discrete form using backward differences:

$$u(t) = \alpha e(t-d) - \beta_1 u(t-1) - \beta_2 u(t-2) \tag{3-33}$$

where d is the electromechanical delay and α, β_1, and β_2 are the coefficients that define the second-order dynamics. Selection of the values for α, β_1, and β_2 should follow the following restrictions:

$$\beta_1 = \gamma_1 + \gamma_2 \tag{3-34}$$

$$\beta_2 = \gamma_1 \times \gamma_2 \tag{3-35}$$

$$|\gamma_1| < 1 \tag{3-36}$$

$$|\gamma_2| < 1 \tag{3-37}$$

$$\alpha - \beta_1 - \beta_2 = 1 \tag{3-38}$$

in order to guarantee the stability of the equation and that neural activation does not exceed 1. The calculation results should be filtered by a low-pass filter (with a cut-off frequency of 3-10 Hz) because the muscle naturally acts as a filter, resulting in that force changing frequency is much lower than amplitude changing frequency of EMG signals, which has been mentioned previously.

3.5 Experimental results

3.5.1 Experimental setup

Seven healthy volunteers (age from 22-28, all male, two left handed and five right handed) participated in the experiment. The elbow flexion and extension, forearm pronation and supination and wrist flexion and extension were the same with experiments in 3.3.1. In the experiment of wrist adduction and abduction, subjects again relax their upper limbs vertically as they did in the previous two experiments, and then performed the adduction and abduction movement (as shown in Fig. 3.13).

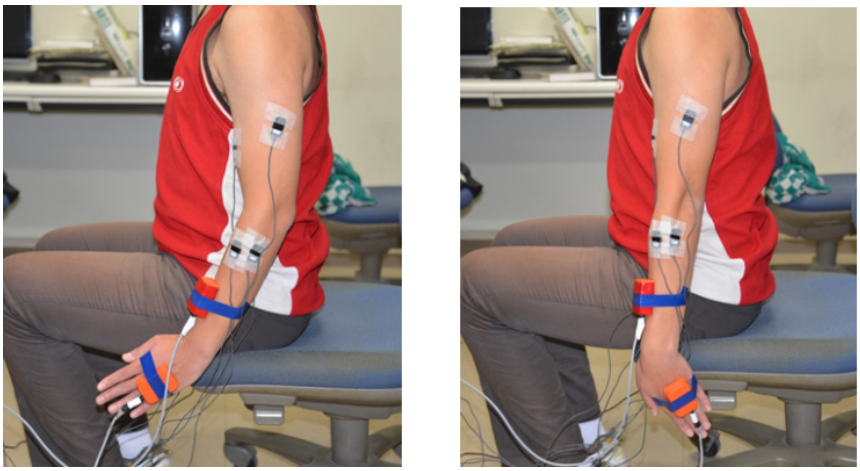

Figure. 3.13: Experiment of wrist adduction and abduction

Each subject repeated the four experiments five times firstly to acquire data to train classifiers. After classifiers training well, another five trials were conducted for each of the four experiments to test the on-line performance of the recognition methods. All the subjects practiced several times following a standard video before experiments. Flexor carpi radialis, flexor carpi ulnaris, extensor carpi radialis, extensor carpi ulnaris, biceps brachii and triceps brachii were selected to record sEMG signals. Apparatus used in the experiment were the same with the ones in section 3.3.1.

3.5.2 Experimental results

Experimental results of the performance of different combination with the four feature extraction methods and two classifiers during training process are listed in Table 3.4. Experimental results shows that WP with NN obtains the highest recognition accuracy rate (with average of 97.6%) and RMS with SVM obtains the lowest recognition accuracy rate (with average of 73.1%). For the feature extraction methods, the performance of WP and MM is better than that of RMS and DFA while WP is a little better

than MM (97.6% to 95.1%). For classifiers, NN performs better than SVM during training process for all the four kinds of features.

Table 3.4. Performance of off-line training.

Features	Subject (NN/SVM)						
	A	B	C	D	E	F	G
AR	75.2/74.2	70.7/66.8	82.2/80.5	81.2/78.9	76.1/71.5	70.1/69.7	73.3/70.1
fAR	87.0/82.0	84.1/83.5	90.6/89.5	89.6/86.8	86.5/85.4	82.1/80.2	85.1/81.2
WP	98.4/97.6	97.2/94.1	97.7/94.5	98.9/96.8	97.5/95.2	97.5/94.5	96.5/92.5
MM	98.8/98.0	95.7/90.9	94.1/91.8	91.4/88.3	93.1/90.1	95.3/93.4	97.3/95.4

Experimental results of on-line performance are listed in Table 3.5. It can still be observed that WP and MM obtain higher recognition accuracy rate than RMS and DFA while MM is a little higher than WP (94.3% to 92.0%). However, the performance of NN is worse than that of SVM during on-line testing experiments (except subject D). The recognition accuracy rates of both of the two classifiers decrease compared with the performance during training period. The amplitude of decreasing for NN is larger than that of SVM.

Table 3.5. Performance of on-line testing.

Features	Subject (NN/SVM)						
	A	B	C	D	E	F	G
AR	70.2/74.1	68.7/68.8	80.1/81.5	77.1/78.0	72.1/73.5	70.0/71.1	69.1/71.2
fAR	79.3/83.0	80.1/84.3	82.3/87.1	81.1/85.3	79.1/81.3	75.1/81.1	77.7/80.2
WP	93.4/95.6	89.8/91.1	90.1/91.8	87.1/90.2	90.3/91.0	89.5/91.7	90.5/93.1
MM	94.8/97.0	91.1/93.0	92.1/95.8	93.3/91.3	92.1/93.1	89.3/93.4	92.3/96.4

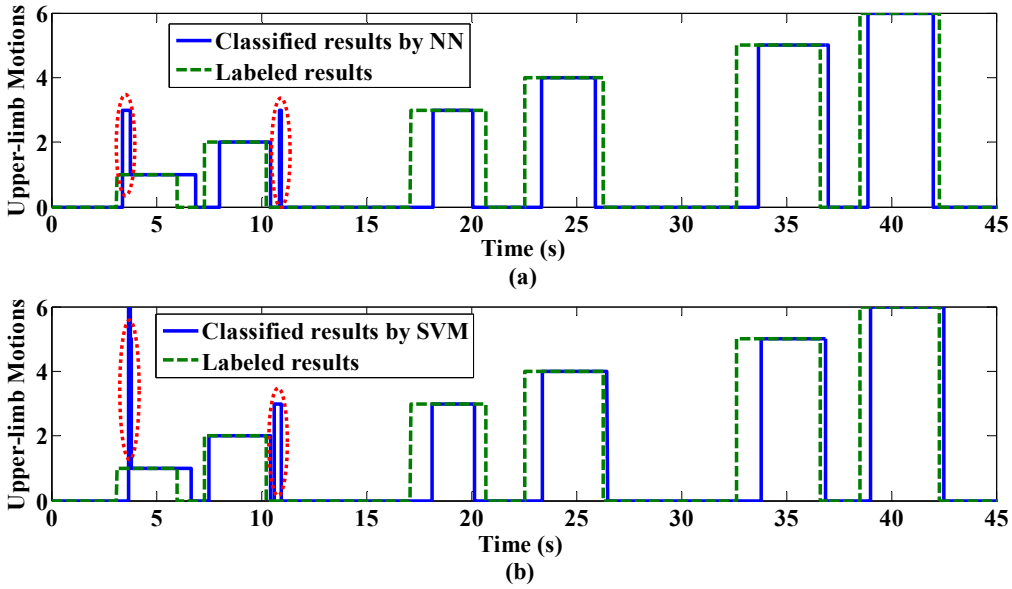

Figure. 3.14: On-line testing performance with MM feature extraction method. (a) shows the classification results by NN. (b) shows the classification results by SVM.

One set of the on-line testing performance is depicted in Fig. 3.14, where the blue lines show the classification results and dashed green lines show the labeled results. The dotted red lines mark the misclassification results. It can be indicated that the misclassification places are similar between NN and SVM.

Another important issue for motion recognition is the time consumption for training and on-line computation, while the latter is more important than the former in our particular circumstance. Experimental results for off-line training process are depicted in Fig. 3.15. The experimental results are average value of off-line training time of the seven subjects on the same feature extraction method and classifier. The light blue bars denote the average training time of NN while the green bars denote the

ones for SVM. It can be found that NN takes much more time than SVM (469.6s to 73.5s) to obtain a good performance. For NN, MM and WP takes more times than RMS and DFA, while the former pair obtains higher recognition accuracy rate than the latter pair. For SVM, MM and WP takes fewer times than RMS and DFA, while the former pair still obtains higher recognition accuracy rate than the latter pair. Experimental results for on-line calculation are depicted in Fig. 3.16. The blue bars denote the time consumption for one sample with NN using different feature extraction methods. There is almost no difference because the structure of the NN is the same. Compared with NN, it is distinct that it takes much more times for SVM to complete one recognition loop than NN (1.0918 ms to 0.0034 ms). As the sampling frequency is 1000 Hz in our experiment and this frequency is also important for sEMG sampling, time consumption longer than 1 ms will give rise to time delay in real-time experiment. Given this condition, RMS and DFA, with time consumption of 1.7ms and 1.2ms respectively, are not suitable for real-time purpose.

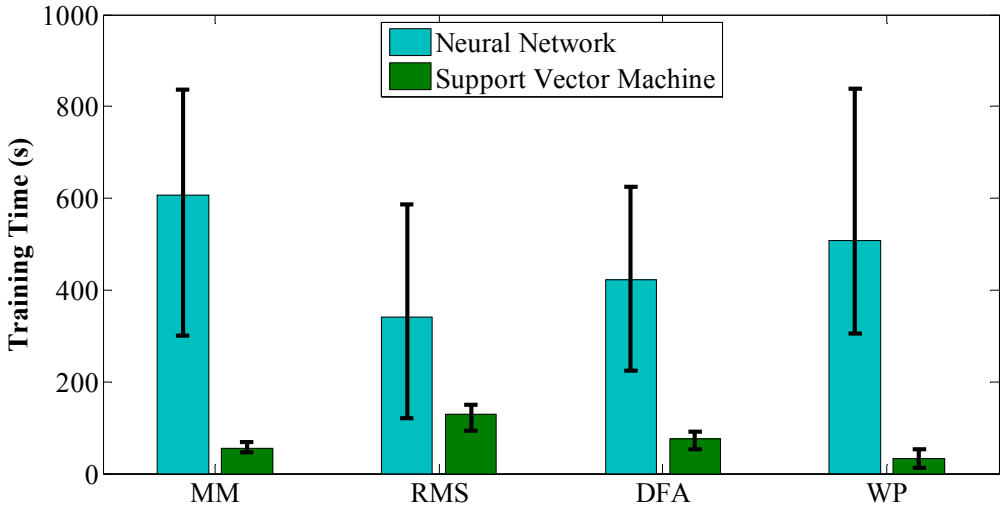

Figure. 3.15: Time consumption on off-line training process

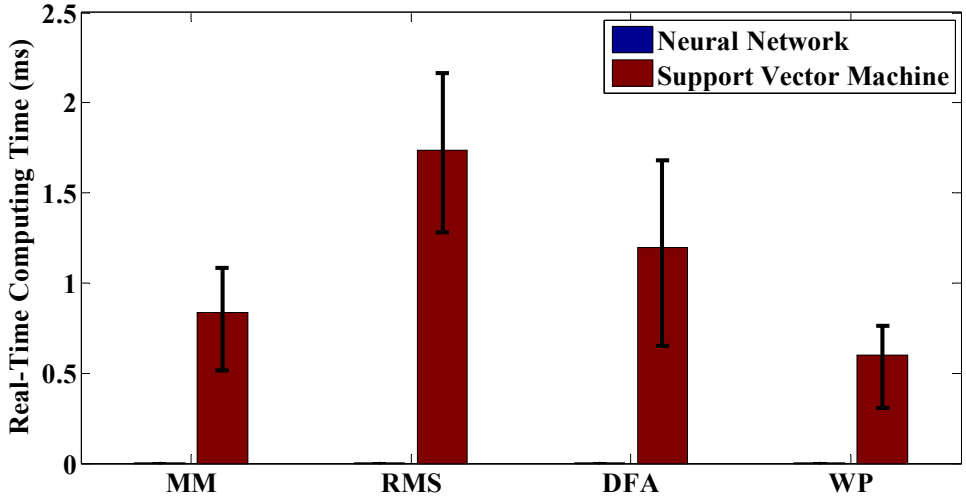

Figure. 3.16: Time consumption for on-line testing process

3.6 Summary

In this chapter, a motion evaluation and recognition with EMG signals were introduced and discussed. A bilateral training function were proposed, in which the patient wears our developed ULERD on his/her impaired arm and performs the upper limb motion bilaterally. The control singles for ULERD are obtained from the EMG signals recorded from the intact arm. In order to map EMG signals to motions, the motion recognition based methods were proposed. Firstly, an AR model based feature extraction combined with NN classifier method were applied. The recognition accuracy rate was around 80%. In order to improve the recognition rate and find the relationship between different feature extraction methods and classifiers for EMG signals, different combinations of four feature extraction methods and two classifiers were tested. The proposed muscular model based method with SVM can acquire a recognition accuracy rate of above 90% with more motions and fewer training time consumption. The

advantage of the proposed bilateral self-training function is that patients can perform the training by themselves with the guiding of their intact arm and the control signals are obtained from EMG signals which are forward to motions and represent the intention of patients. From the neurorehabilitation point of view, patients self-inspired motion can bring more benefit to rehabilitation training than just simple motion following.

Chapter 4 Continuous Motion Prediction using sEMG

4.1 Introduction

Although accuracy rate for motion recognition method can achieve above 90%, this kind of method can only provide binary-like control reference, i.e., it cannot provide exact kinematic value, such as joint angle of human upper limb, to the controller. In many cases, or maybe most of the cases, continuous prediction results are more appreciated than binary-like ones. However, it is a challenging work for all the researchers to find analytical and quantitative relationship between measured sEMG signals and desired kinematic variables. The first problem is the redundancy of human musculoskeletal structure. For a robotic system, engineering can provide one motor for one degree of freedom, however, in human body, every degree of freedom, which in many cases is also complex, is controlled by multiple muscle-tendon pairs. The second problem is the relationship between sEMG signals and musculotendon force. The conclusion is still under discussion although some relations have been studied for particular muscles with different results among researchers. The third problem is that we cannot detect every concerned muscle with surface electrode because some muscles are in the deep layer. It seems like our neural system learned an extremely complex rule to control the redundant musculoskeletal system.

In this chapter, a continuous prediction method for elbow joint angle will be proposed based on the quantitative analysis using Hill-type muscular model and simplified musculoskeletal model. A state switching algorithm will also be proposed to conquer the problem of time-variable property of EMG signals caused by the different contract style of muscle.

4.2 Hill-type based muscular model

The Hill model described the mechanisms of muscular force generation from the mechanical point of view. The famous state equation described the Hill model is shown as:

$$(v+b)(F+a)=b(F_0+a) \tag{4-1}$$

where F is the load in the muscle; v is the velocity of contraction; F_0 is the maximum isometric tension generated in the muscle; a denotes the coefficient of shortening heat and v_0 is the maximum velocity when F equals 0.

There is another kind of description for Hill-type muscular model, named three-element model which is shown in Fig. 4.1.

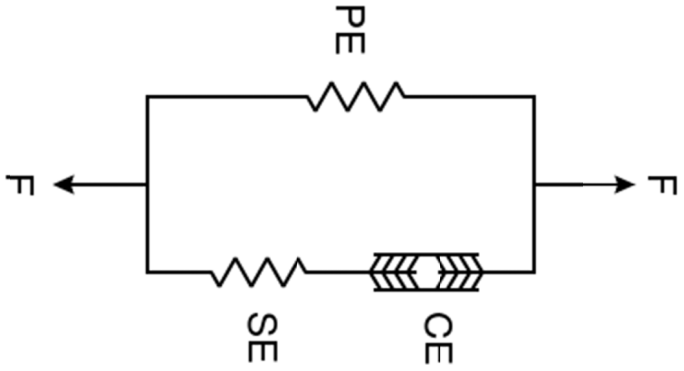

Figure. 4.1: Three-element Hill-type muscular model [75].

Contractile element (CE) represents the active force generation of muscle. This element is capable of shorting when activated. Series element (SE) represents the tendon and the intrinsic elasticity of the myofilaments. It has a soft tissue response and provides energy storing mechanism. Parallel element represents the passive force of the connective tissues and also has a soft tissue mechanical behavior. When muscle is at different status, e.g., different contraction velocity and length, different element responds differently. The equation described these different elements are shown following:

$$F_{PE,SE} = F_{\max}(\exp(S\Delta L / \Delta L_{\max}) - 1) / (\exp(S) - 1) \tag{4-2}$$

$$F_{CE} = F_{\max} u \cdot f_l \cdot f \tag{4-3}$$

$$f_l = \exp\left(-0.5\left(\left(\Delta L_{CE} / L_{CE_0} - 0.05\right) / 0.19\right)\right) \tag{4-4}$$

$$f_v = 0.1433\left(0.1074 + \exp\left(-1.3\sinh\left(2.8V_{CE} / V_{CE_0} + 1.64\right)\right)\right)^{-1} \tag{4-5}$$

$$V_{CE_0} = 0.5(u+1)V_{CE_{\max}} \tag{4-6}$$

$$F_T = F_{CE} + F_{PE,SE} \tag{4-7}$$

where *SE* denotes the passive serial element, *CE* denotes the active contractile element and *PE* denotes the passive element arranged in parallel to the previous two. ΔL is the change in length of the element with respect to the slack length, f_l is the factor of force introduced by the changes of

muscle length and f_v is another factor of force introduced by changes of muscle change velocity. S is a shape parameter, $F_{\max}$ is the maximum force exerted by the element for the maximum change in length $\Delta L_{\max}$, and $F_{PE,SE}$ is the passive force generated by the PE or SE depending on the set of parameters used. F_T is the total force exerted by the muscle. u is the activation level of a muscle.

One of the problems, as can be easily indicated, is that most of the parameters involved in the model are hard to measure. In order to apply the Hill-type model, it is necessary to calibrate these parameters directly or indirectly.

4.3 Upper-limb musculoskeletal model

From simplification consideration, upper-limb elbow flexion and extension motion in sagittal plane was studied in this part. The musculoskeletal model of elbow joint we proposed is depicted in Fig. 4.2.

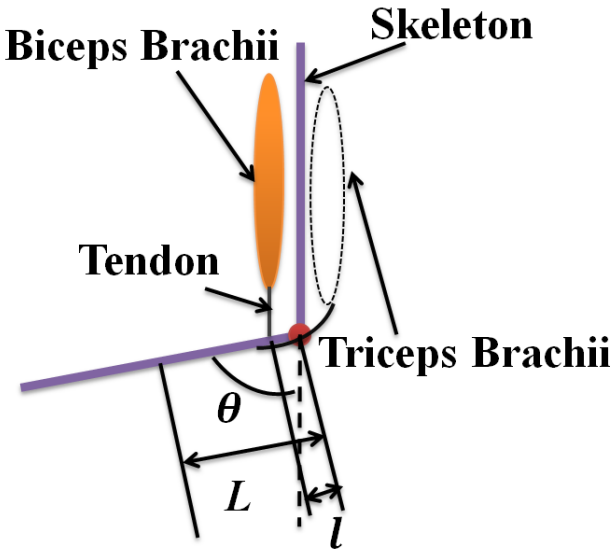

Figure. 4.2: Musculoskeletal model of elbow joint [76]

The distance between the attachment point of the tendon to the skeleton and elbow joint is l. According to a previous study [24], the tendon in the upper arm can be regarded as having high stiffness and thus the tendon deformation is zero. The deformation of the muscle-tendon that results in elbow rotation can thus be regarded as resulting only from muscle contraction. The elbow angle θ is the one to be predicted. L is the distance between the forearm centroid and the elbow joint. In the sagittal plane, it can be considered that the biceps muscle contracts to pull the forearm against the force of gravity during the motion of elbow flexion and extension and that the triceps muscle remains almost unactivated. No obvious EMG signal changes from the triceps muscle can be observed during elbow flexion and extension in the sagittal plane. In the transverse plane, the triceps has to pull the forearm to extend the elbow. As only voluntary motion in the sagittal plane is discussed, the effect from triceps brachii is ignored in this paper.

The following equation describes the motion of elbow flexion and extension in the sagittal plane:

$$F_B l \sin\theta - mgL \sin\theta - \tau_f = I\ddot{\theta} + \tau_e \tag{4-8}$$

where F_B is the musclotendon force exerted by the biceps and τ_f represents the torque from frictional effects, which is assumed to be zero in this paper. τ_e represents the effects of the environmental interaction, which is also assumed to be zero because the subjects held nothing in their hands when they performed the experiments. The mass and inertia of the forearm are *m*

and I, respectively. Dividing (4-8) by $l\sin\theta$ on both sides yields:

$$F_B = mgLl^{-1} + Il^{-1}\ddot{\theta}\sin\theta \tag{4-9}$$

For (4-9), it is difficult to accurately estimate m and I. However, these two parameters can be assumed to be constant during a certain period of time. Using a Hill-type muscular model, the term F_B can be represented as a function of muscular activation level (a), muscle contraction length (L_m), and muscle contraction velocity (dL_m). Equation (4-9) can thus be rewritten as:

$$f(a, L_m, dL_m) = c_1 + A_1\ddot{\theta}\sin\theta \tag{4-10}$$

where c_1 equals mgL_1^{-1} and A_1 equals I_1^{-1}.

An actual musculoskeletal model of human upper limb is more complex than the proposed one, for example not only biceps brachii is involved in the elbow flexion but also brachialis muscle. The brachialis is the deep muscle in the upper arm. It is not easy to record EMG signals from the brachialis using non-invasive surface electrodes. It is assumed that the muscle synergies involved in a certain motion is invariant under the same circumstance (such as the same muscle stiffness, motion speed, and external friction) because the control of the central nervous system keeps the same. Thus the activation level of biceps brachii can be used to predict the angle of elbow joint flexion and extension without considering all involved muscles.

4.4 Equation approximation

Because it is quite difficult or impossible, except by extreme approach, to measure some parameters involved in the dynamic equation, to approximate these parameters becomes one alternative way. During the motion of elbow flexion and extension in sagittal plane, tendon can be regarded as stiff. Given this assumption, ΔL_{CE} in (4-4) can be defined as:

$$\Delta L_{CE} = l\cos\theta = \alpha L\cos\theta = \alpha L_{CE_0}\cos\theta \tag{4-11}$$

where α is the ratio of l to L.

V_{CE} can be defined as:

$$V_{CE} = dl\cos\theta / dt = -\dot{\theta} l\sin\theta \tag{4-12}$$

According to a previous study [27], V_{CE0} can be regarded as $10L_{CE0}$/s for the upper limb muscles in most of cases. Given this condition, the following equation is obtained:

$$\frac{V_{CE}}{V_{CE_0}} = -\frac{\dot{\theta}\alpha L_{CE_0}\sin\theta}{10L_{CE_0}} = -0.1\alpha\dot{\theta}\sin\theta \tag{4-13}$$

Substituting (4-12) and (4-13) back into the Hill-type model and rewriting the term F_B with the detailed equations yields:

$$F_{\max} a\cdot f_l(\cos\theta)\cdot f_v(\dot{\theta},\sin\theta) = C_1 + A_1\ddot{\theta}\sin\theta \tag{4-14}$$

Taking the natural logarithm of both sides yields:

$$C_2 + \ln(\exp(uR^{-1})-1) + \ln(f_v(\dot{\theta},\sin\theta)) = \ln(A_1\ddot{\theta}\sin\theta + c_1) + C_3(\alpha\cos\theta - 0.05)^2 \tag{4-15}$$

where C_2 and C_3 equal $\ln(F_{max}(\exp(A)\text{-}1)^{-1})$ and 0.5×0.19^{-2}, respectively. The value of term $\ln f_v(d\theta,\sin\theta)$ is around zero in this circumstance, and thus ignored. Since the value of c_1 is much larger than that of $A_1 d^2\theta\sin\theta$, the term $\ln(A_1 d^2\theta\sin\theta+c_1)$ can be simplified as $\ln c_1$ and we use C_1 to instead for the purpose of keeping mathematic unification. Equation (4-15) can thus be further simplified as:

$$C_2 + \ln(\exp(uR^{-1}) - 1) = C_1 + C_3(\alpha\cos\theta - 0.05)^2 \qquad (4\text{-}16)$$

where u represents the muscle activation level, which can be calculated from EMG signals, and θ is the upper limb elbow joint angle.

In (4-16), the term $\ln(\exp(uR^{-1})\text{-}1)$ can be represented as a quadratic polynomial with variable uR^{-1}. Then, (4-16) can be transformed into Eq. (4-17), which has a quadratic-like relationship between $\cos^2\theta$ and uR^{-1}. According to the experimental results (discussed in the next section), this quadratic-like relationship is extremely strong during the upper limb elbow flexion period.

$$C_2 + \sum_{i=0}^{2} a_i (uR^{-1})^i = C_1 + C_3(\alpha\cos\theta - 0.05)^2 \qquad (4\text{-}17)$$

4.5 State switch algorithm

Although the relationship between EMG signals (muscle activation level) and elbow joint angle seems simple from (4-17), the actual relation is more complicated. Figure 4.3 shows one set of experimental results of normalized muscle activation level during the motion of elbow flexion and extension. There are four periods: relaxation period, elbow flexion period

(part A in Fig. 4.3), holding period (part B in Fig. 4.3), and elbow extension period (part C in Fig. 4.3). In the flexion period, the activation level has a quadratic-like relation with the elbow joint angle, which corresponds to (4-17). In this period, the type of muscle contraction is concentric contraction. The interesting part is the connection portion between the flexion period and the holding period, where the musclotendon force decreases rapidly and then plateaus, which is similar to overshoot in control theory. This result can be explained by (4-9). During the motion of elbow flexion, the force or torque exerted by the muscle can be represented as:

$$F_B l \sin\theta = mg \sin\theta L + I\ddot{\theta} \tag{4-18}$$

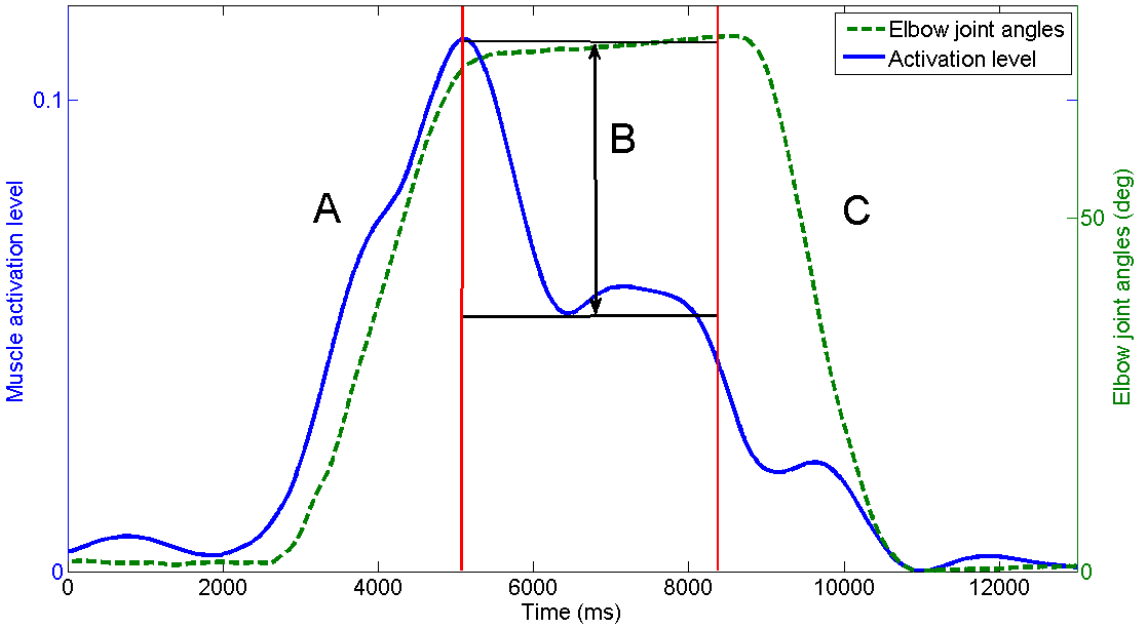

Figure. 4.3: Muscle activation levels compared with elbow joint angles

When the forearm is held at 90° from the upper arm, the desired torque can be represented as:

$$F_B l = mgL, (\theta = 90^\circ) \tag{4-19}$$

Compared with (4-19), there is an extra acceleration term in (4-9), resulting in a higher force level in the elbow flexion period. As the muscle activation level directly reflects the musclotendon force, the activation level is higher in the flexion period than in the holding period. Another reason is the transformation of muscle contraction type from concentric to isometric. However, this issue is beyond the scope of this paper. During the period of elbow extension, the muscle activation level decreases with decreasing elbow joint angle. Furthermore, during the extension period, the muscle contraction type changes to active shortening.

Given this situation, a state switching model (as shown in Fig. 4.4) is developed for elbow joint angle prediction. The input of this switching model is the muscle activation level. There are four states in this state switching model, namely relaxation, flexion, holding and extension states, which correspond to the elbow joint motions with the same names. The relaxation state is the initial state, at which the forearm is 180° from the upper arm in the sagittal plane. When the muscle activation level increases, the state changes to the flexion state. The flexion state changes to the holding state only when the activation level stops increasing and the value exceeds a threshold. When the level decreases, the state changes to the extension state. In the holding state, the state can only change to the extension state when the activation level starts to decrease. The extension state changes to the relaxation state when the value of the activation level

decreases to an inactivation level, and then changes to the flexion state when the force value increases.

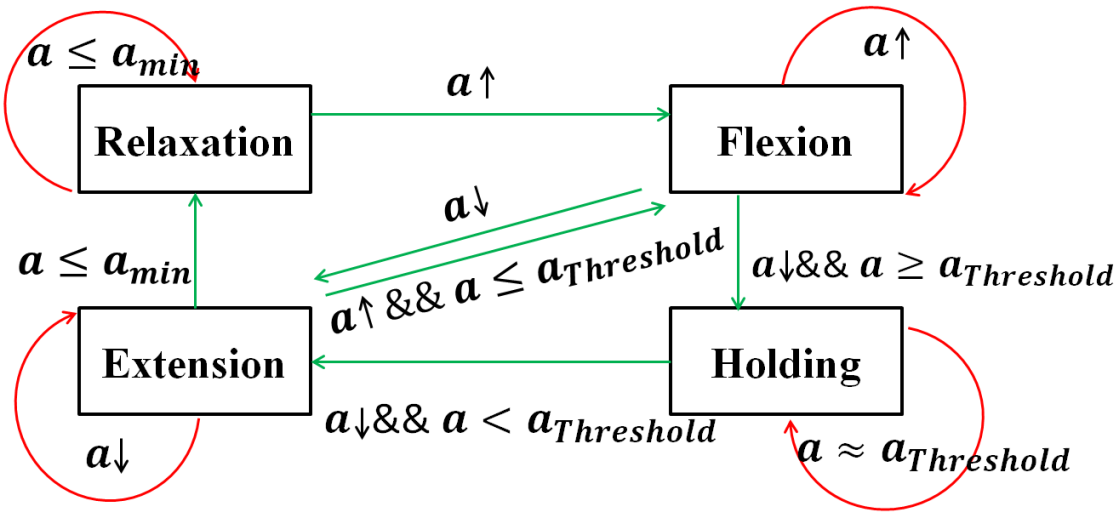

Figure. 4.4: Schematic of state switching method

Although a low-pass filter (with a cut-off frequency of 0.5-1 Hz) was used when transforming EMG signals into muscle activation levels, a further simple value rectification filter with an empirical change range of 1% to 3% was used to stabilize the activation level in the relaxation state.

Another problem in the state switching model is the discontinuity of the representation elbow joint angle value between the flexion state and the extension state, especially when the state changes from the holding state to the extension state. It is assumed that this is caused by the acceleration term in (4-9). The force exerted at the end of the flexion state is higher than that at the beginning of the extension state even though the elbow joint angle is almost the same. Because a continuous quadratic-like function is implemented, the outputs of this function between the two states are discontinuous. In this paper, a simple proportional gain is used to solve this

problem:

$$p = \frac{\theta_{\max}}{\theta`_{\max}} \tag{4-20}$$

where $\theta_{\max}$ is the elbow joint angle at the end of the flexion state and $\theta`_{\max}$ is the elbow joint angle at the beginning of the extension state. According to the definitions of flexion and extension states, the last value at the end of the flexion state is the maximum elbow joint angle at the flexion state and the first value at the beginning of the extension state is the maximum elbow joint angle at the extension state.

In the pre-processing step, raw EMG signals are filtered by a high-pass fourth-order Butterworth filter with a cut-off frequency of 10 Hz and then are processed using (3-33) to get the feature estimation of $u(t)$. After $u(t)$ is filtered with a low-pass second-order Butterworth filter (with 0.5-1 Hz cut-off frequency), the results are divided with the value acquired from MVC test to obtain the muscle activation level (a). Then, the activation level is rectified by 1-3% to reduce the drifting effect caused by the characteristics of EMG signals. The rectified activation level is used as the input to the proposed state switching model to obtain a representation of the elbow joint angle, which is used as the control reference input for the exoskeleton device. The proposed Hill-type-based muscular model is combined in the state switching method.

4.6 Experimental results

4.6.1 Experimental setup

Ten healthy volunteers (age: 24.60±1.67 years, height: 1.70±0.07 m,

weight: 67.66±9.54 kg, two female, eight male, two left-handed, and eight right-handed) participated in the experiments. Process of attaching electrodes is the same with section 3.3.1. The sampling rate was 1000 Hz with differential amplification (gain: 1000) and common mode rejection (104dB). A fourth-order high-pass Butterworth filter with a 10-Hz cut-off frequency was implemented in software to remove the DC offsets in EMG signals before they were rectified. The user interface was programmed using Visual C++ 2010 (Microsoft Co., USA). The analog/digital (A/D) data from the A/D board was collected through the application programming interface and processed with MATLAB (The MathWorks Co., USA). The software was run on a personal computer with a 2.8-GHz quad-core processor (Intel Core i7 860) and 4 GB of RAM. An MTx sensor (Xsens Technologies B.V., USA) was attached on the subject's forearm to record the elbow joint angle for calibration and comparison.

A maximum voluntary contraction (MVC) test at the isometric contraction condition was performed before the experiment. Subjects were asked to hold a dumbbell (from 3 to 18 kg) at an angle of 90° between their upper arms and forearms and the EMG signals from the biceps muscle were recorded. Five trials were performed to determine the MVC EMG value. A sufficient rest time between the five trials was provided to avoid muscle fatigue.

In the experiment of upper limb flexion and extension in the sagittal plane, the subjects were asked to start with both side of their arms relaxed vertically and then flex their forearms to 90°. After having maintained their

forearms in the horizontal position for 3 s, the subjects were asked to extend their forearms to the initial vertical position. Then, a calibration calculation for proposed method was performed offline. After the calibration was finished, the subjects were asked to perform the movement repetitively. A real-time simulation results were conducted on the personal computer by a self-developed software with VS 2010 and OpenGL (as shown in Fig. 4.5).

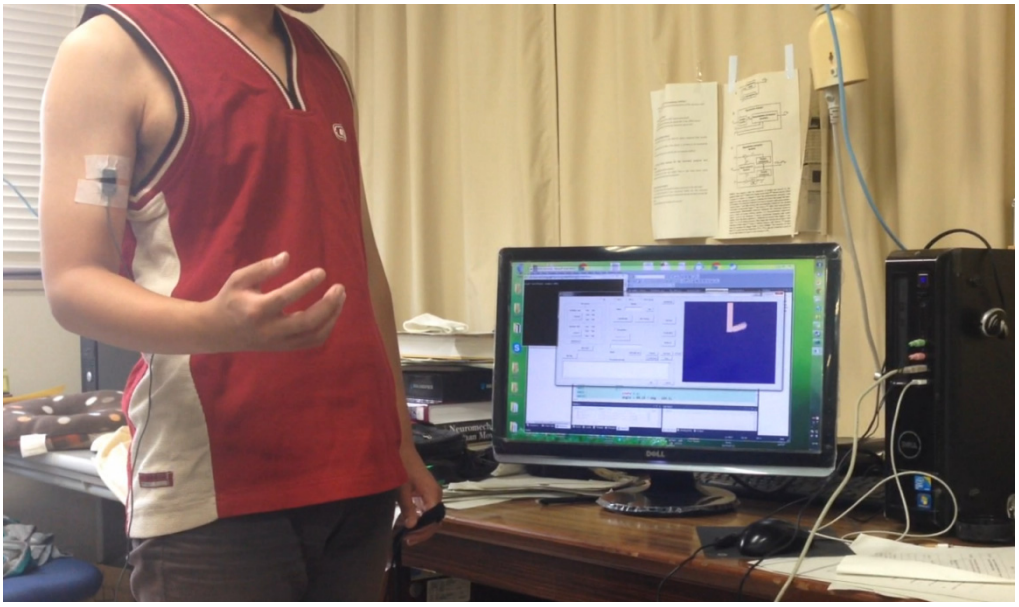

Figure. 4.5: On-line experiment of controlling a virtual arm

Furthermore, a consecutive stepping test was performed by five of the ten subjects. In the consecutive stepping test, the subjects were asked to move their active upper limb to angle of 30°, 20°, and 10°, respectively, and hold for 3 seconds at each step.

A photograph of each subject was taken to record the electrode position on the upper arm. The condition of upper limb movement, such as

forearm rotation speed and upper arm stiffness, should be restricted for the accurate offline calibration. In order to keep the rotation speed and generalize upper limb movement, the subjects were asked to practice the motion by following a prerecorded video. All motions were voluntary without any external force applied on the upper limb. Each subject repeated the three experiments ten times with a relaxation time of 1 min between tests.

4.6.2 Experimental results

To evaluate the proposed musculoskeletal model, all recorded data from the ten subjects during the four days were fitted using the curve fitting tools of MATLAB with quadratic polynomial equations. The inputs were values of the muscle activation level during the flexion motion and the outputs were values of $\cos^2\theta$. Some bad data caused by electrodes sliding on the skin surface were ignored. Figure 4.6 shows one set of model evaluation results from the ten subjects. The dashed lines are the results calculated with data recorded from EMG electrodes (to get the muscle activation level) and from the MTx sensor (to get elbow joint angles). The solid lines are prediction results based on the proposed model. Table 4.1 lists detailed information (mean ± standard deviation). The experimental results show that the average values of the correlation coefficient is above 0.97 for all ten subjects. Although a linear relationship between muscle activation level and $\cos^2\theta$ was found for some subjects (in Fig. 4.6, subjects B and F have correlation coefficients of 0.95 and 0.94, respectively), the quadratic-like relationship has a higher correlation coefficient (with

correlation coefficients of 0.97 and 0.98) than that of the linear one in the same case. In other cases (in Fig. 4.6, subjects I and J), the quadratic-like relationship is more suitable (linear relationship has correlation coefficients of 0.86 and 0.85 and quadratic-like one has 0.97 and 0.98).

Table 4.1 Correlation coefficients between experimental data and proposed model

Day	Subject									
	A	B	C	D	E	F	G	H	I	J
1	0.99±0.01	0.99±0.01	0.98±0.01	0.98±0.01	0.99±0.00	0.98±0.01	0.98±0.01	0.98±0.01	0.97±0.02	0.98±0.01
2	0.98±0.01	0.98±0.01	0.98±0.01	0.98±0.01	0.98±0.01	0.98±0.01	0.98±0.02	0.99±0.01	0.97±0.01	0.97±0.01
3	0.99±0.01	0.97±0.02	0.97±0.02	0.99±0.01	0.97±0.02	0.97±0.01	0.99±0.01	0.97±0.02	0.97±0.01	0.98±0.01
4	0.98±0.01	0.99±0.01	0.97±0.01	0.99±0.01	0.99±0.01	0.98±0.01	0.98±0.01	0.98±0.02	0.97±0.01	0.97±0.01

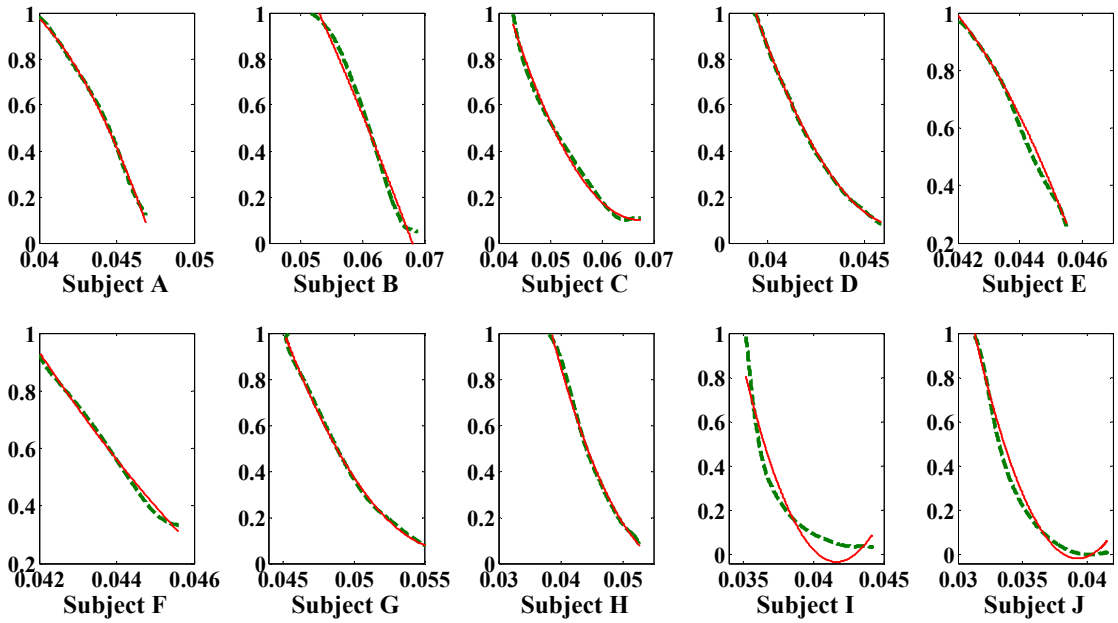

Figure. 4.6: Model validation results of the ten subjects

Figure 4.6 shows one set of the elbow joint angle prediction results obtained using the proposed method. The calculated elbow joint angles are plotted with a solid line and the recorded elbow joint angles obtained using

the MTx sensor are plotted with a dashed line. Trajectory of the exoskeleton device is plotted with a dotted line. The different states are divided using black lines. In state 1 (relaxation state), the prediction results and recorded results are all zero. Actually, small changes in the muscle activation level can be observed in this period due to the small changes in EMG signals. These small changes may make the current state change to the next state and cause errors. A rectification method is thus implemented to stabilize the changes. In state 2 (flexion state), there is usually a time lag (about 100-200 ms) at the end of this state between the recorded data and prediction results. This time lag is caused by the transition from the flexion state to the holding state. The flexion state changes to holding state when the input (the muscle activation level) for the state switching exceeds a threshold, which is pre-determined. However the real desired threshold changes with the variation of EMG signals. As a consequence, the constant pre-determined threshold makes the prediction of holding state backwardly. In state 3 (holding state), the elbow joint remains in a certain position (75° in this case). When the state changes to the extension state, the values of prediction results decrease with decreasing muscle activation level. The correlation coefficients and root-mean-square (RMS) errors between prediction results and recorded ones of the ten subjects are listed in Table 4.2.

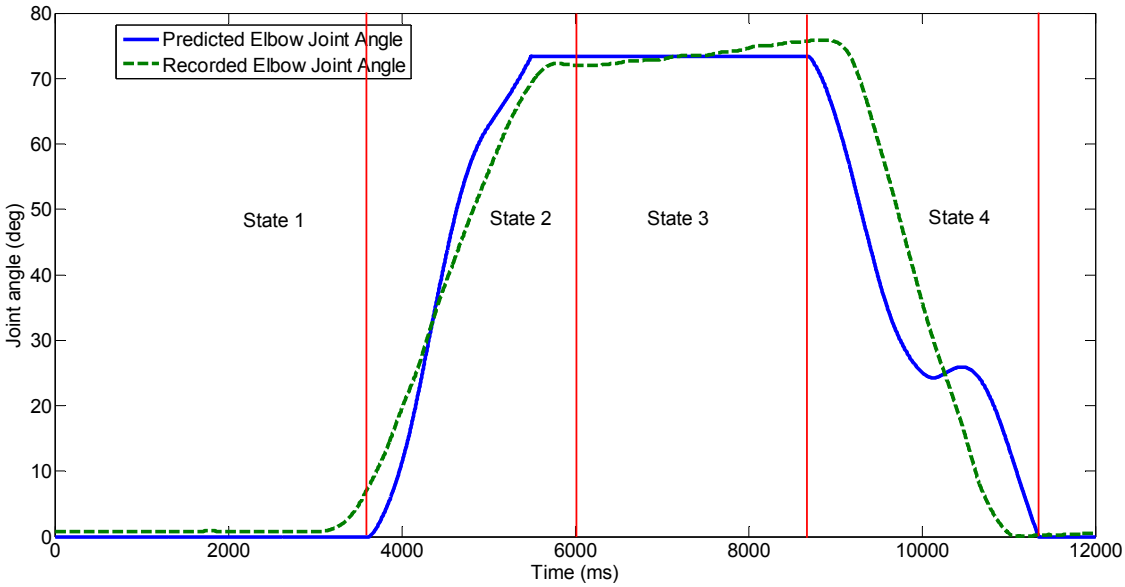

Figure 4.7: Experimental results of continuous elbow joint angle prediction method

Table 4.2 Experimental results of the ten subjects

(a) Correlation coefficients

Day	Subject									
	A	B	C	D	E	F	G	H	I	J
1	0.96±0.02	0.91±0.01	0.94±0.03	0.95±0.01	0.98±0.02	0.96±0.01	0.96±0.07	0.97±0.02	0.94±0.09	0.93±0.05
2	0.98±0.01	0.92±0.05	0.94±0.05	0.95±0.04	0.95±0.04	0.96±0.03	0.98±0.04	0.97±0.03	0.97±0.01	0.97±0.03
3	0.98±0.04	0.91±0.09	0.93±0.07	0.93±0.06	0.95±0.05	0.91±0.08	0.94±0.06	0.97±0.02	0.94±0.01	0.92±0.01
4	0.94±0.06	0.95±0.04	0.97±0.01	0.95±0.07	0.94±0.06	0.97±0.01	0.92±0.08	0.95±0.05	0.95±0.01	0.96±0.02

(b) RMS errors (degrees) between prediction results and recorded results

Day	Subject									
	A	B	C	D	E	F	G	H	I	J
1	9.78±3.79	8.10±2.59	5.20±2.80	9.22±2.12	5.60±0.34	9.17±2.80	9.47±1.37	9.70±0.13	8.64±1.60	5.33±1.27
2	7.33±2.14	7.56±2.31	4.32±2.21	7.31±3.31	5.55±1.21	7.78±2.57	8.33±2.12	9.05±2.11	5.31±2.21	4.21±3.17
3	6.23±4.11	7.71±2.77	5.78±3.33	8.21±2.23	6.04±2.11	7.31±2.23	7.78±3.16	7.73±3.01	7.04±2.13	5.78±2.00
4	7.35±2.11	8.78±2.11	4.32±2.45	5.45±3.13	5.57±3.14	5.32±2.85	9.01±2.11	7.00±1.31	6.66±3.01	6.05±1.15

Nevertheless, the proposed state switching model may give rise to distortion or time lag in some cases. In Fig. 4.8, the motion is forearm flexion and then extension, without a holding period during flexion and extension. There is a time lag between the flexion and extension in the prediction results. This is because the state changes from flexion to holding and then to extension. It takes some time (as long as the time lag) for the model to change state from holding to extension. This time lag depends on the decreasing rate of EMG signals (γ), the difference between peak muscle activation levels (aP), the threshold set for the holding state, and a range value (ar: 1-3%) that is used to reduce the influence of the non-stationarity of EMG signals. The time lag can be defined as:

$$t_{lag} = \frac{F_p - F_t(1 - a_r)}{\gamma} \tag{4-21}$$

where the only parameter which can be controlled is ar. However the influence of a_r is much less than that of the other parameters. Thus, this lag can be regarded as an inherent defect of this model caused by the non-stationarity of EMG signals. Although this time lag appears in certain circumstances, it does not affect all results, i.e. this lag, does not accumulate in the state switching method.

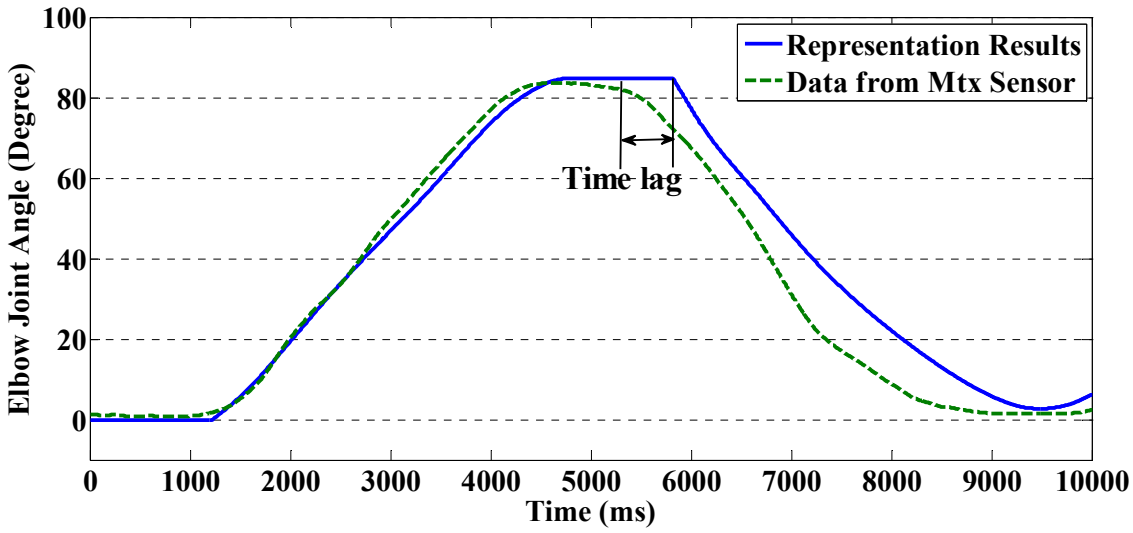

Figure. 4.8: Time lag in real-time caused by state switch algorithm.

To evaluate the proposed method in a more complicated circumstance, a consecutive stepping test was performed by five of the ten subjects. One set of the experimental results is shown in Fig. 4.9 and the detailed information for the five subjects is given in Table 4.3. In the stepping experiment, the subjects were asked to perform the movement with an angular velocity of 30°/s. The experimental results show that the RMS errors between prediction results and recorded ones increase with decreasing increment angle.

The experimental results show that the efficiency of the proposed method decreases with decreasing of increment angle. According to the experimental results, the proposed method provides a “good, faire, and poor” predictions of elbow joint angle with increment angles of 30°, 20°, and 10°, respectively. One of the reasons for that the efficiency of the proposed method decreases with decreasing of increment angle is that the trend of EMG signals tends to become more unstable or the amplitude of

ripple of EMG signals tends to become wider with decreasing increment angle. The wide ripple of EMG signals directly influences the calculation of muscle activation level, i.e., there are ripples in muscle activation levels. The activation levels thus become unstable as well. This phenomenon was found for all five subjects during the consecutive stepping test. But this kind of phenomenon doesn't appear in the continuous motion test. This phenomenon indicates that the subject must provide more effort to achieve the task in the consecutive stepping text than in the continuous motion text and the fluctuation in EMG signals during consecutive stepping test reflects upon this effort. According to the experimental results, the proposed method can provide suitable predictions within increments of 20° to 30°.

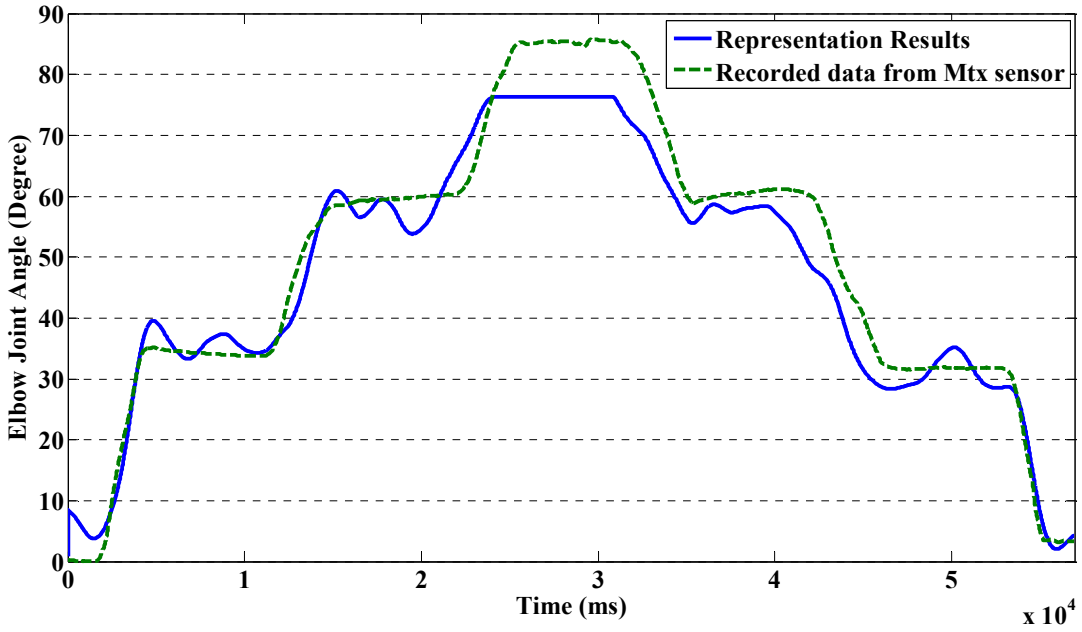

(a)

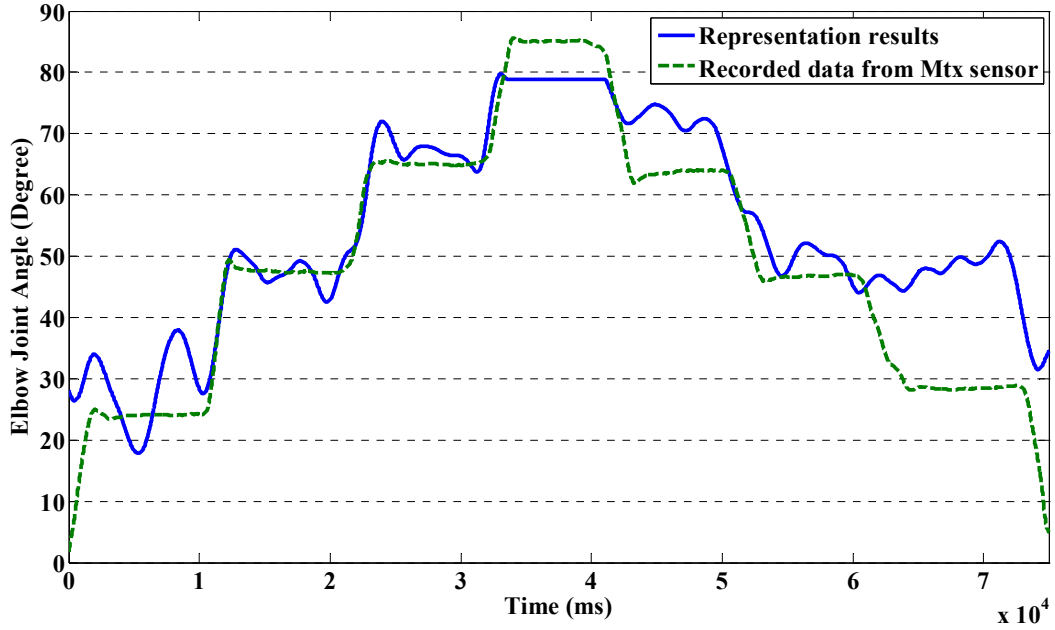

(b)

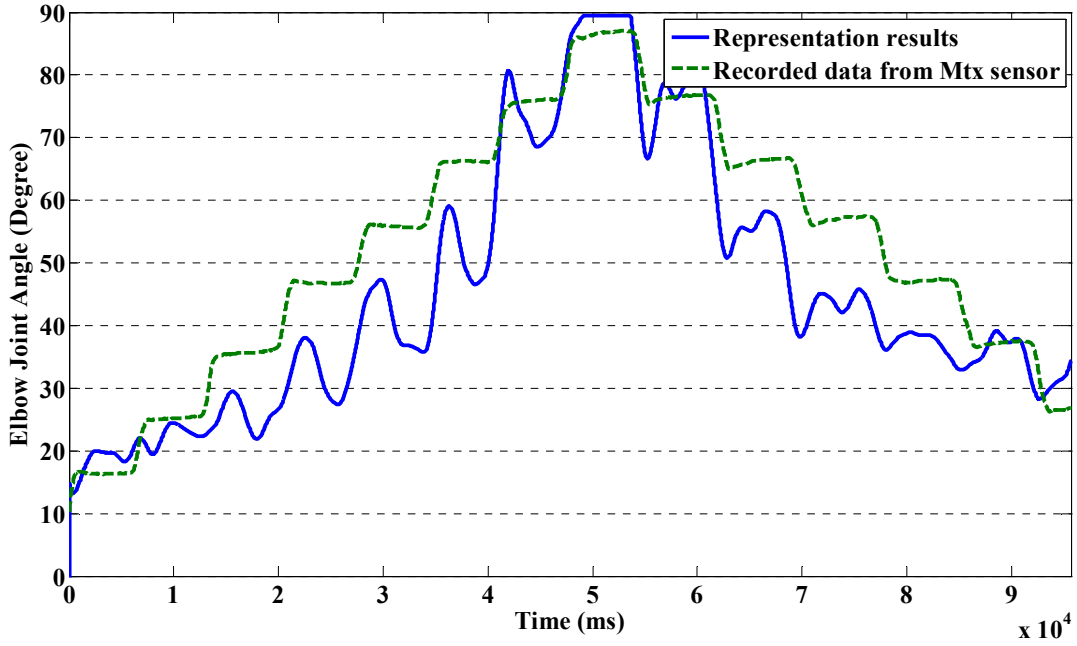

(c)

Figure. 4.9: Consecutive stepping test results for different increment angles. (a) with increment of 30°; (b) with increment of 20°; (c) with increment of 10°.

Table 4.3 RMS errors between prediction results and recorded results in consecutive stepping test

Increment	Subject				
	A	C	E	G	I
30	4.40±3.15	5.40±2.21	6.51±3.11	5.32±4.21	6.71±4.00
20	6.61±3.71	8.83±4.94	7.139±3.90	9.21±2.11	8.31±3.57
10	15.40±3.15	17.40±3.12	17.35±4.12	19.35±3.15	17.44±4.23

4.5 Summary

In this chapter, a continuous prediction method for elbow joint angle was proposed, which is one of the new points in my study. This method aimed to solve the problem that motion recognition based method can only provide binary-like results for control. The proposed method was based on the quantitative analysis of sEMG signals and corresponded elbow position within movement. The dynamic equation was developed on Hill-type muscular model and simplified elbow joint musculotenedon model. With approximation and some assumptions, a quadratic expression was found and evaluated by a four-day-long experiment on ten subjects. A state switching model was developed to avoid the influence of acceleration and transit between muscle contraction states. A consecutive stepping experiment was conducted to test the feasibility of the proposed method with more free motion. Experimental results indicate that this method can provide suitable prediction results with RMS errors of below 10° in continuous motion and RMS errors of below 10° in stepping motion with 20° and 30° increments. With this method, our ULERD can follow the

motion of subject in real-time, not just by pre-defined motions controlled by switch signals. One point should still be noticed that the proposed method is focused on elbow joint, where musculoskeletal structure is relative simple and involved muscles are fewer, compared with the other joints. There is a long way to go if we tend to extend this kind of method on the other joints.

Chapter 5 Force Evaluation and Prediction using sEMG

5.1 Introduction

In this chapter, the relation between force exerted by subject and sEMG signals will be discussed. A prediction method for contact force between subject and the environment will be proposed to provide remote force evaluation function in our home-used rehabilitation system.

The relation between musculotendon force and EMG signals is more direct than the one concerned about motions, as motions are also involved by external variables, e.g., gestures, gravity and status of tendon. However, that is not to say the relation between musculotendon force and EMG signals is simpler. It is still complex, even in a solo isolated muscle. Although the popular Hill-type or Huxley-type muscular models provide a way to explain the force generation function in a muscle, the models themselves are too complex to be directly applied. Nevertheless, there are some arguments about these models that the conclusions were obtained from experiments conducted on isolated muscles which property is different from the one in a living body. It is not hard to tell that to measure the data under a ‘perfect’ condition is quite difficult.

However, it is just the case that using EMG signals is more direct and convenient to predict musculotendon force. Usually, the measurement of muscular force normally cannot be performed by indwelling force

transducers inserted into the tendon but rather by quantifying the reaction force supplied to external loads or ‘‘mechanical ground”. However in some cases it is inconvenient to attach sensors on the surface of the contacting environment. On the other hand, the measurement results from the sensors are the output of the corresponded musculoskeletal system, which is hard to reflect the situation of the individual muscle. On the contrary, using EMG can observe the individual muscle and predict the output of the musculoskeletal system without using a force sensor.

5.2 Muscular model

In this chapter, I focus on two motions: downward touch motion and push motion, given the two motions are very common in daily living. As the redundancy and complex of human musculoskeletal system, only isometric contraction was considered, i.e., subject kept still when he exerted force on the object. EMG signals were recorded from the flexor carpi radialis (FCR), the flexor carpi ulnaris (FCU), the extensor carpi radialis longus (ECRL), the extensor carpi ulnaris (ECU), the extensor digitorum (ED), the biceps brachii (BB), the triceps brachii (TB), and the pectoralis major (PM). These eight muscles are involved in the studied motions. Given these conditions, two muscle-skeleton models were used to derive the dynamic equations for the two motions, respectively.

The sketch of the musculoskeletal model for the downward touch motion is shown in Fig. 5.1 (a) while the one for push motion is shown in Fig. 5.2 (a). The figures on the right column show the corresponded changings of forces for the two motions, respectively. There are mainly

three degree of freedoms (DoFs) on the forearm which are pronation/supination of the forearm, radial/ulnar deviation around the wrist and palm flexion and extension. In our special case of downward touch motion, only palm flexion and extension was concerned. The pairs of flexors and extensors around the forearm act to keep the stiffness of wrist joint and balance the torque from the contact motion. As the motion is isometric, the dynamic function can be written as:

$$\tau_{F\text{lexor}} - \tau_{E\text{xtensor}} + \tau_{mg} = \tau_F \tag{5-1}$$

where τ_{Flexor} denotes the torque derived by the flexors while $\tau_{Extensor}$ denotes the torque derived by extensors. τ_F is the torque derived by the contact force. τ_{mg} is the torque derived by the gravity force of hand. The friction in the joint is ignored here. The singular gesture, in which upper arm and lower arm form in a line, was tried to avoid. In singular condition, the direction of the contact force pass through the wrist joint. Under this circumstance, the main function of flexors and extensors around the forearm is to maintain the stiffness of the wrist joint, and contact force is balanced by the contraction from the other muscle groups.

In push motion, the contact force exerts through the wrist joint (as shown in Fig. 5.2 (a)). This equals an identical force (F') exerts on the elbow joint and couples an additional torque (τ_f) on the forearm. In this case, the contact force also generates a torque on the shoulder joint (τ_s). The BB and TB contract to balance the torque (τ_f) exerted on the forearm. PM contract to balance the torque (τ_s) exerted on shoulder joint. The dynamic

function can be written as:

$$\tau_{Ag} - \tau_{Ant} = \tau \tag{5-2}$$

$$F = \vec{F}_f + \vec{F}_S \tag{5-3}$$

where τ_{Ag} denotes the vector of torque generated by agonist muscles and τ_{Ant} denotes the vector of torque generated by antagonist muscles. τ is the vector with the form of (τ_f , τ_s). $\boldsymbol{F}$ is vector of the desired push force. $\overrightarrow{F_f}$ and $\overrightarrow{F_s}$ can be calculated from the torque equation.

All torques in (5-1) and (5-2) can be expressed as the forces (muscular forces or gravity force) product the corresponded moments. Because the motions are isometric, the moments involved in the equations can be considered as constant. Therefore, (5-1) and (5-2) can be written in a compact form of:

$$\tau = \sum \alpha_i \cdot F_i \tag{5-4}$$

where α_i denotes the constant moment. It should be noticed that subjects were asked to try to perform the motion with the same gesture for each time. Because of the redundancy of human musculoskeletal structure, a motion can be executed with different gestures. The moment arms or muscle status will be different if the gestures are different. Given this condition, the gesture for each motion was constrained. Subjects were asked to perform the motion with a comfortable gesture and keep the same gesture for each time.

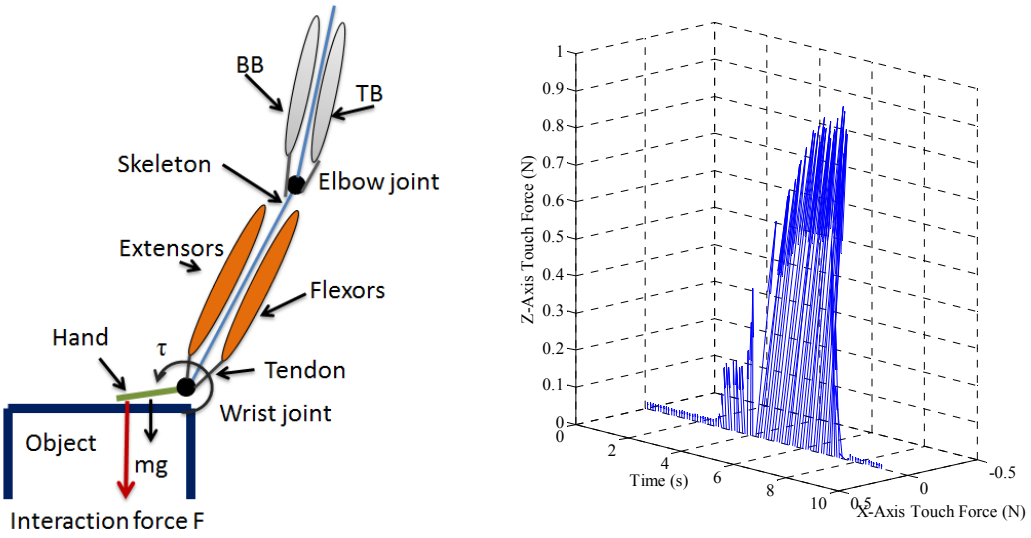

(a) (b)

Figure. 5.1 Downward touch motion. (a) shows the musculoskeletal model and (b) shows the corresponded force.

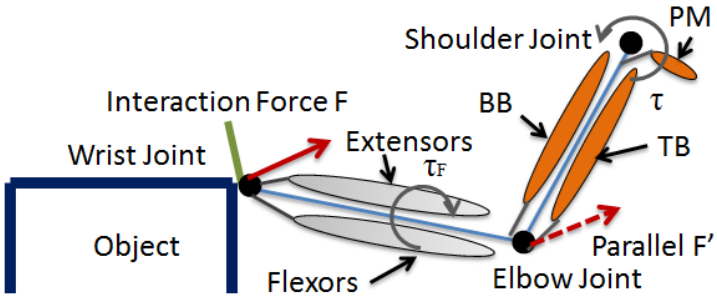

(a) Musculoskeletal model

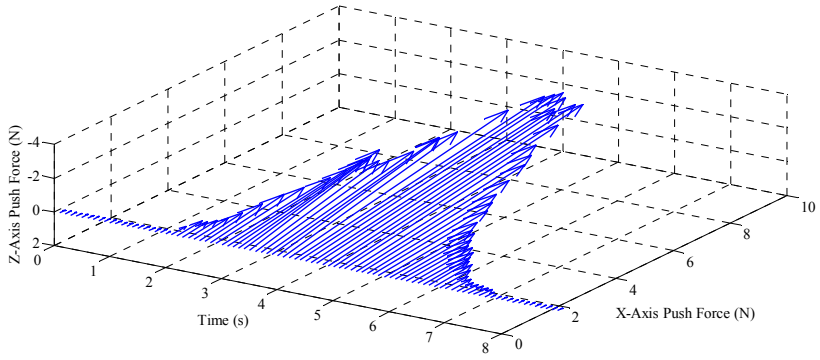

(b) Changing of forces

Figure. 5.2: Push motion

The Hill-type muscular model as introduced in section 4.2 was applied again to predict the musculotendon force with EMG signals. Under the condition of isometric contraction, the term of F_i in (5-4) can be instead with a linear expression of muscle activation level, and (5-4) can thus be rewritten as:

$$\tau = \sum \alpha_i \cdot \beta_i \cdot u \tag{5-5}$$

It should be noticed here that a linear relation between muscle activation level and musculotendon force was assumed, which was not very precise and may be different from individuals. However this assumption is reasonable within a certain range of motion.

5.3 Motion recognition

As dynamic equations are obtained, the time point to apply these equations is needed. A neural network classifier was applied to recognize the motions. As has been discussed in Chapter 3 that SVM costs more time than NN on real-time computation, NN was adopted in this thesis because I do not want to take too much time on motion classification. The inputs were processed EMG signals or muscle activation levels obtained from five muscles, which were BB, TB, FCR, ECRL and ECRB. The outputs of the classifier were binary representation for four motions, which are relaxing, downward touching, pushing, and exerting force motion. Therefore, the input was a vector with five components and the output was a vector with four components. The training data were well labeled, according to the values from MTx sensors and 6-axis force sensor. One set of the

experimental data (push motion) is shown in Fig. 5.3. The relaxing motion was labeled when there were no changings in the value from MTx sensors and no muscle activation level. The pushing motion or touch motion was labeled when there were changings in values from MTx sensors and no changing in force value. The exerting force motion was labeled when force value changes.

There was one hidden layer with seven neurons in the neural network. The hyperbolic tangent sigmoid transfer function and scaled conjugate gradient backpropagation training algorithm were adopted for hidden layer combination and learning process, respectively.

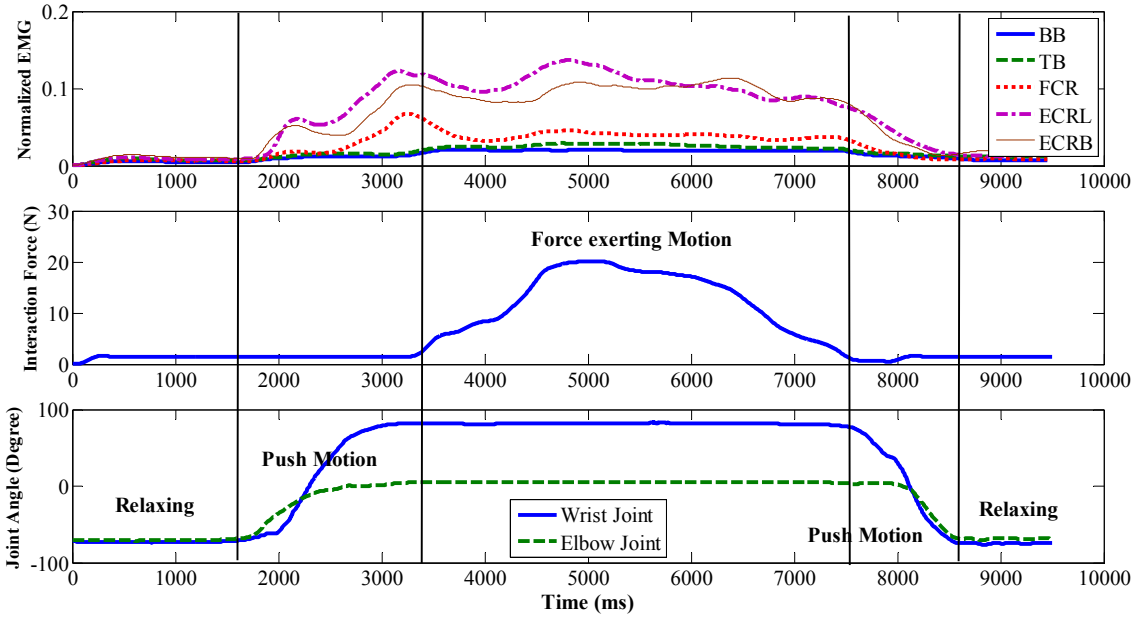

Figure. 5.3: One example of the push motion

5.4 Parameter calibration

The Bayesian linear regression (BLR) algorithm [80] was adopted to calibrate the parameters (ω_i) in the dynamic equations.

Assuming that the noise in prediction function is with the form of

Gaussian, the proposed dynamic equation (5-5) can be written as:

$$\boldsymbol{t} = y(\boldsymbol{a}, \boldsymbol{\omega}) + \varepsilon \tag{5-6}$$

where ε is a zero mean Gaussian random variable with precision β. Thus the following likelihood function can be obtained:

$$p(\boldsymbol{t} \mid \boldsymbol{a}, \boldsymbol{\omega}, \beta) = \prod_{n=1}^{N} N(t_n \mid \boldsymbol{\omega}^{\boldsymbol{T}} \varphi(u), \beta^{-1}) \tag{5-7}$$

On the other hand, we assume that the prior probability distribution over ω is also with the form of Gaussian distribution:

$$p(\boldsymbol{\omega}) = N(\boldsymbol{\omega} \mid \boldsymbol{m}_0, \boldsymbol{S}_0) \tag{5-8}$$

where $\boldsymbol{m}_0$ denotes the mean value of $\boldsymbol{\omega}$ and $\boldsymbol{S}_0$ denotes the covariance.

Because the posterior distribution is proportional to the product of the likelihood function and the prior, the following function is obtained:

$$p(\boldsymbol{\omega} \mid \boldsymbol{t}) = N(\boldsymbol{\omega} \mid \boldsymbol{m}_N, \boldsymbol{S}_N) \tag{5-9}$$

where

$$\boldsymbol{m}_N = \boldsymbol{S}_N(\boldsymbol{S}_0^{-1}\boldsymbol{m}_0 + \beta\Phi^T\boldsymbol{t}) \tag{5-10}$$

$$\boldsymbol{S}_N^{-1} = \boldsymbol{S}_0^{-1} + \beta\Phi^T\Phi \tag{5-11}$$

The $\boldsymbol{m}_N$ denotes the mean of $\boldsymbol{\omega}$ given the condition of $\boldsymbol{t}$, and $\boldsymbol{S}_N$ is the covariance. The evidence approximation method was adopted to calculate $\boldsymbol{m}_N$ and $\boldsymbol{S}_N$. A "cross-validation" selection criteria was adopted to obtain local optimal parameters. In the "cross-validation" criteria, one set of the

experimental data was used to calculate the parameters and the performance of these parameters was assessed by evaluating the root-mean-square (RMS) errors with the remaining data. This procedure was performed on all the experimental data and the ones with the smallest RMS errors were selected as the final optimal parameters.

It should be noticed that the term ‘global’ used here means the entire sEMG data recorded from the target muscles during all the corresponded force exerting motion in a relative long period of one subject’ ADL. It can be easily noticed that it is almost impossible. The term ‘local’, on the contrary, means one set of experimental data for just one or limited number of trials. I tried to use BLR to obtain the global or ‘almost global’ optimal parameters from a limited number of local data. This concept is based on the assumption that there is a constant ‘pattern’ existing in the sEMG data during our expected period and all the data surround the ‘pattern’ with a kind of probability distribution. Although this probability distribution, if existing, is not Gaussian, it is reasonable and nature to assume that the Gaussian is the most-likely one, because there are many uncertain complex ‘disturbances’ exerting on the EMG signals.

5.5 Experimental results

5.5.1 Experimental setup

Five subjects (age: 26.00±1.73 years, height: 1.72±0.04 m, weight: 66.40±10.36 kg, all male, one left-handed, and four right-handed) participated in the experiment. The maximum voluntary contraction (MVC) test was performed for each subject to record the maximum amplitude of

EMG signals for each muscle. As the high redundancy and complexity of human musculoskeletal system, isometric downward touch motion and push motion are considered in this paper. The downward touch motion is defined as that subject uses his figure tips to exert force on the environment with palmar aspect facing downward while the shoulder joint is around 20°, elbow joint around 10°, and wrist joint around 45° in sagittal plane (as shown in Fig. 5.4 (a)). The push motion is defined as that subject uses his palmar to push the object with the shoulder joint around 30°, elbow joint around 100°, and wrist joint around 40° in sagittal plane (as shown in Fig. 5.4 (b)). The experiment for downward touch motion was divided into three trials, with maximum force amplitude of 5 N, 10 N and 15 N, respectively, and there were five trials in experiment of push motion, range from 5 N to 25 N, with an increment of 5 N. During each trial, the subject was asked to contact the object for 2 to 3 s. The subject repeated each trial 10 times with a relaxation time of 1 min between tests.

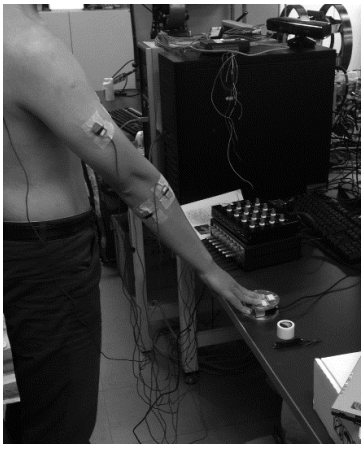

(a) Downward touch motion

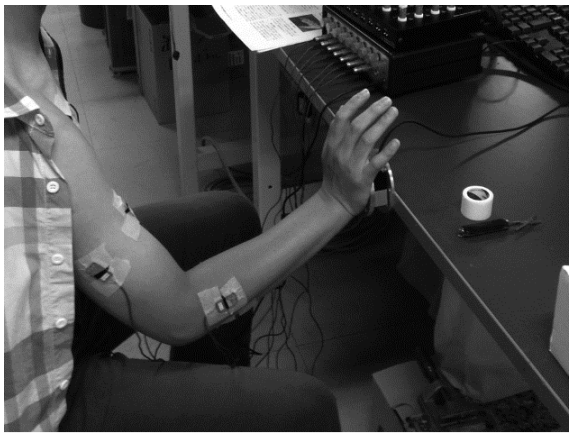

(b) Push motion

Figure. 5.4: Gestures for the two motions

A remote contact force evaluation experiment was designed to evaluate the effectiveness of the proposed method. One of the subjects (named as operator) was asked to perform touch motion and push motion and his contact force was predicted with proposed method and represented by haptic device “Phantom Premium” on the remote side. Another subject (named as observer) was asked to hold the handle of “Phantom Premium” to sense the predicted force (as shown in Fig. 5.5).

(a) (b)

Figure. 5.5: Remote force evaluation experiment. (a) shows the downward touch motion; (b) shows the push motion

Prior to data collection, the skin was shaved and wiped down with alcohol. Dry rectangle electrodes (Ag/AgCl, size: 26x14 mm), with a skin contact surface of 20 mm2, and inter-electrode distance of 15 mm, were placed parallel to the muscle fibers, according to SENIAM references [70]. Electrode placements were confirmed by voluntary muscle contraction and followed the recommendation of [71]. The sampling rate for EMG signals was 1000 Hz with differential amplification (gain: 1000) and common mode rejection (104dB) by the commercial filter box (10-450 Hz band-pass,

Personal EMG, Oisaka Development Ltd., JAP). Two MTx sensors (Xsens Technologies B.V., USA) were attached on subject's hand and forearm to record the joint angles. A six-axis force sensor (ThinNANO, BL AUTOTEC, LTD., JAP) was mounted on the platform to record the contact force.

5.5.2 Experimental results for motion recognition

Experimental results of training performance of motion classifiers are list in Table 5.1. The Recognition accuracy rate of this classifier is 96.0%, and the average accuracy rate for the five subjects is 96.7%. The training needs a few seconds (with average of 41.6 s). One set of on-line experimental results for motion classification is plotted in Fig. 5.7, where the upper plot shows the recognized motions depicted by different line types while the corresponding contact force and joint angles are plotted in the middle and lower plot, respectively. There is an issue about the resolution of the classifier, i.e., in some cases the classifier cannot detect the motion as soon as it happens. The resolution brings one problem to the force prediction which will be described, along with a solution in the following. One confusion plot of the training performance for one subject is shown in Fig. 5.6.

The misclassifications for motion recognition mainly appear during the beginning period and the ending period of the movement. One of the reasons for these misclassifications is that the activation levels of muscles are analogous during these two periods. Although dividing the touch motion and push motion into more detailed patterns, e.g. an initial motion,

touch ending motion, and push ending motion, seems to solve this problem, our experimental results show that a more complicated pattern dividing leads to a lower recognition accuracy rate. Fortunately, these misclassifications do not affect the prediction results because the force exerting motion and the motion right before force exerting happening is recognized correctly. The other motions are just used as reference in this paper.

Table 5.1. Recognition accuracy rate

Subject				
A	B	C	D	E
96.0%	97.4%	94.7%	96.7%	97.1%

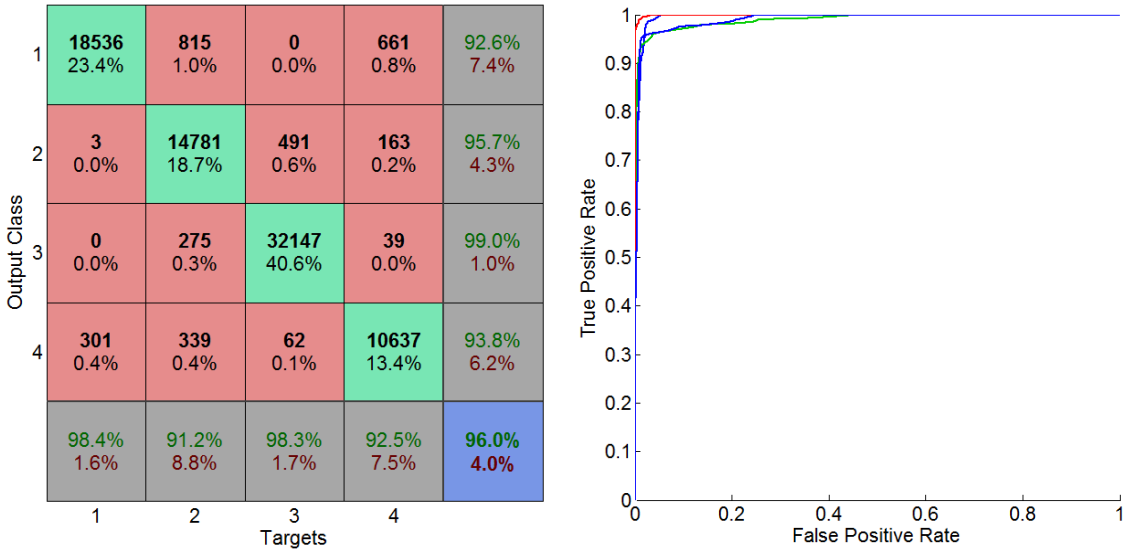

(a) (b)

Figure. 5.6: Training performance of the Neural Network classifier from one subject

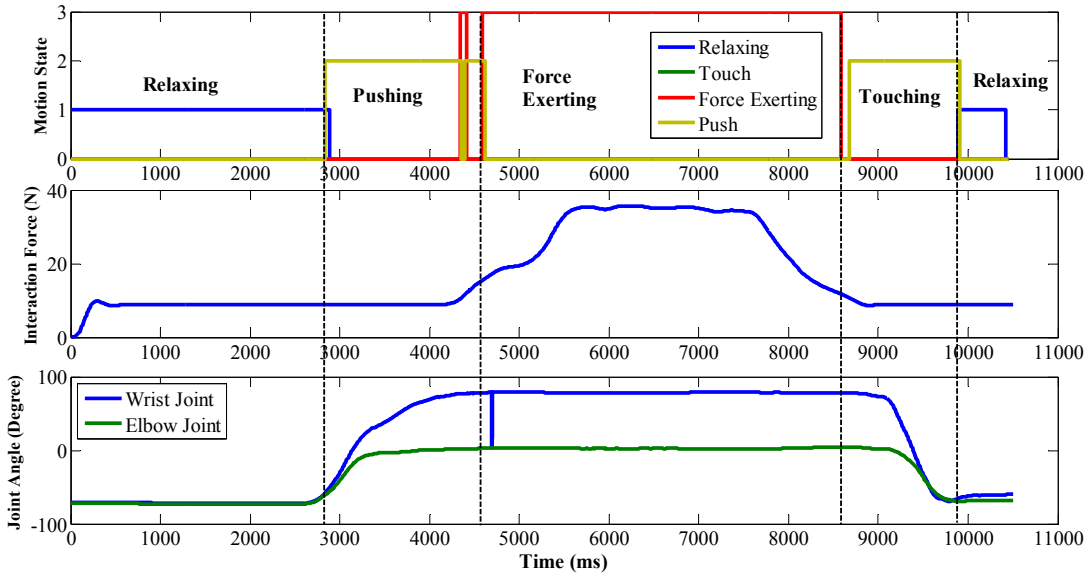

(a) Experimental results for push motion classification

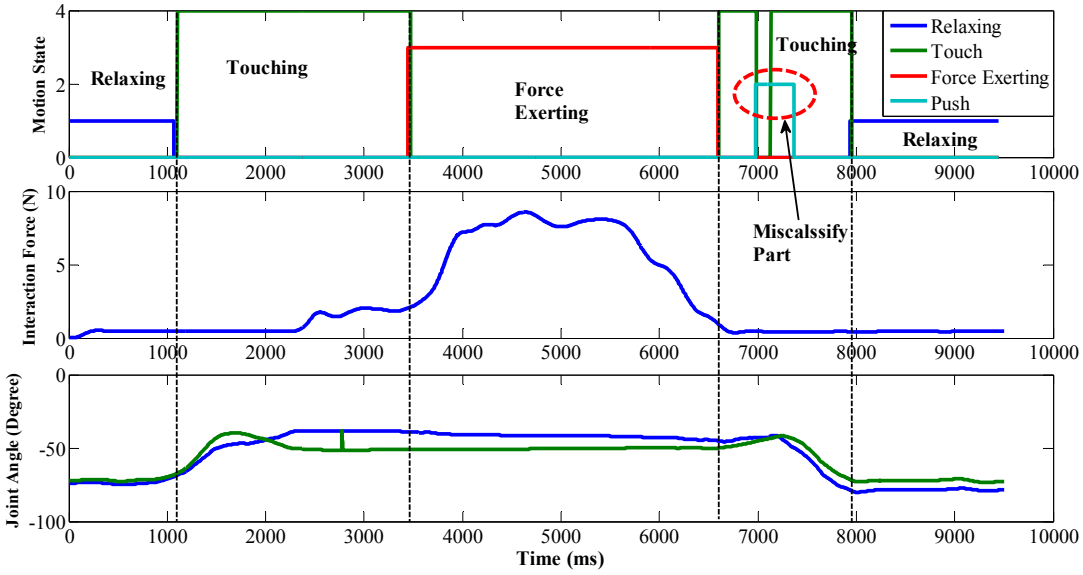

(b) Experimental results for downward touch motion classification

Figure. 5.7: On-line experimental results of motion recognition

5.5.3 Muscle activation during force exerting

Fig. 5.8 depicts all the experimental results of muscle activation levels of FCR, ECRL and ECRB with a function of contact force values. The results were calculated with the mean value of stable period in each trial.

The brown lines represent the linear relationship between the muscle activation levels and interaction forces. For vertical gesture, the correlation coefficients are 0.87, 0.71 and 0.83 for FCR, ECRL and ECRB respectively and for horizontal gesture, they are 0.85, 0.78 and 0.69 respectively. It should be notced that the correlation coefficients which are listed above are calculated ingorning most of the points in relative high interaction force area (as shown by pentagram shape). As indicated by some of other research results, the relationship between muscle activation level and musculotendon force is beyond linear when the musculotendon force is in a relative high level (such as with a level of up 70% MVC). In our particular case, the maximum interaction force which was tested is above 27 N. As a consequence, the range of the pentagram shape points are around 60 to 70%. If the pentagram points are included for calculation, the linear correlation coefficients are 0.78, 0.53 and 0.69 for FCR, ECRL and ECRB respectively for vertical gesture and 0.75, 0.63 and 0.57 fo horizontal gesture. Another interesting result is that the slope or the changing rate for ECRL and ECRB is different. They are 0.0011 and 0.0025 for ECRL and ECRB respectively for vertical gesture and 0.0021 and 0.00114 for horizontal gesture. As both of the two muscles act to extend the hand at wrist joint, the ECRB seems to be more active than ECRL in vertical case and seems to be less active in horizontal gesture.

It can be indicated from the experimental results that there is a ‘pattern’ existing in the EMG data during the force exerting motion, some of them are even linear-like.

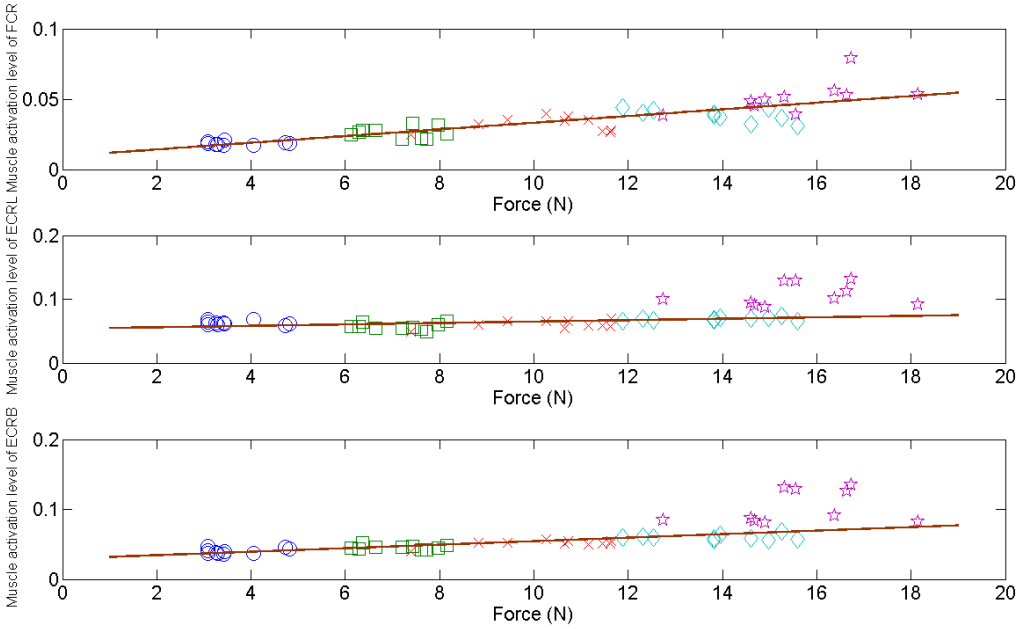

(a) Force exerting of downward touch motion

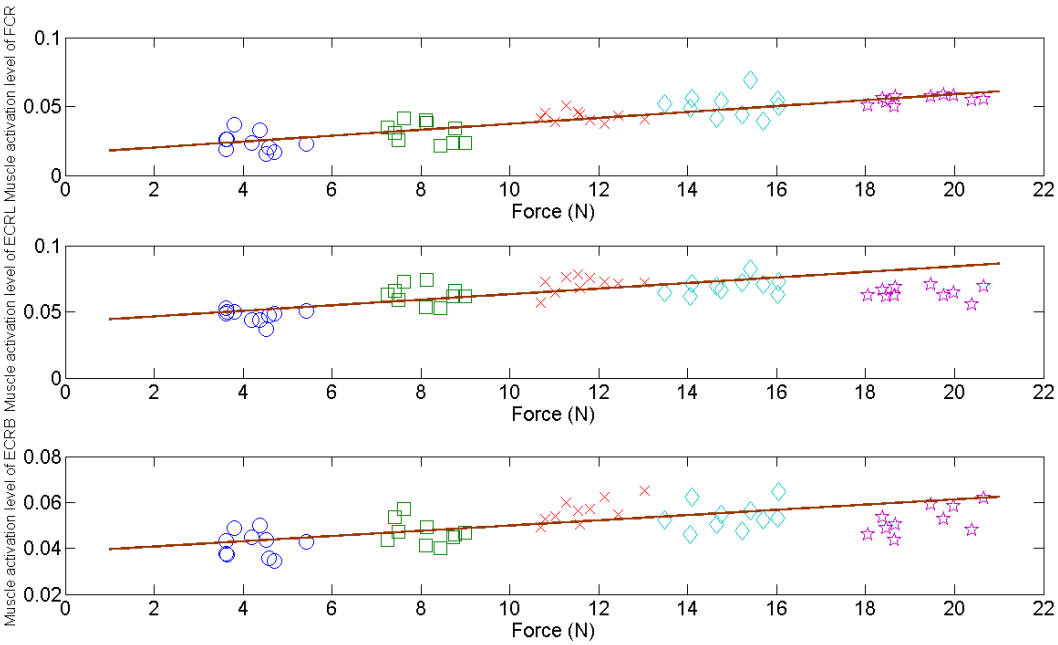

(b) Force exerting of push motion

Figure. 5.8: Muscle activation levels during contact force exerting

5.5.4 Parameter calibration

The off-line parameter calibration procedure for two of the ten

subjects is plotted in Fig. 5.10. The value is the natural logarithm of cost function. It is shown in Fig. 5.10 that the parameters calibrated by the 7th or 8th trial data fitted the entire experimental results best in the local ten trials for subject A and the 5th is the best for subject B. BLR algorithm can obtain a local optimal parameter calibration results based on one set of experimental data. However, these parameters can hardly represent the global optimal values for the entire data. This property can be indicated from the experimental data that the local optimal ones performed differently on the ten test experiments. As up to now I have not found out a proper way to obtain the most global-like ones from local data, a 'cross-validation' method is adopted to find the global-like ones. Actually, there is one question that whether it is enough to find out the global-like ones during ten trials. Fortunately, we found that it doesn't require using all the data to find the optimal parameters although the "cross-validation" was performed on all the off-line experimental data. Among all the subjects, the parameters, which are local optimal for one group of data, are also optimal for the other ones. However just one set of data is not enough to find the optimal parameters. Five to ten sets of data with different force magnitude are suitable. A long-period experiment is also desired to find a more convinced result.

The experimental results of off-line force prediction were plotted in Fig. 5.9. The results show that the BLR has the ability to catch the proper parameters within the given data space under our special cases.

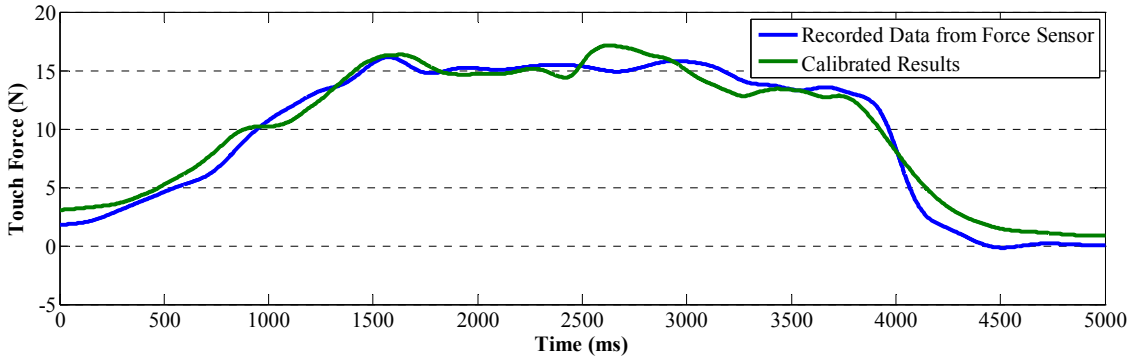

(a) Downward touch motion

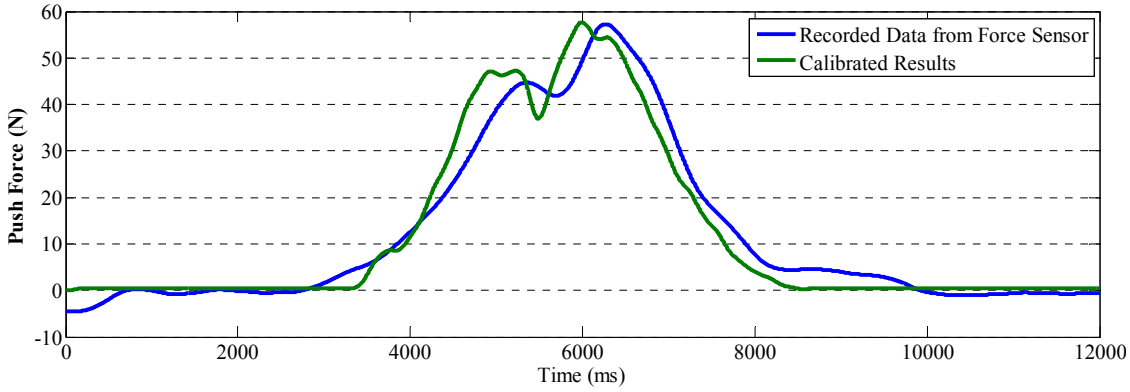

(b) Push motion

Figure. 5.9: Off-line force prediction results

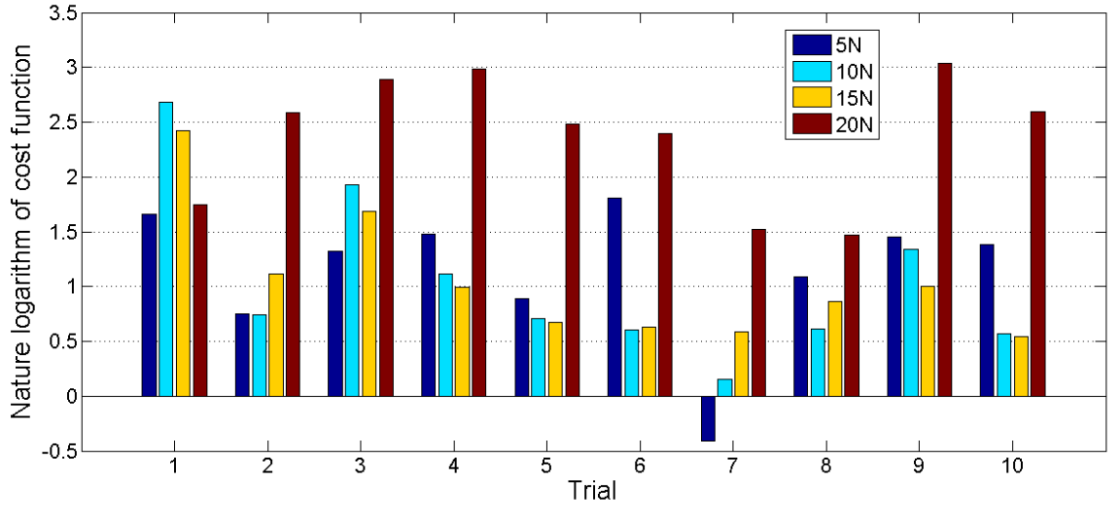

(a) 'Cross-validation' of subject A

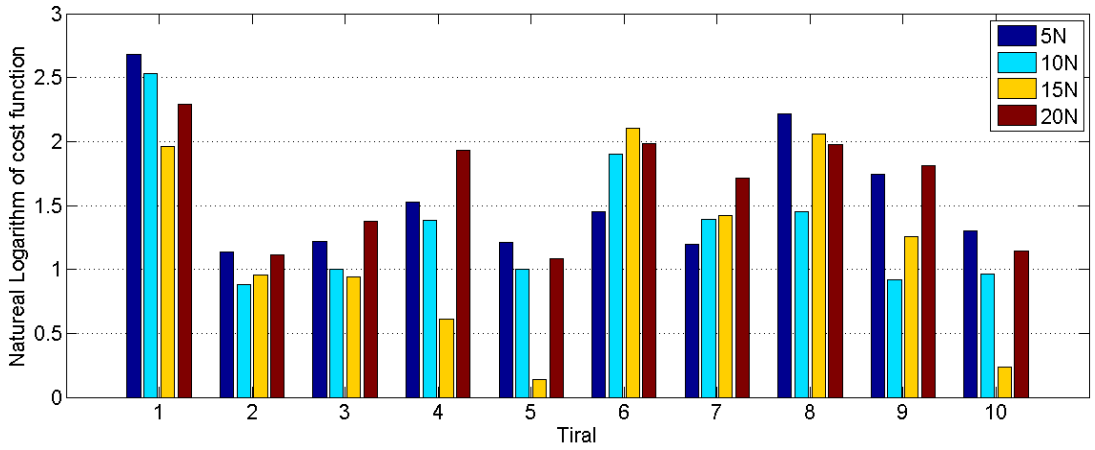

(b) 'Cross-validation' of subject B

Figure. 5.10: 'Cross-validation' of two subjects

5.5.5 On-line experimental results

Experimental results of contact force prediction for the downward touch motion are listed in Table 5.2 and for the push motion are listed in Table 5.3. The RMS errors of downward touch motion for all the five subjects are below 3.0 N (with maximum of 15 N) and for push motion are below 6.2 N (with maximum of 25 N). One set of on-line experimental results are shown in Fig. 5.11 and 5.12. The predicted contact forces are plotted as a solid line, followed by the recorded results from force sensor plotted with dash line. As mentioned previously, the resolution of the proposed classifier gives rise to one problem that there were two discontinuous points in predicted results (shown in upper plot of Fig. 5.11). One was at the beginning of the force exerting motion and the other was at the ending of this motion. As the classifier cannot guarantee to recognize the force exerting motion as soon as the subject exerts the force on the

object, when force exerting motion is recognized, the predicted result is so high that this point is discontinuous from the previous one (zero). For the same reason, the end part is also discontinuous. A proportion smooth algorithm was proposed to address this problem, which is described as follow:

$$x'_i = x_i \mp (a - ai/t) \tag{5-12}$$

where x_i is the original prediction result. a is the difference in the discontinuous point. t is the time interval for smooth processing (we set it as 200 ms). The sign of minus (plus) is for the beginning (ending) part.

In remote evaluation experiment, the observer who held the handle of the haptic device "Phantom Premium" could feel the represented continuous contact force from the operator, like the operator directly touched or pushed the observer himself. Without the smooth processing, the discontinuous prediction will bring impact feeling to the observer at the beginning and ending of force exerting motion.

In downward touching force prediction, the RMS errors increase with the increasing of exerting force magnitude. However, the relative errors keep the same, around 17% to 20%, which indicates that there is a constant relative error existing in the proposed prediction method. As using the surface electrodes, some of the deep muscles around forearm are unable to be detected, which may bring some errors in the proposed model. Another reason may come from using a 2 Hz low-pass filter. Some energy of the EMG signals was filtered by using the low-pass filter. Therefore, some

information in the EMG signals was eliminated. However, the using of the low-pass filter is reasonable and necessary for obtaining acceptable prediction results. Because the muscle naturally acts as a filter, the force changing frequency is much lower than the amplitude changing frequency of the EMG signals. Without using the low-pass filter, the prediction results change so frequently that they are far from the real contact force. Using the low-pass filter to mimic the low-pass property of muscle makes the results smoother and more accurate.

Table 5.2. RMS errors of on-line downward touching force prediction results

Force(N)	Subject				
	A	B	C	D	E
5	1.37±0.27	0.97±0.37	1.45±0.29	2.12±0.58	0.83±0.78
10	2.37±0.55	2.01±0.78	2.49±0.66	2.28±1.16	1.33±0.58
15	3.45±1.10	2.12±1.22	2.93±0.98	2.55±1.08	2.00±0.92

Table 5.3. RMS errors of on-line pushing force prediction results

Force (N)	Subject				
	A	B	C	D	E
5	0.99±0.32	1.23±0.47	1.00±0.19	0.87±0.81	0.81±0.65
10	1.55±0.35	2.11±0.48	2.01±0.36	1.19±1.16	1.31±0.51
15	2.91±1.00	2.56±1.00	2.90±1.98	2.11±0.78	2.11±0.71
20	3.13±1.53	3.75±0.55	2.15±0.65	3.12±0.95	3.71±0.77
25	5.01±1.77	6.11±1.74	4.44±1.15	5.00±1.15	4.98±1.15

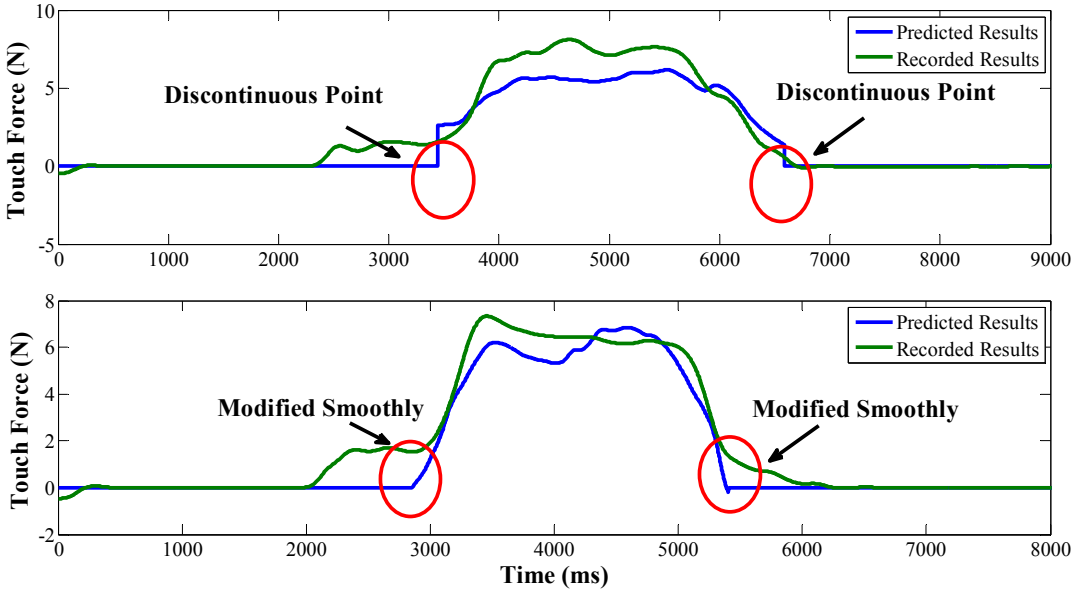

Figure. 5.11: On-line experimental results for downward touch force prediction

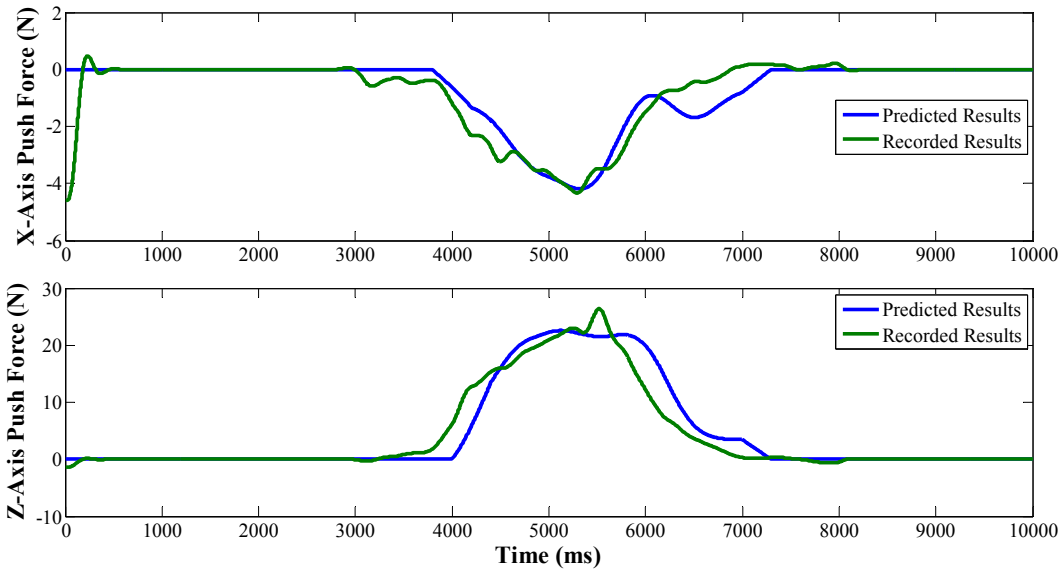

Figure. 5.12: On-line experimental results for push force prediction

5.6 Summary

In this chapter, a force prediction method was proposed using only sEMG signals. This method aimed to provide remote force evaluation

function to our home-used rehabilitation system. Although using force sensor can obtain accuracy measurement results of contact force value, it is inconvenient to attach sensors on the surface of the environment in some cases and the force sensor can just provide a summary output of the entire musculoskeletal system of the patient, not individual behavior of special muscles. The method itself is also the new point of my study.

For simplicity, two motions: the downward touch motion and push motion were studied as these two motions are common in ADL. Two musculoskeletal models were developed for the two motions, respectively. Two dynamic equations were yielded from the two models. The Hill-type model was also applied in the dynamic equations. To calibrate the parameters, BLR algorithm was adopted. As it is still hard to obtain a global-like data space, we used the ‘cross- validation’ method to find the proper optimal values. The experimental results showed that the relative RMS errors using the proper optimal parameters were below 20% with the force amplitude range from 0 N to 25 N in push motion and 0 N to 15 N in downward touch motion. For the remote side, the haptic device ‘Phantom Premium’ was used to represent the predicted force in real-time. The subject who held the handle of the Phantom felt like the performer himself contacted him as real.

Chapter 6 Entire System Evaluation

6.1 Introduction

The purpose of my study is to design a home-used self-training rehabilitation system. According to the requirement of clinical purpose, the system should be able to provide self-training function and remote force evaluation function. In Chapter 3 and 4, a motion prediction method aimed to provide self-training function to the system was proposed, based on pattern recognition method and muscular model method. In Chapter 5, a force prediction method was proposed for the purpose of providing remote force prediction function to the system. In this chapter, the evaluation for the entire system will thus be given from these two points. In addition, some discussions will also be given on the different issues about the methods or the entire system.

This chapter is divided into two parts basically, the first part for self-training function and the second part for remote force evaluation function. For each part, a schematic of the corresponded function will be given firstly, together with a straightforward review of the proposed method. As some methods are actually coupling with each other, the review will make my idea more clear to understand.

6.2 System construction

My study is one part of our rehabilitation project (as shown in Fig. 6.1). The purpose of this project is to provide rehabilitation training for

stroke patients using robotic system. We have developed an exoskeleton device, named Upper-limb Exoskeleton Rehabilitation Device (ULERD) based on anthropometry measurement. This device has three active DoFs (one for the elbow joint and tow for the wrist joint) and four passive DoFs (two for the elbow joint and two for the wrist joint), as mentioned in section 2.2. This device can provide positive training, in which the device resistant force against to the tendency or direction of patient's movement. This function was achieved by impedance control. A passive training can also be provided by following a pre-defined movement. Another property of this device is that it is portable.

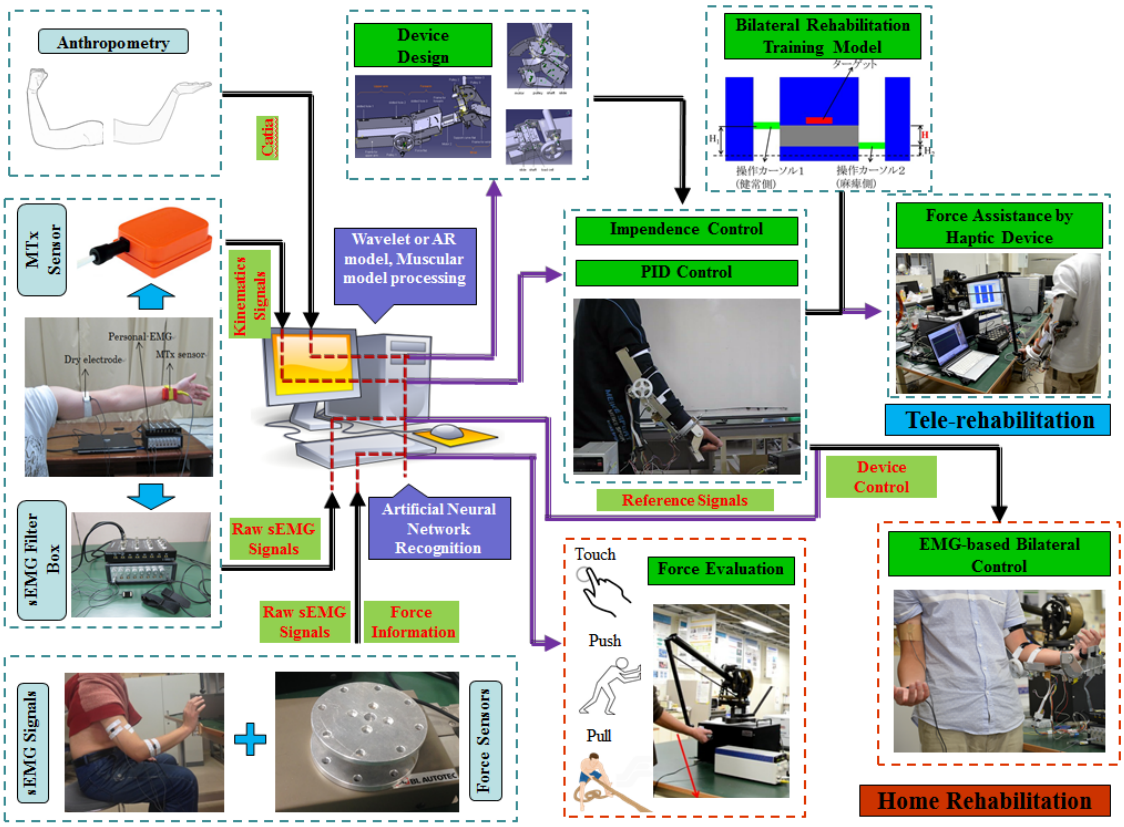

Figure. 6.1: Schematic of the entire project

The purpose of my study is to develop a home-used self-training rehabilitation system. The requirement has been discussed in Chapter 2. The schematic of this system is depicted in Fig. 6.2. The hardware is constructed mainly by a ULERD, 'Phantom Premium', EMG measurement apparatus, DSP control system, and a personal computer. The ULERD is worn by the patient to perform rehabilitation training. The haptic device 'Phantom Premium' is used to represent the force for the therapist to evaluate the training effort. EMG measurement apparatus is combined by the electrodes and a filter box. A personal computer is used to train the classifiers, and collect and save data from patients. The controller for the ULERD is the DSP system. It can communicate with personal computer to modified the parameters and transmit recorded data back to the computer. All these devices, except 'Phantom Premium', are used for patients at home.

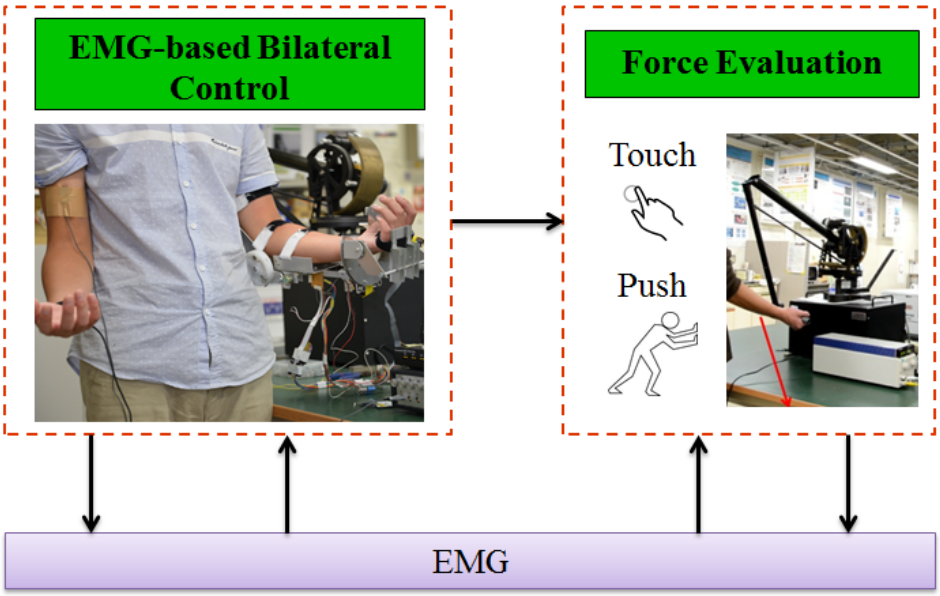

Figure. 6.2: Schematic of the proposed system

6.3 Evaluation of self-training function

6.3.1 Schematic of self-training function

In our system, the 'self-training' was achieved by following the motions of the intact arm and the motions were recognized not by motion sensors, but sEMG signals. As our ULERD can follow the target position quite well via PID control, the point is to provide as accuracy recognition results as possible. As discussed in Chapter 4 that a continuous prediction results are more acceptable than a binary-like ones, the system adopted the continuous elbow joint angle prediction method to the self-training function.

The schematic is depicted in Fig. 6.3. sEMG signals are recorded from the Biceps Brachii of the intact arm. The parameters involved in the calculation can be calibrated off-line in a personal computer, and then uploaded to the MCU, e.g., a DSP as employed in our system. The rest of the calculation can be performed in the MCU system, as the computation is not complex. All the calculation is conducted in real-time.

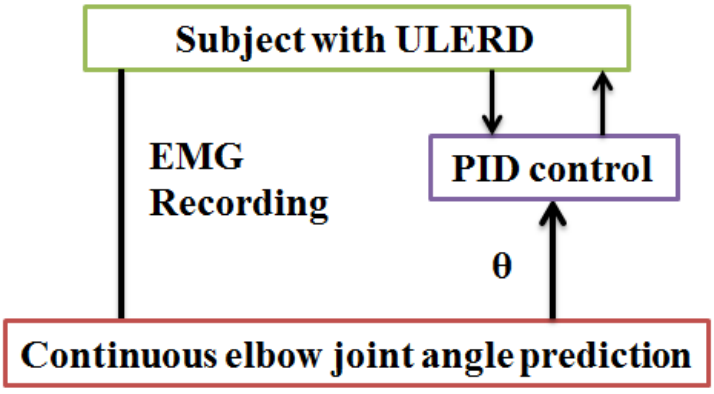

Figure. 6.3: Schematic of the self-training function

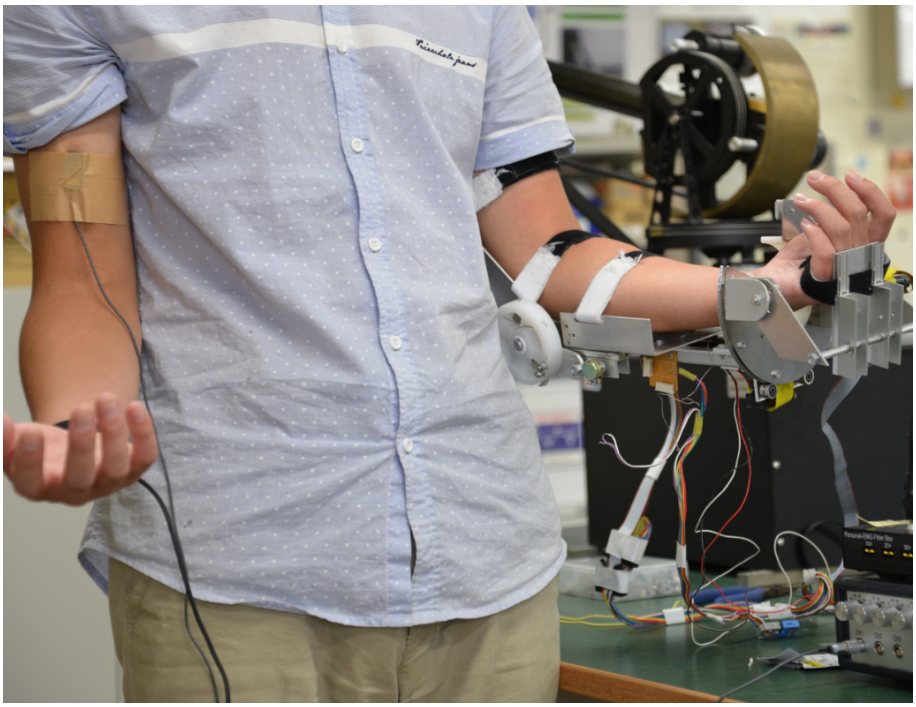

Figure. 6.4: Subject with ULERD

6.3.2 Experimental results

Five healthy subjects (age: 24.60±1.67 years, height: 1.70±0.07 m, weight: 67.66±9.54 kg, all male, right-handed) participated in the experiment. Each subject repeated the movement of elbow flexion and extension five times. The ULERD was worn on either side of their upper limbs, according to the subjects' will (as shown in Fig. 6.4). The sEMG signals were recorded from the other sides (called active side). MTx sensor was attached on the active side to record the real position of upper limb. RMS errors between prediction results and recorded ones were listed in Table 6.1, and one set of the experimental data were plotted in Fig. 6.5, where the blue solid line is the prediction results, red dashed line is the recorded results from MTx sensor and green dotted line is the angle of motor calculated via encoder.

Table 6.1 RMS errors of the on-line experiments

RMS errors	Subject				
	A	B	C	D	E
	3.10±3.10	4.10±1.31	5.31±2.11	7.12±1.31	6.11±2.03

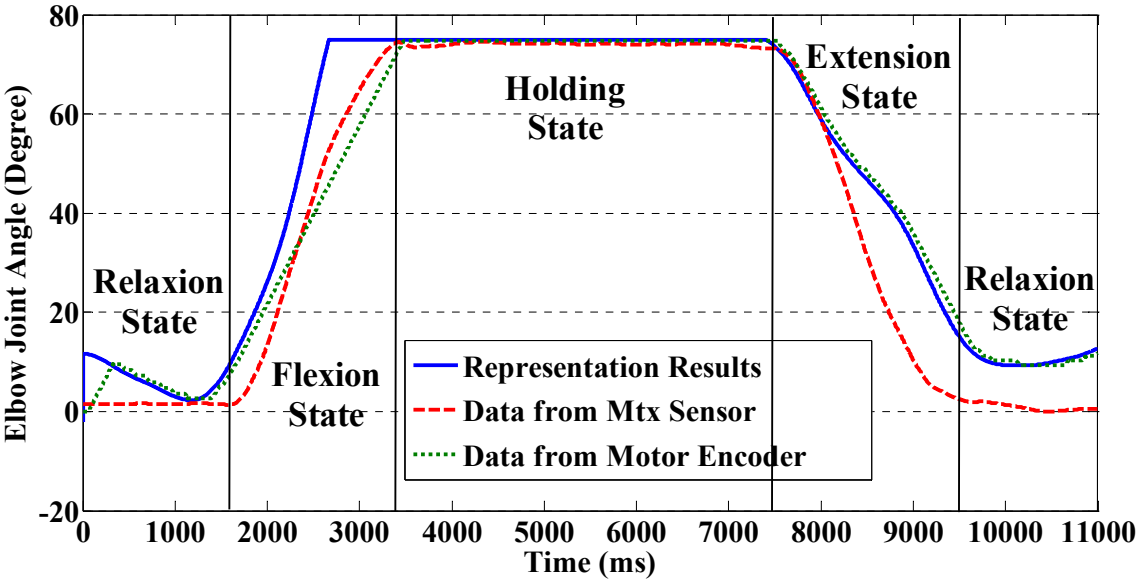

Figure. 6.5: On-line experimental results

It can be indicated from the experimental results that the motor can follow the prediction results quite well in most of the cases. However, unfitted part can be observed at the flexion state (from 2 s to 3 s). It was caused by the PID controller that the motor cannot catch the trend of the prediction results, but interestingly, followed the original elbow motion quite well (i.e. the dotted green fitted the red dashed line better than blue solid line). This phenomenon did not happen quite often. It may be given rise to the reason the PID controller was calibrated with the data recorded from MTx sensor, which represented the 'nature trend' of elbow motion.

When the prediction results are different from the 'nature trend', the controller tended to carry the motion in the original 'nature way'.

One of the issues, which has been mentioned in section 4.6.2, is that the state switching algorithm may bring time lag for prediction. In this experiment, a continuous movement test was thus performed to evaluate the affect. The experimental results are shown in Fig. 6.6. It can be indicated that the affect by state switch can be ignored.

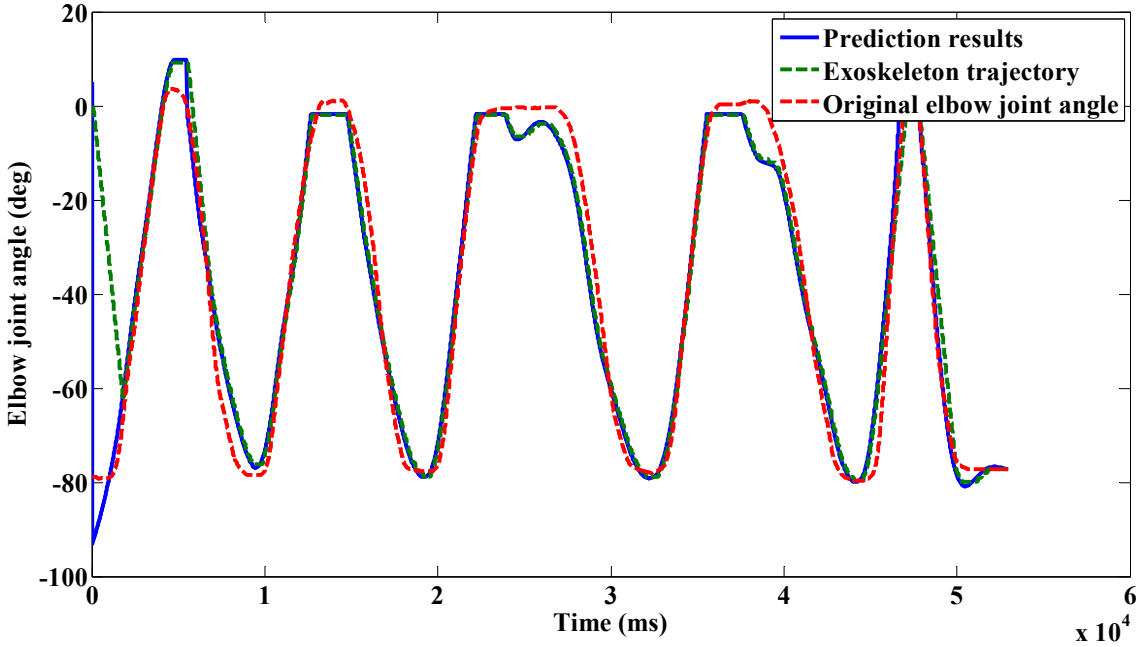

Figure. 6.6: Experimental results of continuous movement

However, another problem really effects the prediction. It is the phenomenon of time shift caused by the Butterworth filter. One set of the data processed with different order of Butterworth filter is shown in Fig. 6.7. It can be indicated that with the increasing of the order of the filter, the time shifts more backwardly. The time lag between the 1st order and 4th order is about 500 ms. The purpose of applying a low pass filter is to obtain

a smooth prediction results and also it has a biological meaning of mimic the low-pass property of muscular structures, as mentioned in Chapter 4. Although the time lag between 1st order results and the raw sEMG data is almost zero, the smooth effort is too limited to acquire a good result. Given this situation, a 2nd order Butterworth filter is recommended, but still it brings about 100 ms time delay compared with the raw EMG data. Observed from the experiment, a time delay within 100 ms affects a little, but a time delay above 300 ms will cause discordant feeling to the subject. If the time delay is above 500 ms, subjects will consider the system as no respond.

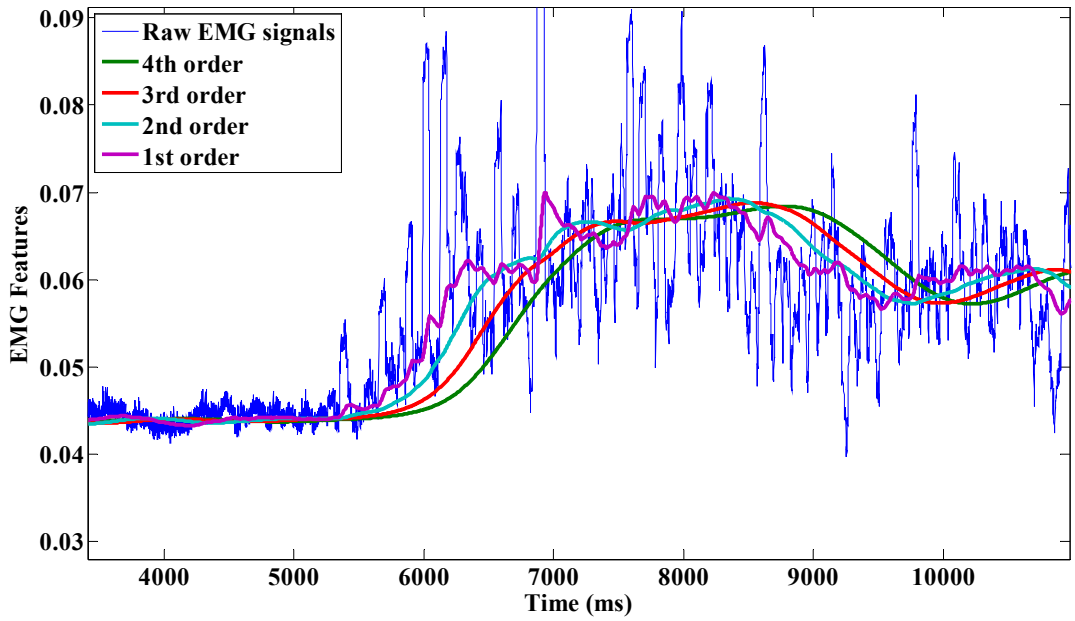

Figure. 6.7: Results with different order of Butterworth filter

The experimental results for consecutive stepping test of elbow joint angle are plotted in Fig. 6.8. As the same with in a simulation experiment, the proposed method can provide a good prediction results with the increment above 30°. For the 30° increment angle case, the prediction

results corresponded to the recorded data well and only small errors were found (with mean RMS error of 5.67°). In this case, the ULED can follow the motions of the active upper limb quickly and no obvious deviation was felt by subjects. In the 20° increment angle case, relatively large deviations or floats from the recorded elbow joint angles were observed in the data (with mean RMS error of 8.02°) and reported by subjects. Although the ULED can follow the motions of the subject's active upper limb, some trembling was sensed. For the 10° increment angle case, the deviations between prediction results and recorded ones were large (with mean RMS error of 12.99°). Only a general trend can be found from the data and obvious trembling was sensed by subjects.

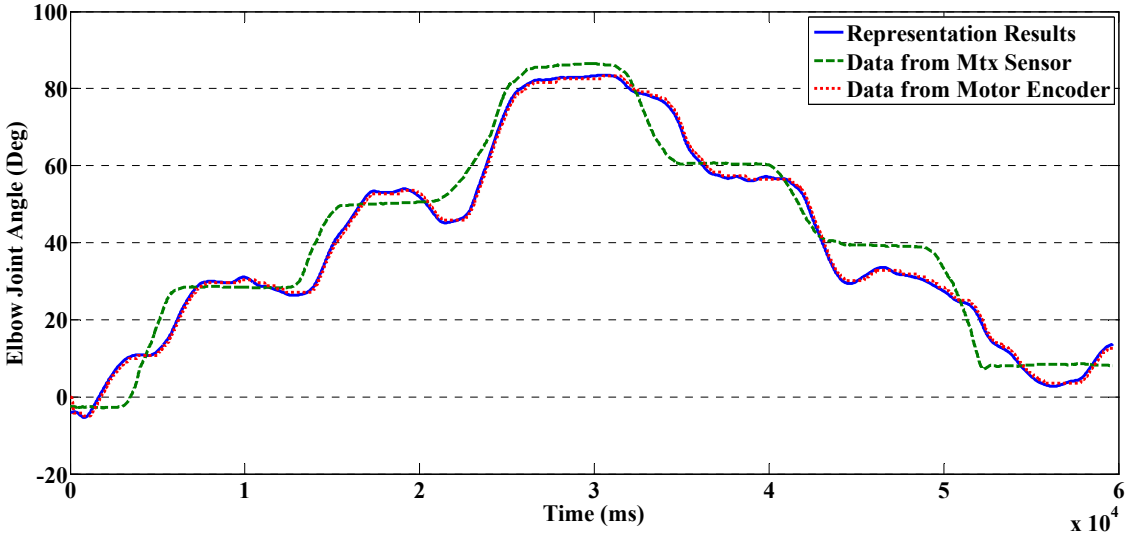

(a) Experimental results of continuous movement with increment of 30°

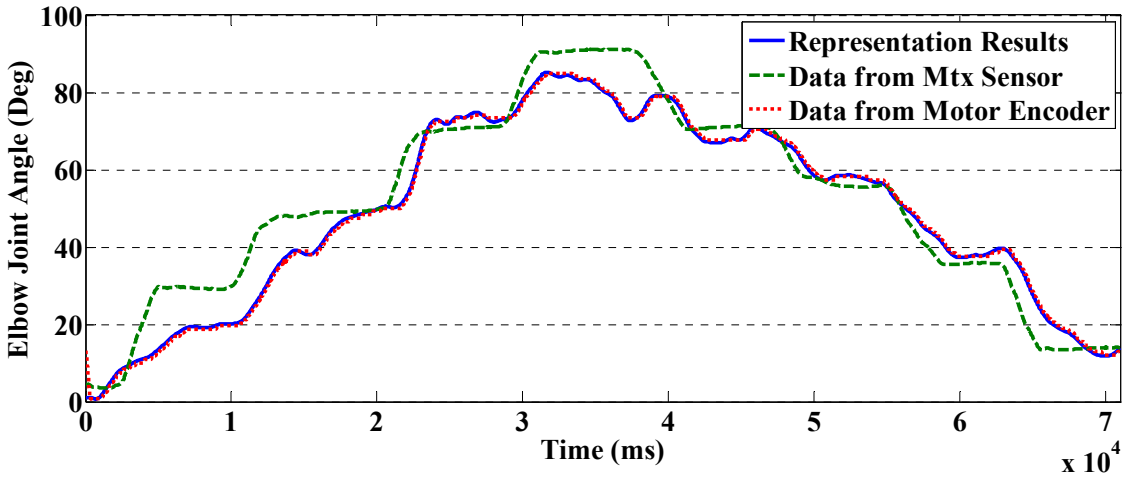

(b) Experimental results of continuous movement with increment of 20°

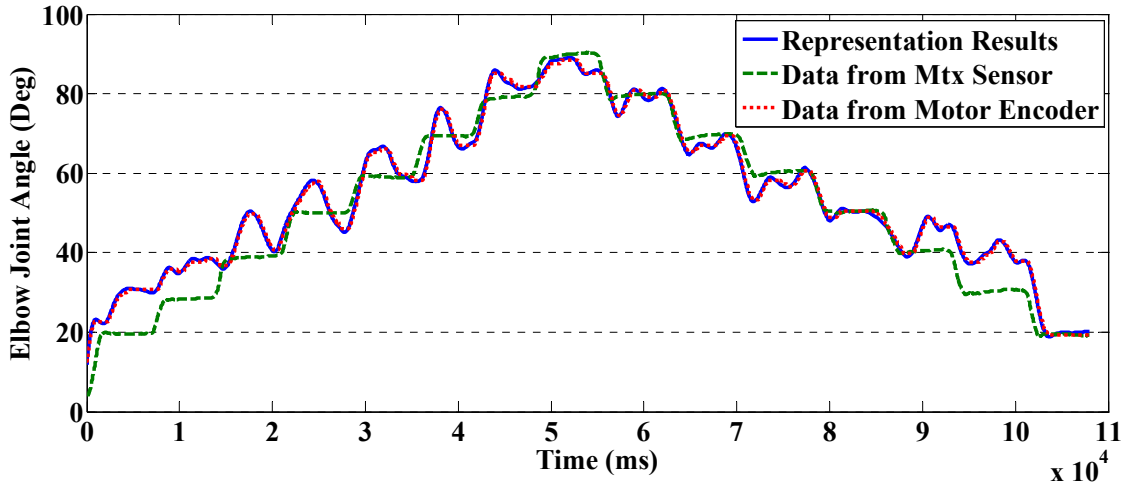

(c) Experimental results of continuous movement with increment of 10°

Figure. 6.8: Experimental results of consecutive stepping test

The evaluation experiment for self-training function shows that the proposed method is able to provide a suitable prediction results for the system to achieve the requirement of self-training at home. The method is easy to calibrated and applied on other kind of purpose, e.g., intuitive control of robot arm and human-machine interaction. It should be noticed that the continuous prediction method has been applied on elbow joint up

to now, because elbow joint is relative simple compared with the other joints of human body. With the increasing of DoFs, the dynamic function, which is approximated to be a quadratic form between sEMG signals and cosθ, may lost the straightforward expression form, especially when the musculoskeletal system involved is redundancy.

6.4 Evaluation of remote force evaluation function

6.4.1 Schematic of remote force evaluation function

The remote force evaluation function aims to solve the problem that the therapist is unable to evaluate the training effect of the patient except patient goes to the rehabilitation center. The remote force evaluation function will allow therapist to sense the contact force of the patient remotely and give effective comments to the patient. Two issues involved in this problem. The first one is the accuracy measurement of force value and the second one is the representation of the force in a remote side. A force sensor is a proper way for the first issue. However it is inconvenient to attach force sensor on the surface in some cases or it may constraint the movement of the patient. Another disadvantage to use the force sensor is that it can only measure the output value of the entire musculoskeletal system, not the performance of the individual muscles. We thus adopted EMG to predict the contact force. For the second issue, a haptic device is a suitable solution.

The schematic of the remote force evaluation function is depicted in Fig. 6.9. Two motions, i.e., downward touch motion and push motion were focused on to predict the contact force. Two musculoskeletal models with

surface muscles involved were adopted for the two motions, respectively. Dynamics equations for the two motions were developed based on the musculoskeletal models. The equations were linear combination of involved musculotendon forces. As the force exerting motion was isometric in this study, a simplified Hill-type model was developed to calculate musculotendon force for the individual muscle. In order to seek for the proper parameters or weights involved in the dynamic equations, we adopted the Bayesian linear regression (BLR). The off-line parameter calibration was needed for BLR to compute the proper parameters. As the whole movement of contact motion is complex, a motion recognition method was used to classify the different motions. When force exerting motion is detected, the well-calibrated dynamic equations will be used to predict contact force. The predicted force is represented by haptic device 'Phantom Premium' on the remote side for the observer or therapist to evaluate. The resolution of the 'Phantom' is good enough to mimic the identical contact force.

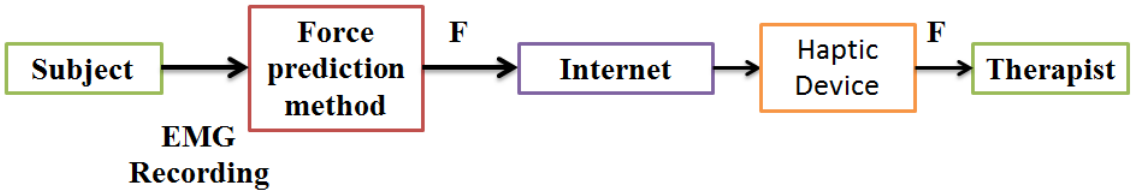

Figure. 6.9: Schematic of proposed remote force evaluation method

6.4.2 Experimental results

Five subjects (age: 26.00±1.73 years, height: 1.72±0.04 m, weight: 66.40±10.36 kg, all male, one left-handed, and four right-handed) participated in the experiment. The pre-experimental process was similar with the one which has been introduced in section 5.5.1. EMG signals were recorded from the flexor carpi radialis (FCR), the flexor carpi ulnaris (FCU), the extensor carpi radialis longus (ECRL), the extensor carpi ulnaris (ECU), the extensor digitorum (ED), the biceps brachii (BB), the triceps brachii (TB), and the pectoralis major (PM). One set of the experimental results for downward touching force prediction were listed from Table 6.2 to Table 6.4. The value is the RMS error between the prediction result and recorded one.

Table 6.2 Force prediction for 5 N group with parameters calculated from 5 N group

Test Trails	Parameter Calibration Trials									
	5.1	5.2	5.3	5.4	5.5	5.6	5.7	5.8	5.9	5.10
5.1	0.05	1.29	1.24	3.82	3.34	5.64	1.68	8.36	**2.35**	3.44
5.2	1.02	0.04	0.93	2.58	2.38	4.00	2.30	6.52	**2.37**	7.65
5.3	1.27	1.38	0.21	4.56	1.74	4.35	2.99	7.22	**1.31**	6.62
5.4	2.76	1.92	1.72	0.51	1.87	2.40	2.35	4.65	**1.80**	3.80
5.5	2.23	1.12	0.91	3.13	0.39	1.93	2.57	4.57	**1.11**	5.07
5.6	3.60	2.54	1.65	3.74	1.12	0.67	2.81	2.23	**1.92**	5.37
5.7	3.64	1.69	1.38	3.42	2.68	3.32	0.41	6.09	**1.44**	7.09
5.8	6.28	4.28	3.00	3.41	2.07	2.63	2.86	0.79	**2.72**	6.15
5.9	2.84	1.86	1.25	3.50	2.10	3.52	1.71	6.05	**1.20**	3.00
5.10	3.04	3.00	2.29	3.47	2.76	4.51	2.45	6.08	**2.40**	0.58

Table 6.3 Force prediction for 10 N group with parameters calculated from 5 N group

Test	Parameter Calibration Trials									
Trails	5.1	5.2	5.3	5.4	5.5	5.6	5.7	5.8	5.9	5.10
10.1	4.45	2.62	3.67	13.63	5.28	2.53	7.13	3.88	**2.55**	11.38
10.2	2.67	4.00	1.12	11.05	3.54	8.13	7.85	12.88	**2.06**	14.45
10.3	3.99	4.85	1.77	12.64	3.53	12.56	8.45	16.77	**2.95**	16.85
10.4	9.23	11.26	3.78	12.07	2.69	18.83	8.10	26.73	**7.56**	17.86
10.5	2.42	4.29	2.02	17.37	5.94	7.40	9.37	12.60	**2.43**	17.98
10.6	7.98	9.37	3.84	12.88	4.34	19.02	8.18	25.54	**5.60**	15.89
10.7	6.19	4.19	7.74	28.98	13.65	8.35	14.53	8.81	**3.95**	26.78
10.8	2.00	2.54	2.73	17.01	6.46	6.72	9.21	11.52	**1.53**	15.89
10.9	2.32	1.54	4.70	23.15	9.18	4.61	11.34	7.85	**2.17**	21.91
10.10	1.94	2.58	3.41	20.21	7.76	7.37	10.34	11.14	**1.60**	20.85

Table 6.4 Force prediction for 15 N group with parameters calculated from 5 N group

Test	Parameter Calibration Trials									
Trails	5.1	5.2	5.3	5.4	5.5	5.6	5.7	5.8	5.9	5.10
15.1	10.71	11.65	2.96	19.22	7.69	22.05	14.62	30.33	**5.43**	28.99
15.2	5.26	2.74	5.84	21.52	10.21	6.73	10.99	12.54	**3.25**	13.74
15.3	4.55	6.83	3.83	29.55	11.38	10.79	15.18	18.16	**3.20**	30.30
15.4	4.10	5.16	3.86	23.37	9.43	9.36	13.67	14.88	**2.10**	26.15
15.5	14.05	8.24	9.60	22.82	12.61	10.49	10.06	3.97	**6.60**	6.26
15.6	4.69	3.87	7.11	26.60	12.44	7.32	14.19	11.16	**3.90**	23.29
15.7	4.30	7.58	6.51	53.61	20.01	6.60	19.40	13.09	**4.36**	41.75
15.8	3.66	4.17	7.18	37.78	15.79	4.57	17.06	9.86	**2.93**	33.43
15.9	1.72	0.46	0.88	11.37	2.68	2.37	2.76	0.48	**1.14**	7.78
15.10	3.98	7.14	3.54	30.43	12.02	9.54	13.46	17.76	**3.77**	23.59

The subtitle in the three tables is with the form of m.n where m denotes the force group and n denotes the n trial in this group. It can be indicated that as the parameters were calibrated by 5 N group, the RMS values in diagonal elements of Table 6.2 is the smallest. BLR can guarantee

to find the optimal parameters in one special data space. However, the time-variable property of EMG signals makes it difficult or impossible to acquire a special data space which is sufficient to represent the entire data space. This kind of property can be indicated from the other groups. Some of the RMS errors from the other groups are quite large.

Given these situations, two questions come naturally. The first one is whether the different groups share the same data space. And the second one is that how long it takes to find the property parameters. The first question is essential. As shown in section 5.5.3 that, there is a constant ‘pattern’ in the trend of muscle activation levels of individual involved muscles during the contact force exerting motion. The linearity of these muscles is different. In other research results [101-103], the relation between muscle activation level and the musculotendon force was also studied and it is certainly not ‘random’. It is also reasonable that the ‘commands’ sent by the CNS are some fixed ‘patterns’. These patterns reflect certainly in the EMG signals as EMG signals are the electrical representation of the CNS commands. For the second problem, it will take only one time calibration to find the proper parameters if a suitable data space can be obtained. Actually, it is extremely luck to acquire such kind of data space at the first time. In the given situation, we tested 10 trials for each group and conducted the ‘cross-validation’ on the total 30 sets of data. Table 6.2 to 6.4 listed the results of calibration with 5 N group and tests on the whole data. The other cases are listed from Table 6.5 to 6.10. The optimal parameters are marked as red for each group. It can be indicated that the optimal ones for one

group are also the optimal ones for the other group. This case happens on the other subjects as well. With the help of computer, it takes not much time to cross-validate the results on the whole 30 sets of data. However it really takes time for the subject to perform 30 times of tests. In this case we suggest that 10 times of tests for one group are performed and then use cross-validation to find the optimal parameters. Another two tests of the other two groups, respectively, are then conducted to test the optimal parameters.

Table 6.5 Force prediction for 5 N group with parameters calculated from 10 N group

Test Trails	Parameter Calibration Trials									
	10.1	10.2	10.3	10.4	10.5	10.6	10.7	10.8	10.9	10.10
5.1	4.50	2.81	0.73	2.06	3.61	4.24	6.02	**4.22**	4.09	2.75
5.2	3.80	2.69	1.02	2.25	3.50	4.80	5.96	**4.24**	3.90	3.55
5.3	3.35	1.34	0.93	2.89	2.01	2.45	5.43	**2.67**	2.93	2.55
5.4	2.04	1.97	2.25	4.01	2.11	2.77	4.36	**2.20**	2.59	3.60
5.5	1.95	0.85	1.68	3.80	1.07	1.64	5.16	**1.62**	1.46	2.84
5.6	1.23	1.50	2.46	4.49	1.50	2.12	4.41	**1.59**	2.39	3.91
5.7	3.13	1.96	2.15	6.00	2.30	2.66	8.91	**2.67**	3.07	5.64
5.8	1.33	2.36	3.99	7.47	2.16	2.18	5.61	**1.72**	4.28	6.81
5.9	2.55	1.35	2.08	4.82	1.56	1.92	5.90	**1.98**	1.81	3.73
5.10	3.21	2.53	2.51	4.41	2.73	2.75	4.25	**2.74**	3.33	3.36

Table 6.6 Force prediction for 10 N group with parameters calculated from 10 N group

Test Trails	Parameter Calibration Trials									
	10.1	10.2	10.3	10.4	10.5	10.6	10.7	10.8	10.9	10.10
10.1	0.54	2.62	4.02	7.17	2.30	3.33	5.06	**1.91**	3.23	5.91
10.2	4.84	0.61	1.04	3.25	0.98	2.22	4.72	**1.43**	4.47	2.15
10.3	6.71	1.81	0.91	2.35	2.38	1.74	4.66	**2.33**	6.31	3.45
10.4	12.51	4.23	3.39	0.97	5.20	1.94	10.33	**5.76**	11.97	7.67
10.5	4.79	1.20	1.69	4.42	0.96	2.96	6.24	**1.20**	3.78	1.91
10.6	11.45	4.08	2.59	2.33	4.90	0.86	8.35	**4.70**	9.89	5.82
10.7	4.72	7.39	6.55	8.93	7.35	7.55	1.92	**6.31**	5.35	6.63
10.8	3.88	1.91	2.46	5.81	1.40	2.88	6.22	**0.75**	2.11	2.46
10.9	2.03	3.82	3.72	6.08	3.34	3.84	3.18	**2.53**	1.06	2.76
10.10	3.71	2.71	2.56	4.40	2.29	3.11	3.56	**1.72**	2.76	1.35

Table 6.7 Force prediction for 10 N group with parameters calculated from 15 N group

Test Trails	Parameter Calibration Trials									
	10.1	10.2	10.3	10.4	10.5	10.6	10.7	10.8	10.9	10.10
15.1	12.23	3.06	2.43	2.47	3.91	4.35	4.37	**3.45**	12.63	8.61
15.2	4.45	5.30	5.95	12.08	4.80	5.91	10.31	**3.59**	3.61	8.45
15.3	6.70	3.01	2.42	5.75	2.33	5.11	6.18	**1.68**	5.43	2.39
15.4	4.94	2.95	2.88	5.37	2.23	4.92	3.39	**1.61**	4.45	3.16
15.5	5.19	9.37	10.64	19.05	9.12	8.72	11.30	**6.80**	12.80	18.52
15.6	4.41	6.48	6.30	9.97	6.02	6.97	4.75	**4.99**	3.86	6.01
15.7	5.40	5.93	3.92	9.39	5.57	6.78	11.57	**3.63**	4.25	4.40
15.8	3.22	6.50	5.42	8.90	6.06	7.51	4.65	**4.88**	3.14	4.56
15.9	0.30	0.16	0.40	1.99	0.07	1.39	4.58	**0.96**	0.45	1.26
15.10	7.16	3.07	2.66	8.61	2.54	5.30	11.43	**1.76**	4.49	3.79

Table 6.8 Force prediction for 5 N group with parameters calculated from 15 N group

Test	Parameter Calibration Trials									
Trails	15.1	15.2	15.3	15.4	15.5	15.6	15.7	15.8	15.9	15.10
5.1	6.78	7.24	3.28	6.64	7.07	3.37	1.92	2.24	16.21	**3.26**
5.2	7.31	7.24	3.56	6.64	6.46	3.39	1.68	2.39	11.33	**3.49**
5.3	6.13	5.32	2.16	4.94	5.46	3.04	2.57	2.36	14.82	**2.04**
5.4	5.81	3.92	2.71	4.13	4.80	1.94	1.68	1.47	9.62	**1.83**
5.5	4.73	3.36	1.58	3.72	4.29	2.67	1.61	1.70	7.48	**1.64**
5.6	5.33	2.39	2.45	2.99	3.44	2.06	1.69	1.67	7.36	**1.59**
5.7	8.98	4.00	2.83	5.91	7.81	5.46	2.19	3.19	13.12	**3.14**
5.8	8.00	2.10	3.79	1.91	3.09	2.78	2.00	1.87	5.46	**1.63**
5.9	6.44	3.68	2.01	4.60	6.13	3.29	2.29	2.31	14.30	**1.95**
5.10	5.43	4.20	2.85	3.88	5.03	1.86	2.19	1.83	12.44	**2.11**

Table 6.9 Force prediction for 10 N group with parameters calculated from 15 N group

Test	Parameter Calibration Trials									
Trails	15.1	15.2	15.3	15.4	15.5	15.6	15.7	15.8	15.9	15.10
10.1	9.23	2.01	3.90	1.61	2.45	2.63	3.86	2.79	11.37	**2.30**
10.2	3.62	5.43	1.43	3.02	3.42	1.95	4.26	1.74	26.97	**1.56**
10.3	2.97	6.88	2.48	3.79	6.05	1.65	4.76	1.74	27.08	**1.40**
10.4	3.09	11.99	6.09	7.59	9.01	5.74	2.87	5.11	51.65	**3.44**
10.5	5.55	4.83	1.36	2.64	3.24	3.01	4.23	2.39	30.99	**1.86**
10.6	2.95	9.67	4.36	6.58	9.54	4.18	4.03	3.47	44.55	**2.16**
10.7	9.70	5.76	6.36	6.33	7.78	3.21	6.68	4.12	20.10	**5.14**
10.8	6.49	3.29	1.59	2.06	3.69	2.64	3.98	1.82	26.08	**1.50**
10.9	6.10	1.26	2.61	2.14	3.59	2.72	5.05	3.04	17.94	**3.12**
10.10	3.94	3.07	1.46	1.75	3.09	2.00	4.64	2.44	21.77	**2.42**

Table 6.10 Force prediction for 15 N group with parameters calculated from 15 N group

Test	Parameter Calibration Trials									
Trails	15.1	15.2	15.3	15.4	15.5	15.6	15.7	15.8	15.9	15.10
15.1	1.60	10.40	4.67	4.39	6.44	2.52	8.67	2.30	57.95	**3.16**
15.2	15.96	2.20	5.75	2.92	6.16	5.37	4.14	3.39	35.60	**3.33**
15.3	6.41	4.81	1.60	1.96	3.29	2.53	5.85	2.20	46.72	**2.95**
15.4	5.24	3.84	1.73	0.97	1.96	2.58	6.71	2.63	37.03	**3.34**
15.5	25.24	8.39	12.09	3.11	1.80	5.92	2.36	2.85	23.56	**3.22**
15.6	10.84	3.43	5.52	4.01	4.66	3.15	6.13	3.72	29.53	**4.93**
15.7	12.57	3.55	3.96	3.11	5.40	6.32	1.74	5.81	60.40	**2.35**
15.8	10.05	3.09	4.86	4.24	5.64	2.67	5.34	2.73	39.47	**4.73**
15.9	1.03	1.50	0.33	1.94	1.09	3.11	2.17	2.63	0.02	**1.86**
15.10	12.29	4.32	2.57	2.73	4.33	6.15	2.41	4.75	55.58	**1.48**

The relative RMS errors for the five subjects are within 20% and this error exists in the entire tests data, i.e., it is more like a constant value rather than an average one. As some muscles involved are at the deep layer, it is impossible to record the accuracy EMG signals from these muscles. The constant 20% errors may be caused by the undetected muscles. Another reason may be given rise to the muscular model. Although Hill-type model is a classic and conventional model for muscle, it is not accuracy enough. On the other hand, many approximations were assumed during the dynamic equation development. All of these bring uncertainty to the results and cause the constant 20% error.

Another important issue is the adoption of proportion smooth algorithm (5-12) which is used to address the problem of force impact caused by the resolution of motion recognition classifier. The resolution of

the classifier defined in this thesis is the time delay between a motion sensor (MTx sensor) detected starting point and the classifier detected starting point for a special movement. According to the experimental results of motion recognition, the resolution is about 100-200ms. That is to say the classifier cannot detect the motion as soon as it happens. However the EMG signals go on as well. This give rise to one problem that when classifier detects the motion and then informs the controller to calculate the contact force, the force is already so high that it is not continuous from the previous time point. That is the reason for the force impact on the remote side. The proportion smooth algorithm increases the force generation time manually with the trade-off of accuracy. As the algorithm only spreads the 'impact' within 100ms, the trade-off is acceptable and the effort of eliminating the impact feeling is helpful for mimicking the original contact force.

The experimental results prove the efficiency of the proposed remote force evaluation function for our rehabilitation system, which will help the therapist to supervise the patient more efficiently.

6.5 Summary

In this chapter, the evaluation for the entire system was conducted. Testing experiments were performed for self-training function and remote force evaluation function. The experimental results coincided with the simulation results in the corresponded chapter, respectively. The self-training function, which was achieved by extraction of reference command signals from EMG signals of the intact arm for the ULERD worn

on the impaired arm, provided a bilateral rehabilitation training function allowed patient to perform the training exercise under the willing of their own without the supervision of therapist. The prediction results with RMS lower than 10° show that the proposed method can provide suitable control effect for the self-training purpose. The remote force evaluation function, which was achieved by using only EMG signals, allows the therapist to evaluate the training effect remotely. This will benefit both the therapists and patients.

Additionally, some issues involved in these methods were also discussed in order to address the problems more clearly and provide some ideas for the similar problems.

Chapter 7 Concluding Remarks

7.1 Thesis summary

Stroke is the second leading cause of disability, which wildly affects peoples' Activities of Daily Living (ADL) and the life style of their families. The tremendous contradiction is the large demand for special clinical care and the limited number of therapists. The purpose of the proposed system is to provide home-used self-training rehabilitation for stroke patients.

Our previous developed Upper-limb Exoskeleton Rehabilitation Device (ULERD) was designed to be portable to guarantee the capability to be used at home. The 'self-training' property was achieved by the proposed bilateral training method, in which the impaired arm was carried by ULERD and the control signals were extracted from the EMG signal from the intact arm. The proposed system also provides remote force evaluation function for therapist to evaluate the training effect of the patient remotely. This function allows the therapist supervises and gives suggestion to patient efficiently, without meeting the patient face to face.

To accurately extract motion information from sEMG signals, we first adopted a motion recognition based method. The Autoregressive (AR) model was applied to extract the features from the sEMG signals and a Neural Network (NN) classifier was trained to recognize the motions. The parameters involved in the AR model were decided by AIC criterion and the recognition results were processed by an experiential method to acquire

the final control command to the ULERD. As the recognition accuracy rate was not good enough and the results were unstable, a Hill-type muscular model based feature extraction method and a Support Vector Machine (SVM) was applied to improve the recognition results. The recognition accuracy rate increased from 85% to 96%.

In order to address the drawback of the motion recognition based method that it can only provide binary-like control reference to the device, a continuous elbow joint angle prediction method was proposed. In this method, a quantitative relation between sEMG signals and elbow joint angle was developed based on the Hill-type based muscular model and our proposed simplified musculoskeletal model of elbow joint in sagittal plane. After some approximation, a quadratic-like equation was found and validated by a four-day experiment on ten subjects. Furthermore, a state switch model was developed to solve the problem of time-variable of sEMG signals. The experimental results showed that the proposed method can provide a prediction results with RMS errors below 10°.

For the purpose of remote force evaluation, a force prediction method using only sEMG signals was designed. As the complex of musculoskeletal structure, isometric downward touch motion and push motion were focused on in this study. Two musculoskeletal models were used to represent the two motions, respectively. The dynamic equations were yielded based on the combination of Hill-type based muscular model and the proposed musculoskeletal models. The motions were recognized by a NN classifier and the desired forces were calculated by the dynamic equations when the

force exerting motion was detected. The force representation was achieved by a haptic device ‘Phantom Premium’ which is a high fidelity device for sensation generation. The experimental results show that the proposed method can predict the contact force with relative RMS errors within 20%.

The entire system was evaluated for the self-training function and remote force evaluation function, respectively, at the last of this thesis. The experimental results indicated that the self-training function supported by the proposed continuous elbow joint angle prediction method is suitable to allow patients to perform the rehabilitation training by themselves. The remote force evaluation function is also sufficient to allow the therapist to evaluate the training effect of the patient.

7.2 Research achievement

(1) Design of the bilateral rehabilitation training based on EMG signals.

The proposed bilateral rehabilitation training aims to allow patient to train his/her impaired arm with the intact arm. In this training, patient performs bilateral movement with both of the arms. The impaired arm wears our developed ULERD under the direction of the intact arm to complete the same movement. In this way, the patients can complete the training exercise by themselves under the wills of their own. The new point here is that we extract the control signals from the sEMG signals which reflect the intention of patients, not just movement. From the neurorehabilitation point of view that the training effort will be better if the motion is inspired by neuro system, not just passive motion following. The system, with our proposed method, can help patients to move their

impaired arms under the control of the neuro system, i.e., by the control command from the EMG signals.

(2) Development of continuous elbow joint angle prediction method using only sEMG signals.

The proposed method aims to address the drawback of the motion recognition method that it can only provide binary-like reference control signals. Pattern recognition based methods have been studied widely around the world. However, the continuous prediction type is seldom proposed. In this study, we combined the Hill-type based muscular model and a simplified elbow joint musculoskeletal model to yield the mathematic expression between sEMG signals recorded from Biceps Brachii and the elbow joint angle. As many parameters involved in the Hill-type based muscular model, some approximations were assumed for simplification. The modified dynamic equation released quadratic-like relation between muscle activation level, which can be calculated from sEMG signals, and the cosθ. Although the situation of elbow joint is relative simple compared with the other joints, this kind of method introduces an alternative way to use EMG signals to predict motions or joint angles.

(3) Force prediction using only EMG signals.

The relationships between musclotendon force and EMG signals have been widely studied. However, seldom focus has been paid on using EMG signals to predict the contact force between human and environment. Although the EMG signal is heavily unstable and time-variable, it has potential to represent the individual muscle status and predict the contact

force even it is very hard to attach force sensor on the contact surface. In order to avoid the complex of redundancy of musculoskeletal structure, a motion recognition method was adopted to classify the different force exerting motions and the period of force exerting. This method combined with a haptic device can form a remote force evaluation system. This kind of system also can mimic the true contact motion between human and human in virtual-reality.

(4) Found of relation between motion recognition and different classification method.

We compared different classification method and feature extraction method to find the relation between them. The experimental results indicated that using the feature processed with a low-pass filter with cut-off frequency with 4 to 10 Hz will make the recognition better than direct using the feature extraction results for classifier training. Furthermore, it is found that the Support Vector Machine (SVM) performs better than Neural Network (NN) in real-time test, while the time consumption is much higher than NN. The reason is that SVM uses massive support vectors to represent the boundary for different motions while the number of parameters involved in NN is constant. Using the low-pass filter processing will reduce the support vectors as well.

7.3 Recommendations for the future

Motion recognition using EMG signals is a compelling topic which will bring benefit to many application fields. However, seldom applies have been sighted outside laboratory environment. The non-stationary,

time-variable and easily affected properties are the primary reasons that prevent the application. Feature extraction plays an important role in this issue. The ideal feature extraction method is the one that can avoid the effect by the external factors and extract the expected features ignoring the non-stationary and time-variable. On the other hand, the concept of muscle synergy could be used for this issue. The muscle synergy releases the relation between EMG signals changing and the command trend from the CNS. There are some constant behavers in the muscle synergy for the same motions. Up to now, only downward touch motion and push motion have been studied. Other types of motions are recommended, such as poll motion and the gait motion. In gait motion, this kind of method may be used to predict the interaction force from the ground.

For the home-used rehabilitation system, a human-like arm for the therapist side is recommended. Actually, a very simple prototype is being designed in our group. This kind of device will be designed to own the ability to mimic the status of real human arm, which will help the therapist more to estimate the rehabilitation effort of the patient.

References

[1]. http://www.world-heart-federation.org/cardiovascular-health/stroke/

[2]. J. H. Carr, R. B. Shepherd, editors. Movement Science: Foundations for Physical Therapy in Rehabilitation. Rockville, MD:Aspen; 1987.

[3]. J. A. Kleim, E. Lussnig, E. R. Schwarz, T. A. Comery and W. T. Greenough. Synaptogenesis and FOS expession in the motor cortex of the adult rat after motor skill learning, *J. Neurosci*, Vol.16, pp.4529-4535, 1996.

[4]. F. W. George, R. Chen, K. Ishii, K. Obushara, S. Eckloff, E. Croarkin, E. Taub, L. H. Gerber, M. Hallett and L. G. Cohen. Constraint-induced therapy in stroke: Magnetic-stimulation motor maps and cerebral activation, *Neurorehabl. Neural Repair.*, Vol.17, pp.48-57, 2003.

[5]. B. H. Dobkin, D. Apple, H. Barbeau, M. Basso, A. Behrman, D. Deforge, J. Ditunno, G. Dudley, R. Elashoff, L. Fugate, S. Harkema, M. Saulino and M. Scott. Methods for a randomized trial of weight-supported treadmill training versus conventional training for walking during inpatient rehabilitation after incomplete traumatic spinal cord injury, *Neurorehabil. Neural Repair*, Vol.17, pp.152-67, 2003.

[6]. S. J. Page. Intensity versus task-specifity after stroke: how important is intensity? Am J. *Phys Med Rehabi.*, Vol. 82, pp.730-732, 2003

[7]. J. Furusho, K. Koyanagi, Y. Imada, Y. Fujii, et al. A 3-D

rehabilitation system for upper limbs developed in a 5-year NEDO project and its clinical testing. *Proceedings of the 2005 IEEE 9th International Conference on Rehabilitaiton Robotics*, pp.53-56. 2005.

[8]. P. S. Lum, C. G. Burgar, M. V. Loos, et al. MIME robotic device for upper-limb neurorehabilitation in subacute stroke subjects: A follow-up study. *J. Rehabil. Res. Dev.*, Vol. 43, pp 631-642, 2006.

[9]. R. E. Schleenbaker, and A. G. Mainous. Electromyographical biofeedback for neuromuscular re-education in the hemiplegic stroke patient: a meta-analysis, *Arch. Phys. Med. Rehabil.*, 74, pp. 1301-1304, 1993.

[10]. L. SONDE, C. Gip, S. E. Fernaeus, C. G. Nilsson, and M. Vitanen. Stimulation with low frequency (1.7Hz) transcutaneous electric nerve stimulation (low-tens) increases motor function of the post-stroke paretic arm, *J. Rehabil. Med.*, Vol. 30, pp. 95-99, 1998.

[11]. J. W. Krakauer. Motor learning: its relevance to stroke recovery and neurorehabilitation. *Current opinion in neurology*, Vol. 19, pp 84-90, 2006.

[12]. G. Kwakkel, B. J. Kollen, and R. C. Wagenaar. Long term effects of upper and lower limb training after stroke: a randomised trial, *J. Neurol. Neurosurg. Psychiat.*, Vol. 72, pp. 473-479, 2002.

[13]. H. Kwee, J. Duimel , J. Smit, A. T. Mold, J. Woerden, and L. V. D. Kolk. The manus wheelchair-mounted manipulator: developments toward a production model. *Proc. 3rd Int. Conf. Assoc. Advancement Rehab. Technol.*, pp. 460-462, 1988.

[14]. L. Leifer. Rehabilitive robotics, *Robot Age*, pp. 4-11, 1981.

[15]. V. D. Loos, H. F. M. Michalowski, and J. L. Leifer. Development of an omnidirectional mobile vocational assistant robot. *Proc. 3rd Int. Conf. Assoc. Advancement Rehab. Technol.*, pp. 468-469, 1988.

[16]. N. Hogan, H. I. Krebs, A. Sharon, and J. Charnnarong. Interactive robotic therapist. U.S. Patent, 5466213, 1995.

[17]. H. I. Krebs, N. Hogan, M. L. Aisen, and B. T. Volpe. Robot-aided neurorehabilitation, *IEEE Trans. Rehab. Eng.*, Vol. 6, pp. 75-87, 1998.

[18]. T. Nef, R. Riener. ARMin – design of a novel arm rehabilitation robot. *Proceedings of the 2005 IEEE 9th International Conference on Rehabilitation Robotics*, pp. 57-60, 2005.

[19]. T. Nef, M. Mihelj, R. Riener. ARMin: a robot for patient-cooperative arm therapy. Med. Bio. Eng. Comput., Vol. 45, pp. 887-900, 2007.

[20]. P. S. Lum, C. G. Burgar, V. Loos, P. C. Shor, M. Majmundar, R. Yap. The MIME robotic system for upper-limb neuro-rehabilitation: results from a clinical trial in subacute stroke. *Proceedings of the 2005 IEEE 9th International Conference on Rehabilitation Robotics*, pp. 511-514, 2005.

[21]. C. Beurskens, P. Heymans. Mime therapy improves facial symmetry in people with long-term facial nerve paresis: A randomised controlled trial. Aust, J. Physiother., Vol. 52, pp. 177-183, 2006.

[22]. R. Riener, T. Nef, G. Colombo. Robot-aided neurorehabilitation of the upper extremities. *Med. Biol. Eng. Comput.*, Vol 43, pp. 2-10,

2005.

[23]. M. Zinn, B. Roth, O. Khatib, and J. K. Salisbury. A new actuation approach for human friendly robot design, *Int. J. Robot. Res.*, Vol. 23, pp. 379-398, 2004.

[24]. N. Hogan. Impedance control: An approach to manipulation: Part II – Implementation. *J. Dyn. Sys., Meas., Control.*, Vol 107, pp. 17-24, 1985.

[25]. V. G. Popescu, G. C. Burdea, M. Bouzit, V. R. Hentz. A virtual-reality-based telerehabilitation system with force feedback. *IEEE T. Inf. Technol. B.*, Vol. 4, pp. 45-51, 2000.

[26]. D. Jack, R. Boian, A. S. Merians, M. Tremaine, G. C. Burdea, S. V. Adamovich, M. Recce, H. Poizner. Virtual reality-enhanced stroke rehabilitation. *IEEE T. Neur. Sys. Reh.*, Vol. 9, pp. 308-318, 2001.

[27]. A. Henderson, N. Korner-Bitensky, M. Levin. Virtual reality in stroke rehabilitation: A systematic review of its effectiveness for upper limb motor recovery. Top. Stroke. Rehabil., Vol. 14, pp. 52-61, 2007.

[28]. C. J. Luca. The Use of Surface Electromyography in Biomechanics, *J. of Appl. Biomech.*, Vol.13, pp. 1-38, 1997.

[29]. D. Stashuk, EMG signal decomposition: how can it be accomplished and used, *J. Electromyogr. Kines.*, Vol.11, pp. 151-173, 2001.

[30]. T. S. Buchanan, D. G. Lloyd, K. Manal and T. F. Besier. Neuromusculoskeletal modeling: estimation of muscle forces and joint moments and movements from measurements of neural command, *J. Appl. Biomech.*, Vol. 20, pp. 367-395, 2004.

[31]. D. G. Lloyd, T. F. Besier. An EMG-driven musculoskeletal model for estimation of the human knee joint moments across varied tasks. *J. Biomech.*, Vol. 36, pp. 765-776, 2003.

[32]. D. G. Lloyd, T. S. Buchanan. A model of load sharing between muscles and soft tissues at the human knee during static tasks. Journal of Biomechanical Engineering, Vol. 118, pp. 367-376, 1996.

[33]. K. Manal, R. V. Gonzalez, D. G. Lloyd, T. S. Buchanan. A real-time EMG driven virtual arm. *Comput. Biol. Med.,* Vol. 32, pp. 25-36, 2002.

[34]. O. Fukuda, T. Tsuji and A. Otsuka. A human-assisting manipulator teleoperated by EMG signals and arm motions, *IEEE T. Robot. Autom.*, Vol. 19, pp. 210-222, 2003.

[35]. M. V. Liarokapis, P. K. Artemiadis, P. T. Katsiaris, K. J. Kyriakopoulos and E. S. Manolakos. Learning human reach-to-grasp strategies: towards EMG-based control of robotic arm-hand systems, *Proc. IEEE Int. Conf. Robot.*, 2287-2292, 2012.

[36]. P. K. Artemiadis and K. J. Kyriakopoulos, A switching regime model for the EMG-based control of a robot arm, *IEEE T. Syst. Man CY. B.*, 41: 53-63, 2009.

[37]. Z. Ju, G. Ouyang, M. Wilamowska-Korsak, et al. Surface EMG Based Hand Manipulation Identification Via Nonlinear Feature Extraction and Classification. IEEE SENSORS JOURNAL, Vol 13, pp 3302-3311, 2013.

[38]. A. F. Huxley. Muscle structure and theories of contraction. *Progr.*

Biophys. Biophys. Chem., Vol. 7, pp. 255-318, 1958.

[39]. A. F. Huxley and R. M. Simmons. Proposed mechanism of force generation in striated muscle. *Nature*, Vol. 233, pp. 533-538, 1971.

[40]. A. V. Hill. The heat of shortening and the dynamic constants of muscle. *Proc. Roy. Soc. Lond. B. Biol. Sci.*, Vol. 126, pp. 136-195, 1938.

[41]. E. Cavallaro, J. Rosen, J. C. Perry, S. Burns and B. Hannaford. Hill-based model as a myoprocessor for a neural controlled powered exoskeleton arm -parameters optimization. *Proc. IEEE Int. Conf. Robotics & Automation*, 4525-4530, 2005.

[42]. K. Manal, R. V. Gonzalez, D. G. Lloyd and T. S. Buchanan. A real-time EMG-driven virtual arm. *Comput. Biol. Med.*, Vol. 32, pp. 25-36, 2002.

[43]. C. Fleischer, G. Hommel. A Human–Exoskeleton Interface Utilizing Electromyography. *IEEE T. Robot.*, Vol. 24, pp. 872-882, 2008.

[44]. T. Lenzi, S. M. M. Rossi, N. Vitiello, et al. Intention-Based EMG Control for Powered Exoskeletons. *IEEE T. BIO-MED. ENG.,* Vol. 59, pp. 2180-2190, 2012.

[45]. S. Kwon, Y. Kim, J. Kim. Movement Stability Analysis of Surface Electromyography-Based Elbow Power Assistance. *IEEE T. BIO-MED. ENG.,* Vol. 61, pp. 1134-1142, 2014.

[46]. A. Ajoudani, N. Tsagarakis, A. Bicchi. Tele-impedance: Teleoperation with impedance regulation using a body–machine interface. *Int. J. Robot. Res.*, Vol. 31, pp. 1642-1655, 2012.

[47]. X. Chen and Z. J. Wang. Pattern recognition of number gestures based on a wireless surface EMG system. *Biomed. Signal. Proces.*, Vol. 8, pp. 184-192, 2013.

[48]. X. Tang, Y. Liu, C. Lv and D. Sun. Hand motion classification using a multi-channel surface electromyography sensor. *Sensors*, Vol. 12, pp. 1130-1147, 2012.

[49]. A. Phinyomark, F. Quaine, S. Charbonnier, C. Serviere, F. Tarpin-Bernard and Y. Laurillau. A feasibility study on the use of anthropometric variables to make muscle-computer interface more practical. *Eng. Appl. Artif. Intell.*, Vol. 27, pp. 1681-1688, 2013.

[50]. L. Lucas, M. DiCicco, and Y. Matsuoka. An EMG-controlled hand exoskeleton for natural pinching. *J. Robot. Mechatron.*, Vol. 16, pp. 482-488, 2004.

[51]. P. Wojtczak, T. G. Amaral, O. P. Dias, A. Wolczowski and M. Kurzynski. Hand movement recognition based on biosignal analysis. *Eng. Appl. Artif. Intell.*, Vol. 22, pp. 608-615, 2008.

[52]. N. Bu, M. Okamoto and T. Tsuji. A hybrid motion classification approach for EMG-based human-robot interfaces using bayesian and neural networks. *IEEE T. Robot.*, Vol. 25, pp. 502-511, 2009.

[53]. E. A. Clancy, and N. Hogan. Single site electromyograph amplitude estimation. *IEEE T. Bio-Med. Eng.*, Vol. 41, pp. 159-167, 1994

[54]. E. A. Clancy. Electromyogram amplitude estimation with adaptive smoothing window length. *IEEE T. Bio-Med. Eng.*, Vol. 46, pp. 717-729, 1999.

[55]. C. J. Luca, L. D. Gilmore, M. Kuznetsov, et al. Filtering the surface EMG signal: Movement artifact and baseline noise contamination. J. Biomech., Vol. 43, pp. 1573-1579, 2010.

[56]. Z. Song, S. Guo, Y. Fu. Development of an upper extremity motor function rehabilitation system and an assessment system. *Int. J. Mechatronics and Automation*, Vol 1, pp. 19-28, 2011.

[57]. Z. Song, S. Guo. Development of a new compliant exoskeleton device for elbow joint rehabilitation. *Proceeding of the 2011 IEEE/ICME International Conference on Complex Medical Engineering*, pp. 647-654, 2011.

[58]. Z. Song, S. Guo, N. Xiao, L. Shi, B. Gao. Implementation of human-machine synchronization control for active rehabilitation using an inertia sensor, *Sensors*, Vol. 12, pp. 16046-16059, 2012.

[59]. Z. Song, S. Guo. Study on impedance generation using an exoskeleton device for upper-limb rehabilitation, *Proceedings of 2012 IEEE International Conference on Multisensor Fusion and Integration for Intelligent Systems*, pp. 281-286, 2012.

[60]. C. Cipriani, C. Antfolk, C. Balkenius, B. Rosén, G. Lundborg, M. Carrozza, and F. Sebelius. A novel concept for a prosthetic hand with a bidirectional interface: A feasibility study," IEEE Trans. Biomed. Eng., vol. 56, no. 11, pp. 2739-2743, Nov. 2009.

[61]. A. Arieta, H. Yokoi, T. Arai, and W. Yu. Study on the effects of electrical stimulation on the pattern recognition for an EMG prosthetic application. *Proc. IEEE Int. Conf. Eng. Med. Biol. Soc.*, pp.

6919-6922, 2006.

[62]. D. Zhang, X. Chen, S. Li, P. Hu, and X. Zhu. EMG controlled multifunctional prosthetic hand: Preliminary clinical study and experimental demonstration. *Proc. IEEE Int. Conf. Robot. Autom.*, pp. 4670-4675, 2011.

[63]. P. R. Cavanagh, P. V. Komi. Electromechanical delay in human skeletal muscle under concentric and eccentric contractions. *Eur. J. Appl. Physiol.* Vol. 42, pp. 159-163, 1979.

[64]. M. B. I. Reaz, M. S. Hussain, and F. Mohd-Yasin. Techniques of EMG signal analysis: detection, processing, classification and applications. *Biomedical and Life Sciences*, Vol. 8, pp. 11-35, 2006.

[65]. M. Pang, S. Guo, and Z. Song. Study on the sEMG driven upper limb exoskeleton rehabilitation device in bilateral rehabilitation. *Journal of Robotics and Mechatronics*, Vol. 24, No. 4, pp. 585-594, 2012.

[66]. W. S. McCulloch, W. Pitts. A logical calculus of the ideas immanent in nervous activity. *B. Math. Biophys.*, Vol. 5, pp. 115-133, 1943.

[67]. B. Widrow, M. E. Hoff. Adaptive switching circuits. Ire Wescon Convention record, Vol. 4, pp. 96-104, 1960.

[68]. C. V. Malsburg. F. Rosenblatt: Principles of neuraldynamics: perceptrons and the theory of brain mechanisms. *Brain Theory*, pp. 245-248, 1986.

[69]. A. M. Chen, H. Lu, R. Hecht-Nielsen. On the geometry of feedforward neural network error surfaces. Neural. Comput., Vol. 5, pp. 910-927, 1993.

[70]. SENIAM project. [http://www.seniam.org/]

[71]. H. L. Lew, S. J. Tsai. Johnson's practical electromyography. 4th ed. Philadelphia: Lippincott Williams & Wilkins, 2007.

[72]. C. Cortes, V. Vapnik. Support-Vector Networks. Machine Learning, 20(3): 273-297, 1995.

[73]. J. C. Platt. Fast training of support vector machines using sequential minimal optimization. In B. Scholkopf, C. J. C. Burges, and A. J. Smola, Advances in kernel methods - Support Vector Learning, pp. 185-208. MIT press.

[74]. Z. Song, S. Guo, M. Pang, S. Zhang. Study on Recognition of Upper Limb Motion Pattern Using surface EMG signals for Bilateral Rehabilitation, *Proceedings of 23rd 2012 International Symposium on Micro-NanoMechatronics and Human Science*, pp. 425-430, 2012.

[75]. http://en.wikipedia.org/wiki/File:Hill_muscle_model.svg.

[76]. M. Pang, S. Guo, Q. Huang, H. Ishihara, H. Hirata. An EMG-based Quantitative Representation Method for the Upper Limb Elbow Joint Angle in Sagittal Plane. *J. Med. Biol. Eng*, doi:10.5405/jmbe.1843, 2014.

[77]. M. Pang, S. Guo, Z. Song and S. Zhang. A Surface EMG Signals-based Real-time Continuous Recognition for the Upper Limb Multi-motion. *Proceedings of 2012 IEEE International Conference on Mechatronics and Automation*, pp.1984-1989, 2012.

[78]. S. M. Kay. Modern spectral estimation: Theory and application.

Englewood Cliffs, NJ: Prentice Hall, pp. 480–481, 1988.

[79]. H. Akaike. A new look at the statistical model identification. *IEEE T. Automat. Contr.*, Vol. 19, pp. 716–723, 1974.

[80]. C. M. Bishop. Pattern Recognition and Machine Learning. *New York: Springer*, 2006.

[81]. http://lifehealthcare.com.au/neuro-newsletter/

[82]. S. Zhang, S. Guo, M. Qu, M. Pang. Development of a bilateral rehabilitation training system using the haptic device and inertia sensors. *Proceedings of 2014 IEEE International Conference on Mechatronics and Automation*, pp. 1237-1242, 2014.

[83]. S, Zhang, S. Guo, M. Pang, M. Qu. Training Model-based Master-slave Rehabilitation Training Strategy using the Phantom Premium and an Exoskeleton Device. *Proceedings of the 2014 ICME International Conference on Complex Medical Engineering*, pp. 105-110, 2014.

[84]. M. Mihelj, T. Nef, R. Riener. ARMin II – 7 DoF rehabilitation robot: mechanics and kinematics. Proceedings of the 2007 IEEE International Conference on Robotics and Automation, pp. 4120-4125. 2007.

[85]. T. Nef, M. Guidali, R. Riener. ARMin III – arm therapy exoskeleton with an ergonomic shoulder actuation. *Appl. Bionics. Biomech*., Vol. 6, pp. 127-142, 2009.

[86]. N. Hogan. Adaptive control of mechanical impedance by coactivation of antagonist muscles. *IEEE T. Automat. Contr.*, Vol. AC-29, pp.

681-690, 1984.

[87]. J. Perry, G. A. Bekey. EMG-force relationships in skeletal muscle. Crit. Rev. Biomed. Eng., Vol. 7, pp. 1-22, 1981.

[88]. W. Herzog, J. Sokolosky, Y. T. Zhang, A. C. S. Guimaraes. EMG-force relation in dynamically contracting cat plantaris muscle. *J. Electromyogr. Kines.*, Vol. 8, pp. 147-155, 1998.

[89]. M. M. Liu, W. Herzog, H. H.C.M. Savelberg. Dynamic muscle force predictions from EMG: an artificial neural network approach. *J. Electromyogr. Kines.*, Vol. 9, pp. 391-400, 1999.

[90]. A. Rainoldia, J.E. Bullock-Saxton, F. Cavarretta, N. Hogan. Repeatability of maximal voluntary force and of surface EMG variables during voluntary isometric contraction of quadriceps muscles in healthy subjects. J. Electromyogr. Kines., Vol. 11, pp. 425-438, 2001.

[91]. K. Manal, T. S. Buchanan. A one-parameter neural activation to muscle activation model: estimating isometric joint moments from electromyograms. *J Biomech.*, Vol. 36, pp. 1197-1202, 2003.

[92]. J. A. Mercer, N. Bezodis, D. DeLion, T. Zachry, M.D. Rubley. EMG sensor location: Does it influence the ability to detect differences in muscle contraction conditions. J. Electromyogr. Kines., Vol. 26, pp. 198-204, 2006.

[93]. L. Mesin, R. Merletti, A. Rainoldi. Surface EMG: The issue of electrode location. J. Electromyogr. Kines., Vol. 19, pp. 719-726, 2009.

[94]. T. R. Farrell, R. F. Weir. The optimal controller delay for myoelectric prostheses. *IEEE T. Neur. Sys. Reh.*, Vol. 15, pp. 111-118, 2009.

[95]. E. Scheme, K. Englehart. Electromyogram pattern recognition for control of powered upper-limb prostheses: State of the art and challenges for clinical use. *J Rehabil. Res. Dev.*, Vol. 48, pp. 643-660, 2011.

[96]. P. Artemiadis. EMG-based robot control interfaces: Past, present and future. *Advances in Robotics & Automation*, Vol. 1, pp.1-3, 2012.

[97]. A. H. Oskouei, M. G. Paulin, A. B. Carman. Intra-session and inter-day reliability of forearm surface EMG during varying hand grip forces. *J. Electromyogr. Kinesiol.*, Vol. 23, pp. 216-222, 2013.

[98]. J. E. Earp, R. U. Newton, P. Cormie, A. J. Blazevich. Knee angle-specific EMG normalization: The use of polynomial based EMG-angle relationships. *J. Electromyogr. Kinesiol.*, Vol. 23, pp. 238-244, 2013.

[99]. J. Vogel, J. Bayer, P. Smagt. Continuous robot control using surface electromyography of atrophic muscles. *Proceedings of 2013 IEEE/RSJ International Conference on Intelligent Robots and Systems*, pp. 845-850, 2013.

[100].Q. An, Y. Ishikawa, T. Funato, S. Aoi, H. Oka, H. Yamakawa, A. Yamashita, H. Asama. Generation of human standing-up motion with muscle synergies using forward dynamic simulation. *Proceedings of 2014 IEEE International Conference on Robotics & Automation*, pp. 730-735, 2014.

[101].J. Duque, D. Masset, J. Malchaire. Evaluation of handgrip force from EMG measurements. *Applied Ergonomics*, Vol. 26, pp. 61-66, 1995.

[102].S. H. Westing, A. G. Cresswell, A. Thorstensson. Muscle activation during maximal voluntary eccentric and concentric knee extension. *Eur. J. Appl. Physiol.*, Vol. 62, pp. 104-108, 1991.

[103].E. Todorov. Direct cortical control of muscle activation in voluntary arm movement: a model. *Nature Neuroscience*, Vol. 3, pp. 391-398, 2000.

Publication List

International Journal Papers

1. **Muye Pang**, Shuxiang Guo and Zhibin Song, Study on the sEMG Driven Upper Limb Exoskeleton Rehabilitation Device in Bilateral Rehabilitation, Journal of Robotics and Mechatronics. Vol. 24(4), pp. 585-594, 2012.

2. **Muye Pang**, Shuxiang Guo, Qiang Huang, Hidenori Ishihara, and Hideyuki Hirata, Electromyography-based Quantitative Representation Method for Upper-limb Elbow Joint Angle in Sagittal Plane, Journal of Medical and Biological Engineering. DOI:10.5405/jmbe.1843., 2014.

International Conference Papers

1. **Muye Pang**, Shuxiang Guo, Zhibin Song, and Songyuan Zhang, A Surface EMG Signals-based Real-time Continuous Recognition for the Upper Limb Multi-motion, Proceedings of the 2012 IEEE International Conference on Mechatronics and Automation, pp. 1984-1989, 2012.

2. **Muye Pang**, Shuxiang Guo, and Songyuan Zhang, Finger Joint Continuous Interpretation based on sEMG Signals and Muscular Model, Proceedings of the 2013 IEEE International Conference on Mechatronics and Automation, pp. 1435-1440, 2013.

3. **Muye Pang**, Shuxiang Guo, Zhibin Song, and Songyuan Zhang, sEMG Signal and Hill Model based Continuous Prediction for Hand Grasping Motion, Proceedings of the 2013 ICME International Conference on Complex Medical Engineering, pp. 329-333, 2013.

4. **Muye Pang**, and Shuxiang Guo, A Novel Method for Elbow Joint Continuous Prediction using EMG and Musculoskeletal Model, Proceedings of the 2013 IEEE International Conference on Robotics and Biomimetics, pp. 1240-1245, 2013.

5. **Muye Pang**, Shuxiang Guo, and Songyuan Zhang, Interaction Force Transfer for Characteristic Evaluation of Touch Motion, Proceedings of the 2014 IEEE International Conference on Mechatronics and Automation, pp. 1237-1242, 2014.

6. Shuxiang Guo, **Muye Pang**, Youichirou Sugi, and Yuta Nakatsukao, Study on the Comparison of Three Different Upper Limb Motion Recognition Methods, Proceedings of the 2014 IEEE International Conference on Information and Automation, pp. 208-212, 2014.

7. Shuxiang Guo, Songyuan Zhang, Zhibin Song, and **Muye Pang**, Development of a Human Upper Limb-like Robot for Master-slave Rehabilitation, Proceedings of the 2013 ICME International Conference on Complex Medical Engineering, pp. 693-696, 2013.

Biographic Sketch

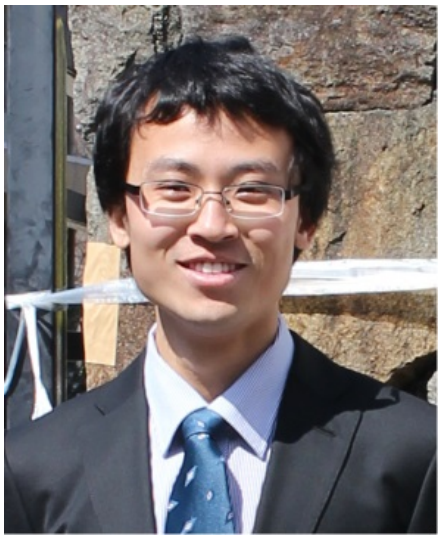

Muye Pang received his B.Sc. and M.Sc. degree from University of Electronic Science and Technology of China, Chengdu, Sichuan, China, in 2008, and in 2011, respectively. Currently, he is a Ph.D. candidate in Kagawa University, Japan. He researches on development of exoskeleton robot for upper limb rehabilitation and Electromyography technology based signal processing.

He has published over 9 refereed journal and conference papers in recent three years. He is an IEEE student member.